Dissertation

Preparation and characterization

of curcumin solid dispersions

(クルクミン固体分散体の調製と評価)

March 2021

NGUYEN NGOC SAO MAI

Acknowledgement

One of the greatest challenges in my life is passing four years in Japan. I am aware that the success does not only depend on my efforts but also tremendous supports from many people and organizations as well. From the bottom of my heart, I express my enormous and most heartfelt gratitude.

I would like to give my sincere appreciations to my supervisor, Professor Takehisa Hanawa for your knowledge, your academic advices, and your daily encouragements. Thank you so much for your acceptance at the beginning and your kind helps during my Ph.D. life in Noda campus at Tokyo University of Science. I would like to give my gratitude to my second supervisor, Associate Professor Yayoi Kawano for your academic advices in doing experiments and for your inspirations of life in Japan. Three years and a half in Hanawa ken is the most memorable experience in my life. I am grateful to all members in Hanawa ken for your kind helps in instructing me on using the equipment and facilities, analyzing data, and learning Japanese.

I would also like to thank Professor Hideyo Takahashi and Assistant Professor Kosho Makino (in Takahashi lab.), Professor Satoru Goto and Assistant Professor Yuta Otsuka (in Goto lab.), Professor Yoshikazu Higami, Professor Chikamasa Yamashita, and Associate Professor Hideshi Yokoyama for your enthusiastic helps in doing experiments and in giving useful academic advices for my researches.

I would like to give thanks to my colleagues in Nguyen Tat Thanh University for first supporting in getting the MEXT scholarship. I am also grateful to all my friends in Vietnam and Japan for watching every step I took and for your cheers, your

understandings, and your bonds. Thank you for becoming an essential part and precious memories of my life. I will miss all of you in my love.

I would like to give special thanks to the Japanese Ministry of Education, Culture, Sports, Science and Technology for having granted me the scholarship for the past 4 years. Your financial supports have helped me to focus on my studies and researches. I would also like to acknowledge the dedicated staff of Chiba University and Tokyo University of Science who are responsible for the scholarship logistics and helping out with every administrative formalities.

With a big hug and immense love in my heart, I give this success to my family, especially my husband, for all your wonderful efforts in raising children and for being my important spiritual supports during the years I was living alone in Japan. After every experience that we had, I would like to replenish all the time passed without me, I pray I stand by you, my giant love and for the rest of my lifetime.

Chiba, March 2021

Sao Mai

Abstract

Solubility is one of the most important physicochemical properties affecting drug bioavailability. One of the approaches to improve drug solubility is the preparation of solid dispersions (SDs) where the active pharmaceutical ingredients (APIs) are dispersed within (a) hydrophilic carrier(s) such as cyclodextrins, celluloses and their derivatives.

Curcumin (CUR), a diarylheptanoid consisting of two aromatic rings joined by a seven-carbon chain, exhibits numerous pharmacological properties such as anticancer, antioxidant, anti-inflammation, anti-tumor, anti-invasion, and wound healing. The efficient first-pass and intestinal metabolism of CUR might explain its poor systematic availability, and a daily oral dose of 3.6 g of CUR might be sufficient to exert pharmacological activity.

It is suggested that there are three majors approaches to overcome the bioavailability problems of CUR: (1) pharmacokinetics approach done by synthesizing its derivatives; (2) pharmaceutical approach realized by modifying formulation, manufacturing processes or physicochemical properties (e.g. complexation, and nano-formulation); and (3) biological approach by altering route of administration (e.g. intravenous, inhalation, and dermal delivery).

Particularly, converting crystalline drug to amorphous drug is a remarkable technique to achieve faster dissolution rate and higher apparent solubility due to changing physicochemical characteristic of API. There are two types of amorphous solids: pure amorphous drug and amorphous solid dispersion (ASD). Amorphous forms show a tendency towards crystallization to reduce the total energy content and pure amorphous forms convert to crystalline forms more rapidly than ASD's. Therefore, dispersing APIs within polymers to form an ASD might improve drug dissolution rate and solubility while

assuring the thermodynamic stability of drugs.

Enhancing the solubility of curcumin using a solid dispersion system with hydroxypropyl-β-cyclodextrin prepared by grinding, freeze-drying and common solvent evaporation methods

Cyclodextrins are cyclic oligosaccharides consisting of six, seven, or eight α-(1,4) linked glucopyranoside units, corresponding to α-, β-, and γ-CD, respectively. The CDs can increase the solubility of drugs that are entrapped within their hydrophobic cavity because of their superior hydrophilic exterior when exposed to water. Moreover, modified CDs using hydrophilic functional groups express a superior possibility of improving drug solubility than conventional CDs.

In this study, SDs of CUR and modified β-CD (hydroxypropyl-β-CD, HPβCD) were prepared using the grinding, freeze drying (FD), and common solvent evaporation (CSE) methods, and their physicochemical properties were evaluated with solubility, PXRD, FTIR, DSC, and dissolution studies. The second or higher order complex of CUR-HPβCD indicated the co-existence of inclusion complexes (ICs) and/or non-ICs, known as the SD system. When comparing the soluble drug amount with CUR crystals, the solubility of SDs were increased by up to 299-, 180-, and 489-fold, corresponding to the ground mixtures (GMs), FDs, and CSEs, respectively. The total transformation into the amorphous phase of CUR were observed in GMs and several ratios of CSEs. The drug was well dispersed within HPβCD in GMs and CSEs. The melting temperature of CUR in SDs increased in order of CUR in 1:2 ICs (CUR: HPβCD = 1:2), CUR in 1:1 ICs (CUR: HPβCD = 1:1), and CUR crystals. The dissolution rate of CUR increased with increase in the amount of HPβCD in SDs. The SD system consisting of CUR and HPβCD significantly increased the drug solubility compared to ICs.

Preparation and characterization of solid dispersions composed of curcumin, hydroxypropyl cellulose and/or sodium dodecyl sulfate by grinding with vibrational ball milling

Hydroxypropyl cellulose (HPC) has been used in SD formation to improve drug solubility. In this study, vibrational ball milling, a dry milling method was used to develop ground and co-ground CUR. It is applicable not only in laboratory research but also in pilot and industrial scale studies. During the grinding process, various parameters can influence the efficiency of grinding, such as the frequency of the vibration, type of grinding jar (volume, material), type of grinding media (quantity, material, and diameter), amount of powder filling, percentage of components, and grinding time.

Here, amorphization of CUR and CUR SDs consisting of CUR, HPC and/or SDS were developed by the vibrational ball milling. The resulting ground samples were characterized using PXRD, FTIR, DSC, and a dissolution study. The 60-min GM containing 90% HPC significantly increased the CUR solubility. Presence of SDS in GMs containing 90% HPC reduced grinding time from 60 min to 30 min in forming a ground SD which significantly increased the drug dissolution rate. This amorphous state was stable for 30 days when stored at 40 °C/ relative humidity 75%.

Effects of polymer molecular weight on curcumin amorphous solid dispersion: at-line monitoring system based on attenuated total reflectance mid-infrared and near-infrared spectroscopy

An at-line process analysis is defined as a method characterized by manual sampling followed by discontinuous sample preparation, measurement, and evaluation. Analytical instruments (e.g. near-infrared, mid-infrared, and ultra-violet spectroscopy) and chemometric techniques (e.g. multivariate analysis, principal components analysis (PCA),

and partial least-squares) are applied in pharmaceutical science for at-line monitoring process. Chemometrics is used in learning the relationships and structure of the system by analyzing very huge and highly complex datasets.

In this study, a ternary SD system containing CUR, HPC (HPC-SSL, HPC-L, or HPC-M), and SDS were prepared with grinding method, and the physicochemical and mechanochemical properties of this system were characterized. The grinding process, such as the grinding time and HPC Mw could be monitored by analyzing data obtained from MIR and NIR spectra. There were two steps in SD formation: (1) simple dispersion with grinding time under 30 min and (2) random dispersion of mixtures with grinding time from 30 to 120 min. The critical Mw of HPC (700,000 Da) could help select HPC(s) for more effectively forming SD systems.

[Conclusion]

CUR SDs were developed using grinding, FD, and CSE method and physicochemically characterized using PXRD, FTIR, DSC, dissolution study as well as scanning electron spectroscopy, particle size measurement, near- infrared. The carrier(s) where the drug was dispersed could influence the SD forming process due to its (their) chemical structure, molecular weight, proportion, and interactions with other components. The CUR-HPβCD SD consists of ICs and non-ICs and significantly increased the dissolution rate of CUR. Particularly, the grinding method with vibrational ball milling performed a total transformation from crystalline to the amorphous phase. The HPC in ground SDs could significantly increase CUR solubility at 90%. Also, the small amount of SDS might reduce the grinding time up to 30 min to manifest a significant enhancement in drug solubility. The forming of SDs can be at-line monitored using simple techniques such as MIR, NIR associated with chemometric.

Table of content

List of abbreviations

ASD – Amorphous solid dispersion

API – Active pharmaceutical ingredient

ATR – Attenuated total reflection

BCS – Biopharmaceutical Classification System

CD – Cyclodextrin

CSE – Common solvent evaporation

CUR – Curcumin

DE – Dissolution efficiency

DoE – Design of experiment

DSC – Differential scanning calorimetry

DW – Distilled water

FD – Freeze-drying

FTIR – Fourier transform infrared spectroscopy

GMs – Ground mixtures

HDF – Human dermal fibroblast

HPβCD – Hydroxypropyl-β-cyclodextrin

HPC – Hydroxypropyl cellulose

IC – Inclusion complex

MeOH – Methanol

MIR – Mid-infrared

Mw – Molecular weight

NIR – Near infrared

PC – Principal component

PCA – Principal component analysis

PET – Polyethylene terephthalate

PMs – Physical mixtures

PXRD – Powder X-ray diffraction

SEM – Scanning electron microscopy

SD – Solid dispersion

SDS – Sodium dodecyl sulfate

SNV – Standard normal variate

Std – Standard deviation

SVD – Singular value decomposition

UV – Ultraviolet

Chapter 1.   Introduction

Solubility is one of the most important physicochemical properties affecting drug bioavailability. According to Biopharmaceutical Classification System (BCS), active pharmaceutical ingredients (API) are classified into four classes due to their solubility and permeability. It is estimated that approximately 70% of the currently new drug candidates are BCS class II and IV which have poor solubility [1]. One methodology that can enhance the solubility of poorly water-soluble drugs and their bioavailability is amorphization [2-5]. Indeed, the solubility of amorphous drugs can be up to a 1000-fold higher than that of their crystalline forms [6-9].

Amorphous substances can be classified into two categories: molecularly pure drug and solid dispersions (SDs) where the API is dispersed within (a) carrier(s). The SDs are divided into crystalline and amorphous SDs according to the physical state of the carrier(s) which is (are) crystalline or amorphous. Vo et al. has demonstrated that SDs can be categorized into four distinct subcategories [10]: (1) SDs that use a crystalline carrier such as urea [11-13]or sugar [11]; (2) SDs that use a polymeric carrier such as povidone [14], polyethylene glycol [15], hydroxypropyl cellulose (HPC) [16], or cyclodextrins (CDs) [17-21]; (3) SDs that use a carrier with surface activity such as surfactant(s) or a mixture of polymers and surfactants [22]; (4) controlled release SDs or SDs that use swellable/water insoluble polymers such as Eudragit® [23] and Carbopol® [23]. As the result, the amorphous SDs containing APIs, a polymer or a mixtures of a polymer and surfactant are considered.

Various methods have been used to prepare the SDs with an aim to enhance solubility and dissolution rate of drugs. Aftab et al. investigated valdecoxib SD with polyvinyl pyrrolidone (PVP) using kneading technique [24]. Anant et al. developed curcumin-PVP

SDs by spray-drying [25]. Melting method and hot-melt extrusion method has been used in forming carbamazepine-nicotinamide cocrystal SDs [26]. Solvent evaporation method was applied in piroxicam SDs [27] and in carbamazepine SDs [28]. Betageri et al. described the preparation of SDs by melt and solvent methods following by lyophilization [29] and reported that the dissolution of lyophilized SDs further increased the dissolution of glyburide significantly. Ball milled aripiprazole SD increased the drug solubility over 100-fold in comparison with pure drug [30].

Curcumin (CUR), an API of BCS IV, was selected as a model of water poorly soluble API. CUR is a diarylheptanoid consisting of two aromatic rings joined by a seven-carbon chain. CUR compound exists both keto-enol forms and di-keto forms [31,32] (Figure 1.1). The di-keto forms are higher energy than the keto-enol forms by approximately 5~7 kcal/mol in different conditions [33].
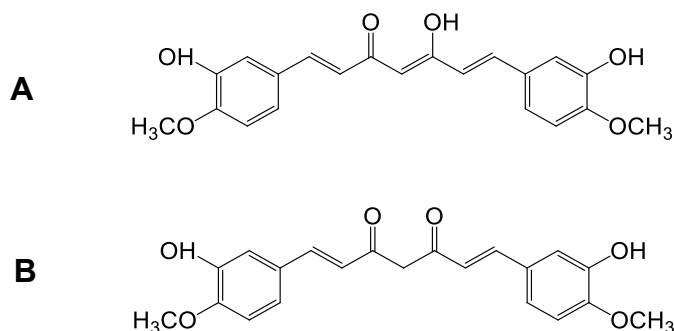
Figure 1.1. Curcumin compound exists both (A) keto-enol form; and (B) di-keto form

CUR exhibits various pharmacological properties such as analgesic, anti-inflammatory, anti-oxidant, anti-malarial, and insect repellant activities [34-40]. Because CUR is low aqueous soluble (~28.9 ng/mL) and dramatically metabolized through the first pass in liver (maximum serum concentration at 1 h: 0.006 ± 0.005 µg/mL) [41]. Particularly, CUR has been used in accelerating wound healing process. Kulac et al. described CUR as a wound dressing agent that protects wound tissue from microbial

infection, reduces inflammation, and stimulates cell proliferation to re-build damaged tissue [42]. Cianfruglia et al. reported that CUR at high concentration (≥ 20 µM) reduced the cell viability of human dermal fibroblast (HDF) with regard to the control of 57% [43]. Protective effect on HDF from UVA was recorded at 5 µM CUR pretreated for 2 h prior to 10 J/m^2 UVA irradiation exposure [44].

Mohanty et al. summarized different topical formulation of CUR for wound healing [45]. They are films (collagen films [46], methoxy poly(ethylene glycol)-graft-chitosan composite film containing CUR nanoformulation [47]), fibers (poly(ε-caprolactone) nanofibers [48]), emulsion (gel-core bioadhesive emulsion [49], nanoemulsion gel [50]), hydrogel (nanocomposite hydrogel [51], hydrogel system containing micellar CUR [52]), and different nanoformulations (hyalurosomes [53], CUR-loaded poly (lactic-co-glycolic acid) nanoparticles [54]).

Numerous pharmaceutical activities of CUR encouraged researchers to develop the CUR SDs to attain a significant enhancement in CUR solubility. Seo et al. prepared CUR SDs with Solutol® HS15 using solvent evaporation method [55]. The same method following by lyophilization was applied in forming CUR SDs with Eudragit® E PO which revealed a sustain release in solutions at various pH [56]. Hu et al. reported a novel SD system of CUR with Cremophor RH40, poloxamer 188, and polyethylene glycol 4000 using melt mixing methods [57]. A complexation agent: an arabinogalactan was demonstrated to form an SD with CUR using ball miller and host-guest complexes were present in this SD system [58]. An up-to-date method preparing CUR SDs was developed by Dharmalingam et al. using microwave-induced diffusion [59].

The fact of loading CUR SDs on a dermal delivery system instead of CUR helps in improving the CUR bioavailability and administration convenience. However, several

studies have been reported. Loading CUR SDs on hydrogels was studied for local treatment of injured vaginal infection [60]. Du et al. demonstrated an *in situ* forming hydrogel loading CUR-phospholipid complex which revealed wound healing effect [61]. An SD system consisting of CUR and monomethyl poly(ethylene glycol)-poly(ε-caprolactone) copolymer was loaded on thermosensitive hydrogels based on poly(ethylene glycol)-poly (ε-caprolactone)-poly(ethylene glycol) copolymer, which applied in colorectal peritoneal carcinomatosis [62].

The basic purpose of this study is to improve CUR solubility by forming an SD system. CUR SDs were developed with hydroxypropyl-β-cyclodextrin and hydroxypropyl celluloses of various grades, using freeze-drying, solvent evaporation or ball milling methods. The prepared SDs were then evaluated their physicochemical characterizations to reveal the effects of selected carriers and preparation methods on the SD formation process. During this, the role of sodium dodecyl sulfate, a surfactant demonstrated its power in increasing the drug solubility and in shortening the SD formation time even with a very small amount. Moreover, the characteristic evaluation methods were computer-assisted using software such as Design Expert and Unscrambler X which base on mathematical analysis. As a result, the global figures of SD formation were revealed, and valuable information of all factors was obtained. Therefore, the SD formation process is completely monitored to economize and validate resources before industrial manufacturing.

Chapter 2. Evaluation of curcumin solid dispersion with hydroxypropyl-β-cyclodextrin prepared by milling, freeze-drying, and common solvent evaporation methods [63]

2.1. Introduction

From their first isolation in 1891, cyclodextrins (CDs) have been introduced as powerful substances to enhance drug solubility by forming host–guest inclusion complexes (ICs) [64-72]. CDs are cyclic oligosaccharides consisting of six, seven, or eight α-(1,4) linked glucopyranoside units, corresponding to α-, β-, and γ-CDs, respectively. They have toroid shapes with a larger and a smaller opening.

The CDs can increase the solubility of drugs that are entrapped within their hydrophobic cavity because of their superior hydrophilic exterior when exposed to water. For decades, CD ICs have been prepared using co-precipitation, freeze-drying, solvent evaporation, and supercritical antisolvent method [73-75]. However, a drug/CD system not only consists of ICs but non-ICs as well [76,77]. In other words, the host–guest ICs are dispersed in the matrix of "empty" CDs as an SD system, which further enhances the solubility of ICs due to the hydrophilic exterior of CDs. Moreover, modified CDs using different functional groups express a superior possibility of improving drug solubility than conventional CDs [78,79].

Akbik et al. proved that the ability of CDs to enhance CUR solubility gradually increased in the order of γ-CD, β-CD, methyl-β-CD, and hydroxypropyl-β-cyclodextrin (HPβCD) [80]. HPβCD is a derivative of β-cyclodextrin and its water solubility is over 500 mg/mL at room temperature [81]. Besides, the amorphous nature of HPβCD helps with the amorphization when dispersing drugs or drug/HPβCD ICs in the matrix of

HPβCD in the SD system [82].

Here, CUR-HPβCD SDs were developed at molar ratio CUR:HPβCD 1:1, 1:2, 1:4, and 1:8, using common solvent evaporation (CSE), freeze-drying (FD), and grinding methods. The obtained SDs were characterized using PXRD, FTIR, DSC, and dissolution study to access their physicochemical properties, and to evaluate the ability of CUR:HPβCD molar ratio and preparation methods on enhancement of CUR solubility and dissolution rate. Instead of the only presence of ICs in CUR-HPβCD mixtures, we also supposed the coexistence of non-ICs which further enhance the drug solubility than conventional ICs.

2.2. Materials

CUR was purchased from Tokyo Chemical Industry Co. Ltd (Tokyo, Japan). HPβCD was purchased from Nihon Shokuhin Kako Co. Ltd (Tokyo, Japan). Methanol (MeOH) (purity min 99.5%) was purchased from Kanto Chemical Co., Inc. (Tokyo, Japan). Ammonia (10% solution) was purchased from Wako Pure Chemical Industries, Co. Ltd (Osaka, Japan).

2.3. SD preparation methods

2.3.1. Grinding method

The defined weights of CUR and HPβCD were mixed in a 30-mL glass sample tube with a vortex mixer for 60 sec to obtain the physical mixtures (PMs). Each PM (500 mg) was transferred to a 5 mL stainless steel jar on a mixer mill (MM400, Retsch, Haan, Germany) containing a ball (stainless steel, Φ7 mm). The jar was immersed in liquid nitrogen for 5 min and then the material was ground using the MM400 for 15 min at 30 Hz. The stroke immersion for 5 min in liquid nitrogen and the grinding was repeated twice,

thus corresponding to 30 min of grinding time. Following this, the ground mixtures were passed through a 36-mesh sieve and stored in a desiccator until further evaluation.

2.3.2. Freeze-drying (FD) method

The definite weights of HPβCD were dissolved in 20 mL DW with a small amount of 10% ammonia solution (pH = 10). Once CUR was added to the solution, the dispersions were stirred at 500 rpm for 15 min at 30°C. Next, the dispersions were sonicated for 4 h at a temperature under 30°C. The samples were then dried overnight using a freeze-dryer (EYELA DFU-2110, Tokyo Rikakikai Co, Ltd., Tokyo, Japan) with a cold trap temperature -80°C, in a dry chamber (EYELA DRC-1N, Tokyo Rikakikai Co, Ltd., Tokyo, Japan). The samples were passed through a 36-mesh sieve and stored in a desiccator until further evaluation.

2.3.3. Common solvent evaporation (CSE) method

The defined weights of HPβCD and CUR were dissolved in 50 mL MeOH. The mixtures were stirred at 30°C, 400 rpm until a clear solution was obtained. The solvent was evaporated using a rotary vacuum evaporator (EYELA, Tokyo Rikakikai Co. Ltd, Tokyo, Japan) at 40°C at a speed of 50 rpm. Then, the samples were placed in a vacuum dryer (vacuum sample drying oven HD-120, Ishii Laboratory Works Co. Ltd, Osaka, Japan) for 24 h to completely evaporate the solvent. The dried samples were passed through a 36-mesh sieve and stored in a desiccator until further evaluation.

2.4. Characteristic evaluation methods

2.4.1. Quantification of curcumin

The CUR content was analyzed using Ultraviolet (UV)-visible spectroscopy at 432 nm (Shimadzu 1800 UV-visible spectrophotometer, Shimadzu Co. Ltd., Kyoto, Japan). The analytical method was validated for specificity, linearity, accuracy, and precision [83].

The standard CUR solution used for quantification was prepared in 50% v/v MeOH/distilled water (DW).

2.4.2. Phase solubility analysis

The phase solubility analysis was conducted according to the method of Higuchi and Connors [84]. Several concentrations of HPβCD (0, 5, 10, 15, and 20 mM) were dissolved in 10 mL DW in 20 mL L-tubes. CUR (20 mg) was added to the solution. Each tube was capped and shaken continuously for 72 h in a water bath at 30 ± 1 °C. These samples were filtered through a 0.45-µm membrane filter (Captiva, Agilent technologies Inc.) and assayed for the CUR content using UV-visible spectroscopy at 432 nm as described in the section 2.4.1. The results were represented as mean ± standard deviation (std) of three measurements.

2.4.3. Solubility

Prepared samples containing 5 mg CUR were dispersed in 10 mL DW in 20-mL L-tubes. These tubes were capped and shaken continuously for 2 h in a water bath at 30 ± 1°C. Supersaturated solutions were filtered through a 0.45-µm membrane filter and further diluted with MeOH 50% v/v to obtain a suitable concentration within the calibration range. The content of CUR was analyzed using UV-visible spectroscopy at 432 nm as described in the section 2.4.1. The results were represented as mean ± std of three measurements.

2.4.4. Powder X-ray diffraction (PXRD)

PXRD were performed using a diffractometer (RINT 2000, Rigaku Co. Ltd., Tokyo, Japan) using CuKα radiation, an X-ray tube voltage of 40 kV, and an X-ray tube current of 40 mA. The range (2θ) of the scans was from 5° to 30° at a speed of 2°/min.

2.4.5. Fourier transform infrared (FTIR)

The attenuated total reflection (ATR) method was used, and FTIR spectra were

recorded using a Fourier transform infrared spectrometer Frontier T-UATR (KRS5) (Perkin-Elmer Inc., Shelton, CT, USA). The scanning range was 4000-500 cm^{-1} with 16 times the accumulation count, a sample thickness of 1 mm, and a resolution of 1 cm^{-1}. The obtained spectra were normalized by the standard normal variate (SNV) method [85].

2.4.6. Differential scanning calorimetry (DSC)

DSC measurements were obtained using a DSC-60 Plus Differential Scanning Calorimeter (Shimadzu Co. Ltd., Kyoto, Japan) connected to a TA-60WS thermal analyzer (Shimadzu Co. Ltd., Kyoto, Japan) and an FC-60A flow controller (Shimadzu Co. Ltd., Kyoto, Japan). Approximately 3-5 mg of samples were weighed in aluminum pans and were sealed. An empty pan was used as the reference. The samples were scanned at 10°C/min from 25°C to 250°C under N_2 gas with a flow rate of 50 mL/min.

2.4.7. Dissolution test

The dissolution profiles of CUR in the samples were evaluated using the dissolution apparatus specified in the 17th Japanese Pharmacopoeia [86]. Samples of SD containing 5 mg of CUR were accurately weighed and poured into a vessel containing 500 mL of DW. The temperature was controlled at 37°C ± 0.5°C, and the rotating speed of the paddle was set at 100 rpm throughout the study. At defined time intervals (1, 3, 5, 10, 15, 30, 45, 60, 90, and 120 min), 5-mL aliquots were withdrawn and replaced with an equal volume of fresh DW. The sample solutions were filtered through a 0.45-µm membrane filter (Captiva, Agilent technologies, Inc) and assayed for CUR content using UV-visible spectroscopy at 432 nm, as described in the section 2.4.1. The results were presented as the mean ± std of three measurements.

2.4.8. Dissolution efficiency (DE)

Khan and Rhodes suggested DE as a suitable parameter for the evaluation of in vitro dissolution [87]. The term DE for a pharmaceutical dosage form is defined as the area under the dissolution curve up to a certain time t, expressed as a percentage of the area of the rectangle described by 100% dissolution at the same time. It can be calculated using the following equation:

$$DE = \frac{\int_0^t y \times dt}{y_{100} \times t} \times 100 \qquad 2.1$$

where y is the drug percent dissolved at time t.

Although the CUR SD formation can increase the solubility of drug, the DE hardly attains 100%. As a result, we define DE to be the percentage of soluble drug at the same time. Therefore, the DE over 120 min of dissolution study was calculated as a comparative parameter to evaluate the variation of drug kinetic solubility.

2.5. Results and discussion

2.5.1. Phase solubility analysis

The phase solubility diagram of CUR and HPβCD is presented in Figure 2.2. The plot shows that the aqueous solubility of CUR increases with increasing HPβCD concentration up to 20 mM. According to Higuchi and Connors [84], this diagram is classified as A_P-type, indicating formation of second and/or higher order complexes with regard to HPβCD. However, the profile is not fitted to any equations which are used to calculate the stability constant of complex. It has been suggested that A_P-type profiles are strongly similar to phase solubility diagrams of lipophilic water insoluble drugs in aqueous surfactant solution [77].

10
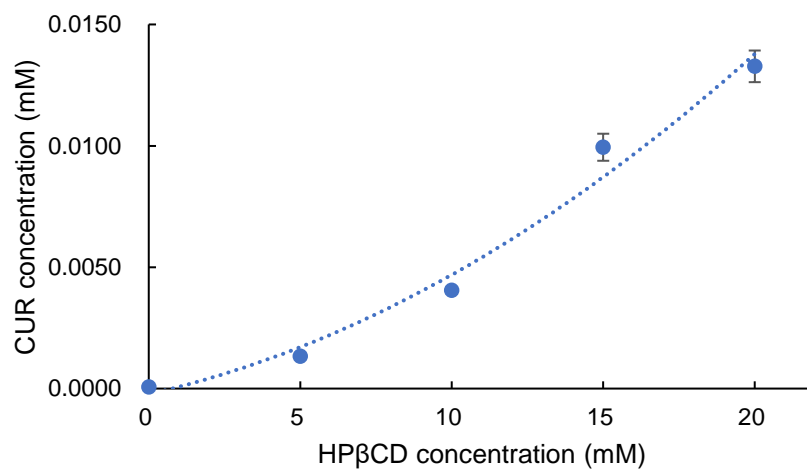
Figure 2.2. Phase solubility diagram of curcumin in various concentration of hydroxypropyl-β-cyclodextrin from 0 to 20 mM suggested Ap-type profile according to Higuchi and Conor [63]
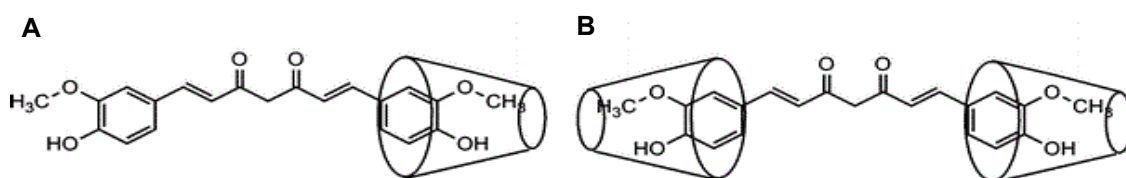
Figure 2.1. Inclusion complex scheme of (A) 1:1 curcumin (CUR): β-cyclodextrin (βCD), and (B) 1:2 CUR: βCD [88]

Using ^{1}H nuclear magnetic resonance (NMR) and 2D rotating frame overhause effect spectroscopy, Jahed et al. reported that one or two aromatic rings of CUR entered the β-CD cavity [88] corresponding to 1:1 or 1:2 host-guest ICs (Figure 2.1A and Figure 2.1B), respectively. Because of the existence of ICs and non-ICs in CUR/HPβCD SD system, it is supposed that the SD consists of free CUR molecules, CUR in ICs, CUR in non-ICs, and "empty" HPβCD molecules. Thus, the components of CUR-HPβCD SD are observed as in Figure 2.3. Moreover, the number of these components is belonging to the molar ratio of CUR-HPβCD and the preparation methods. For example, if there is an excess amount of HPβCD and dispersed force from preparation method is large enough to form the ICs, the free CUR crystals and 1:1 ICs will disappear.
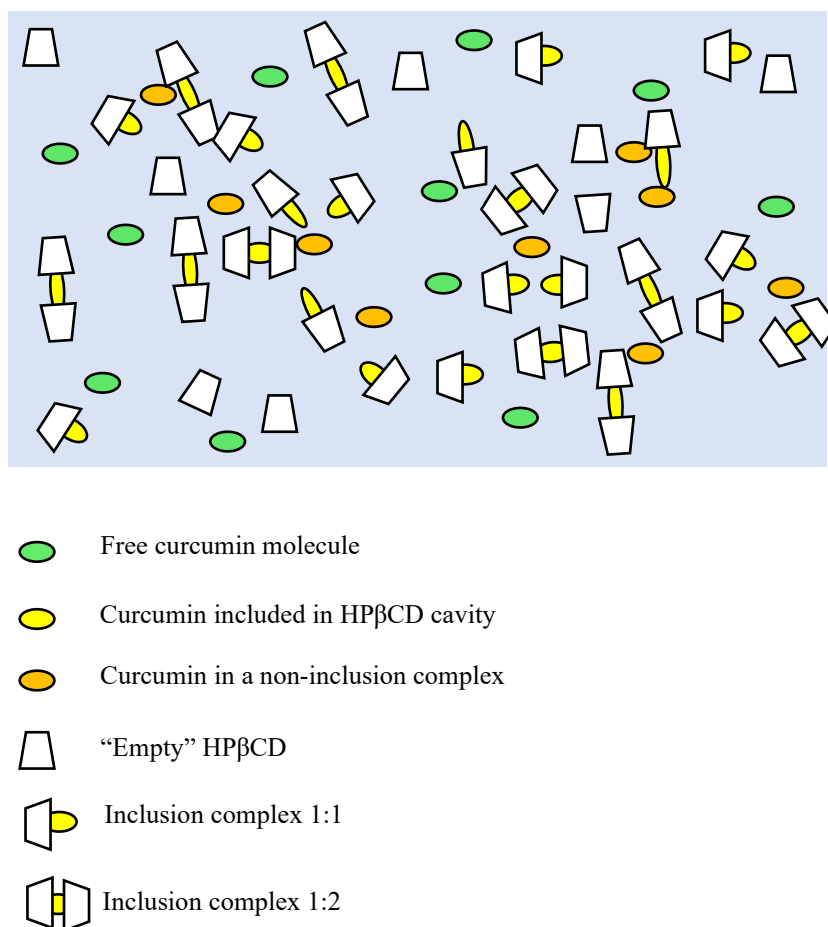
Figure 2.3. Components of curcumin/hydroxypropyl-β-cyclodextrin (HPβCD) solid dispersion: free curcumin (CUR), inclusion complex (IC) 1:1, IC 1:2, and "empty" HPβCD [63]

2.5.2. Solubility

The CUR solubility results are shown in Table 2.1. As the HPβCD molar was increased from 1 to 8 while the CUR molar ratio was kept constant at 1, the solubility ranged from 0.89-6.61, 0.27-5.23, and 2.64-14.16 µg/mL, corresponding to the grinding mixtures (GMs), freeze-drying mixtures (FDs), and common solvent evaporation mixtures (CSEs) methods, respectively. An increase in the amount of HPβCD enhanced the solubility of CUR regardless of the preparation method. When comparing the soluble drug amount with CUR crystal, the solubility was enhanced by up to 299-, 180-, and 489-fold corresponding to GMs, FDs, and CSEs, respectively.

Table 2.1. Molar ratio of different samples, their solubility (µg/mL) in water at 30ºC and their dissolution efficiency (%) calculated from dissolution data [63]

Sample	[1]CUR:[2]HPβCD ratio (mol/mol)	Solubility (µg/mL)	[3]DE (%)
CUR	-	0.03 ± 0.01	0.36±0.02
[4]GM11	1:1	0.89 ± 0.17	0.66±0.12
GM12	1:2	1.25 ± 0.25	2.55±0.13
GM14	1:4	2.55 ± 0.24	4.17±0.26
GM18	1:8	6.61 ± 0.15	4.31±0.10
[5]FD11	1:1	0.27 ± 0.02	1.48±0.27
FD12	1:2	0.54 ± 0.01	2.30±0.31
FD14	1:4	1.61 ± 0.13	4.02±0.46
FD18	1:8	5.23 ± 0.18	4.69±0.60
[6]CSE11	1:1	2.64 ± 0.11	2.82±0.18
CSE12	1:2	3.08 ± 0.19	10.00±0.45
CSE14	1:4	4.70 ± 0.29	31.27±0.31
CSE18	1:8	14.16 ± 1.27	52.21±0.75

Li et al. reported that the CUR-HPβCD IC prepared by cosolvency-lyophilization had a drug loading capacity of 1:7 of the drug:CD molar ratio [89]. Thus, the aqueous solubility of CUR was enhanced to 15.2 mg/mL. Because two benzene groups of one molecule of CUR will be entrapped within two molecules of CD, corresponding to 1:2 of the CUR/CD molar ratio, Li et al. formed an SD system consisting of ICs and non-ICs but named it an IC only.

---

[1] CUR, Curcumin

[2] HPβCD, Hydroxypropyl-β-cyclodextrin

[3] DE, Dissolution efficiency

[4] GM, Ground mixture

[5] FD, Freeze-drying mixture

[6] CSE, Common solvent evaporation mixture

2.5.3. PXRD

Figure 2.4A presents the PXRD patterns of CUR crystals, HPβCD, and PMs of CUR-HPβCD with various molar ratios. CUR crystals show prominent peaks at $2\theta = 8.88$, 12.3, 14.54, 17.26, 21.2, 23.32, and 24.72º, whereas HPβCD showed two broad peaks in the range of 10–15º and 15–20º, suggesting its amorphous nature. In PMs, the characteristic peaks of CUR are visible, but there are reductions in the intensity as the amount of HPβCD in the SDs increased.
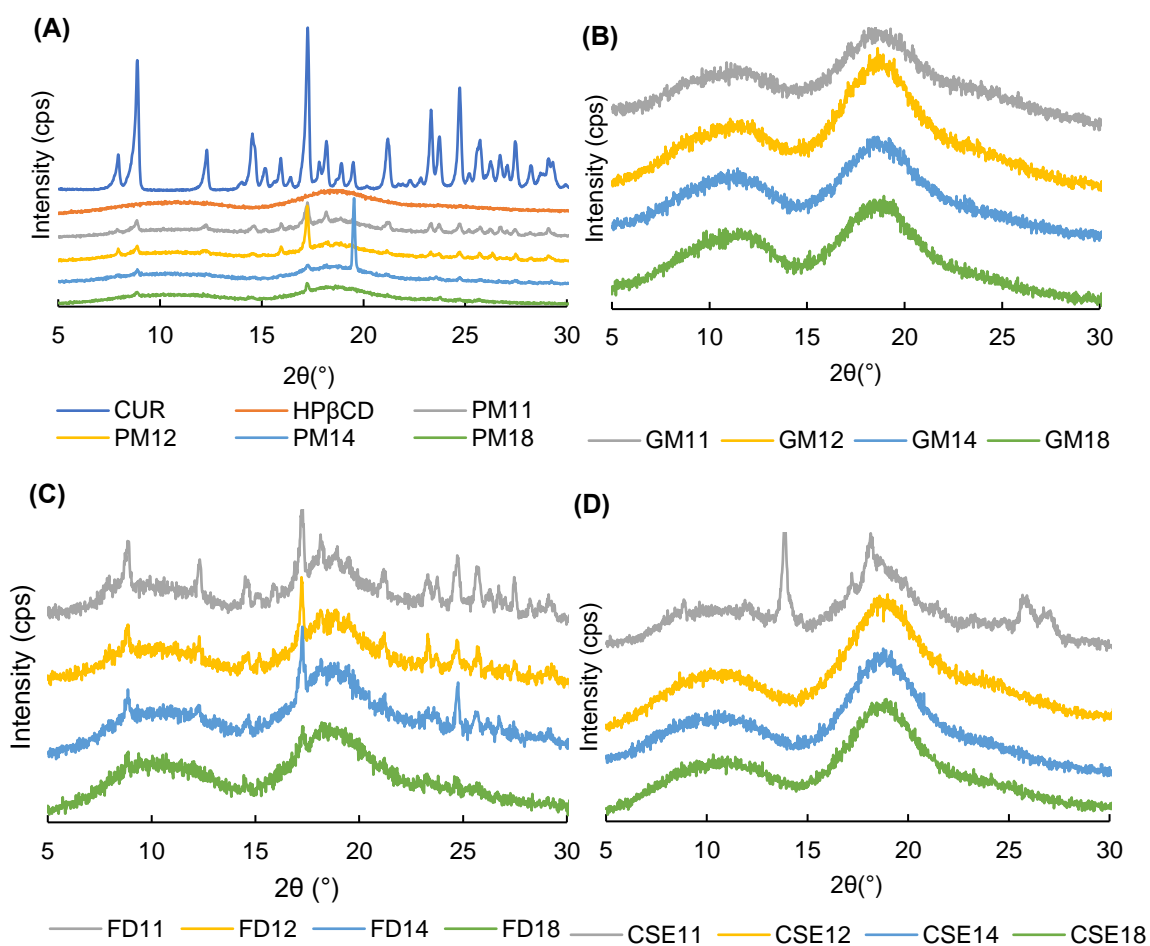
Figure 2.4. X-ray patterns in the range 2θ of 5-10º for (A) curcumin (CUR), hydroxypropyl-β-cyclodextrin (HPβCD), and physical mixtures (PMs) which showed crystalline, amorphous, and crystalline nature, respectively; (B) ground mixtures (GMs) which showed amorphous form of CUR; (C) freeze-drying mixtures (FDs) showed decreases in the intensity of CUR prominent peaks as the amount of HPβCD increased; and (D) common solvent evaporation mixtures (CSEs) showed some prominent peaks of CUR for CSE11 and amorphous forms of CUR for other CSEs [63]

Figure 2.4B halo patterns of CUR-HPβCD SDs prepared by the grinding method, indicating a total transformation from a crystalline form to an amorphous form. In Figure 2.4C, some prominent peaks of CUR were observed at 2θ = 8.92, 12.34, and 17.32°. However, peaks in the FD18 sample almost disappeared, thus demonstrating the amorphization of CUR. Figure 2.4D shows that in the PXRD patterns of the CSE11 sample, a peak at 2θ = 13.86° was observed, resulting in the crystalline form of CUR. However, in the CSE12, CSE14, and CSE18 samples, the prominent peaks of CUR are invisible, which suggests CUR exists as amorphous phase in the system.

2.5.4. FTIR

The prominent peaks observed in CUR are as follows: (1) 1602 cm^{-1} for the stretching
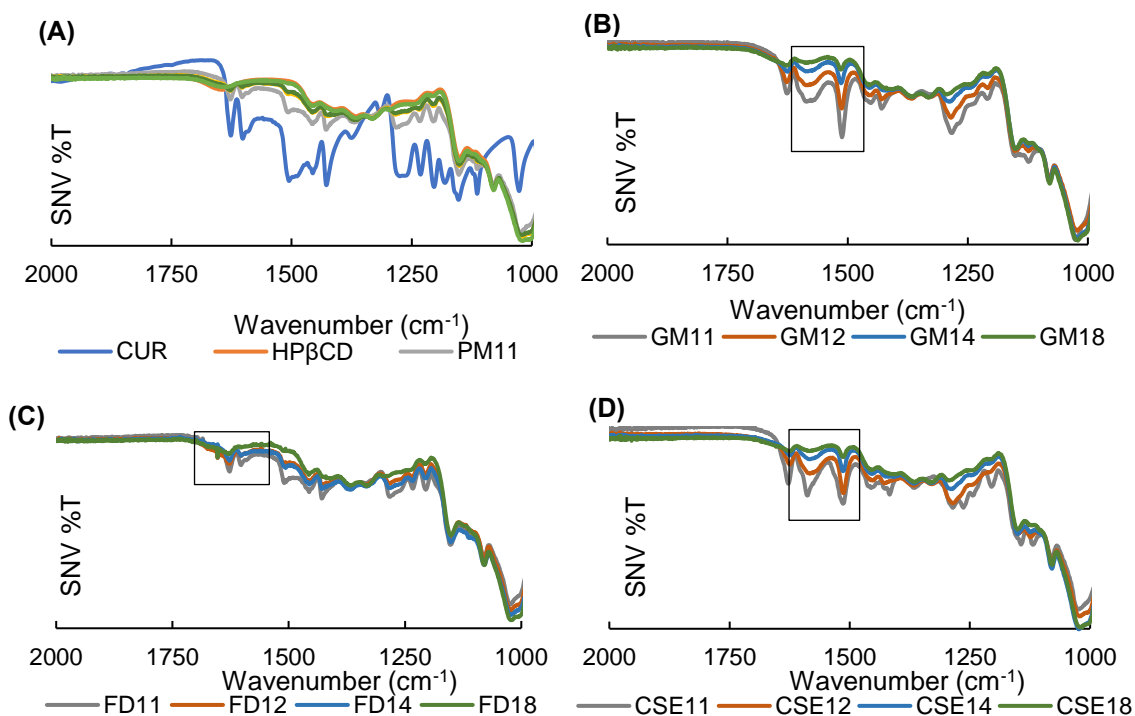
Figure 2.5. FTIR spectra of (A) curcumin (CUR), hydroxypropyl-β-cyclodextrin (HPβCD), and physical mixtures (PMs) in considering peaks at 1506 and 1275 cm^{-1} corresponding to carbonyl group (C=O) and benzyl methyl ether (OCH$_3$), respectively; (B) ground mixtures (GMs) showing appearance of new peaks at 1506 cm^{-1}; (C) freeze-drying mixtures (FDs) showing similar profiles to PMs; and (D) common solvent evaporation mixtures (CSEs) showing appearance of new peaks at 1506 cm^{-1} suggesting the hydrogen bond formation between CUR and HPβCD [63]

15

vibration of the benzene ring skeleton; (5) 1506 cm^{-1} for the mixed (C=O) and (C=C) vibrations; and 1275 cm^{-1} for the methyl aryl ether (O-CH$_3$) stretching vibrations [90]. Representatively, the peaks at 1506, 1602, and 1275 cm^{-1} were analyzed. Figure 2.5A shows the FTIR spectra of CUR crystals, HPβCD and PMs of CUR-HPβCD with various molar ratios at wavelength from 2000-1000 cm^{-1}. As the amount of HPβCD in PMs increased, CUR peaks were obscured by HPβCD spectra.

New peaks could be observed at 1506 cm^{-1} in case of GMs and CSEs (Figure 2.5B and Figure 2.5D respectively), whereas FDs showed the similar peaks as PMs (Figure 2.5C). It was supposed that CUR was well dispersed within HPβCD in GMs and CSEs and the dispersed behavior of FDs was similar to that of PMs. Additionally, the intensity of these new peaks positively decreased as the amount of HPβCD in mixtures increased. These new peaks were suggested to due to hydrogen bond formation between the oxygen of the CUR carbonyl group and the hydrogen of the HPβCD hydroxyl group.

2.5.5. DSC

The DSC curve for CUR crystals showed one endothermic peak at 188°C, corresponding to the melting point of CUR. An endothermic peak at 222°C was observed in the DSC curve of HPβCD, thus indicating its decomposition peak (Figure 2.6A). In thermograms of PMs, the melting peaks of CUR and decomposition peaks of HPβCD were detected, but they were shifted to lower temperatures because the mixtures of CUR and HPβCD are considered impure substances [91]. Furthermore, the shift range positively corresponds to the amount of HPβCD in PMs. On the other hand, the impurity of the 1:2 IC is considered to be lower than that of the 1:1 IC. Therefore, the endothermic peak of the 1:2 IC might be detected at a lower temperature than that of the 1:1 IC.

Figure 2.6B shows the DSC thermograms of GMs at various molar ratios. In the GM11 curve, it is supposed that the small and broad endothermic peak at 167.5°C indicates the formation of ICs. It is well known that some sublimable drug is included in CD cavities, the endothermic peak corresponds to the formation of inclusion complex was observed. In this study, though this small endothermic peak might be due to the formation of ICs, it should need further study. In the case of GM12, there were two glass transitions
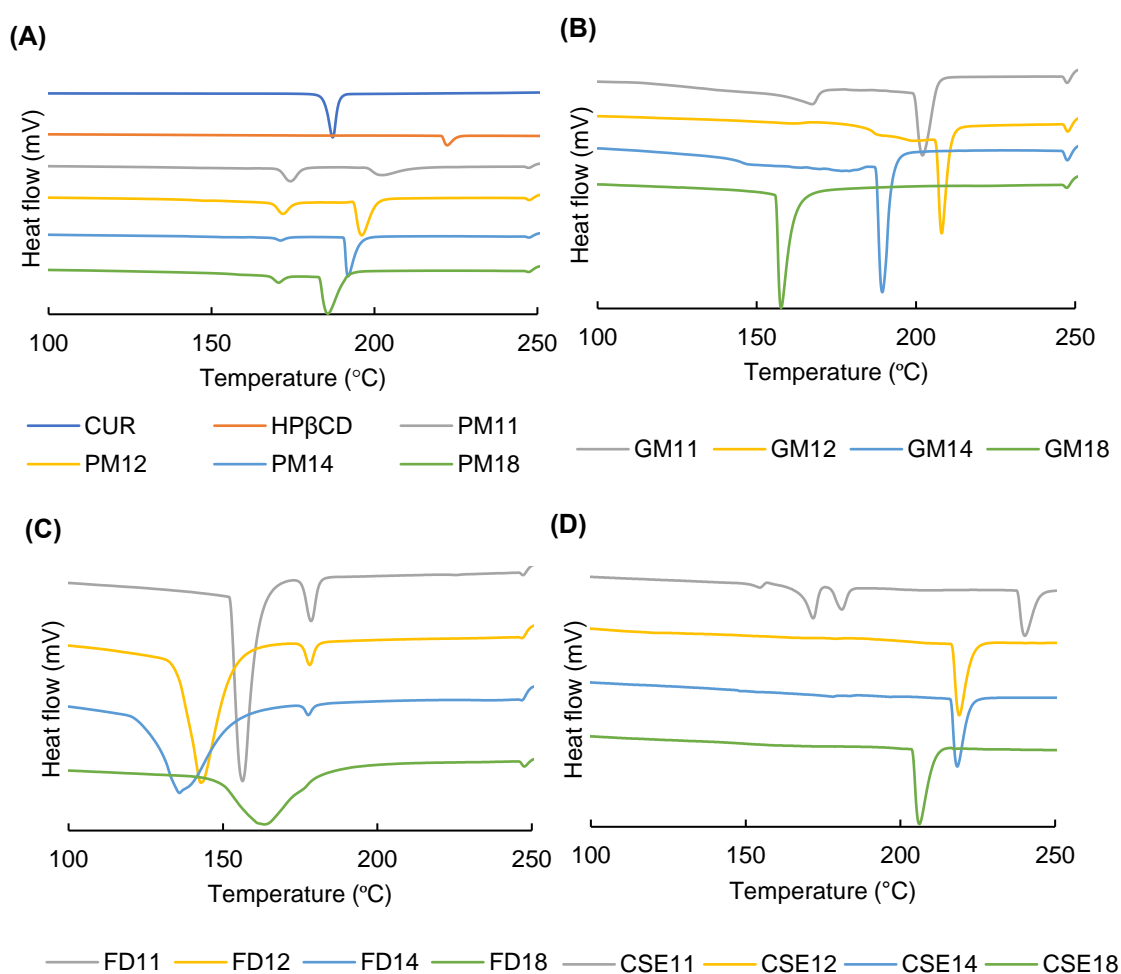
Figure 2.6. DSC curves of (A) curcumin (CUR) showing its melting temperature at 188ºC, hydroxypropyl-β-cyclodextrin (HPβCD) showing its decomposition temperature at 222ºC, and physical mixtures (PMs) showing shifts in the temperature of endothermic peaks for CUR and HPβCD; (B) ground mixtures (GMs); (C) freeze-drying mixtures (FDs); and (D) common solvent evaporation mixtures (CSEs) referring to 4 endothermic peaks for CSE11 corresponding to that of inclusion complex (IC) 1:2, IC 1:1, CUR, and HPβCD [63]

at 163 and 188.9°C, which correspond to the 1:2 and 1:1 complexes, respectively. In the GM14 curve, one glass transition was identified at 147°C, which corresponds to the 1:2 complexes. However, in the GM18 graph, the glass transition is invisible because of a large amount of HPβCD, which may over-impose the signal of the transition peak.

Figure 2.6C and Figure 2.6D reveal the DSC figures of FDs and CSEs, respectively. Because the melting point of a pure substance is higher and has a smaller range than the melting point of an impure substance [91], the melting temperature of CUR crystals is higher than that of 1:1 complexes and 1:2 complexes. Therefore, four endothermic peaks in CSE11 (Figure 2.6D) at 154.7, 171.7, 181.5, and 240.9°C corresponded to the 1:2 complex, 1:1 complex, CUR crystals, and HPβCD, respectively.

2.5.6. Dissolution study

The dissolution profiles of CUR crystals and SDs that were prepared by the grinding, FD, and CSE methods were depicted over a 120 min period (Figure 2.7). In general, mixtures containing a higher amount of HPβCD were expected to release a higher concentration of CUR and at the same molar ratios, CSEs had a higher dissolution rate than GMs and FDs.

According to the dissolution profiles of PMs (Figure 2.7A), CUR was gradually released, and its concentration tended to increase over 120 min of this study. However, SDs prepared by the grinding method exhibit different behavior as the molar ratios of components differ. With molar ratios 1:1 and 1:2, the released CUR peaks at 3 min, and then slightly decreases before plateauing over the remaining time (5-120 min) in the GMs. Alternatively, in GM14 and GM18, the soluble CUR rapidly peaks after one minute, decreases from 3-30min, and plateaus over the remaining time (45-120 min) (Figure 2.7B). It is observed that there is a similarity in the dissolution behavior of GM14 and GM18.

The dissolution profiles of the FDs (Figure 2.7C) showed the fast release of CUR concentration over 1-5 min, a slight variation over 10-60 min and stable release over the remaining time (90-120 min). For SDs prepared using the CSE method, CUR is released very quickly during the first minute and continues to increase its concentration up to 15 min (Figure 2.7D). However, the concentration of released CUR slightly decreases over the remaining time (30-120 min).
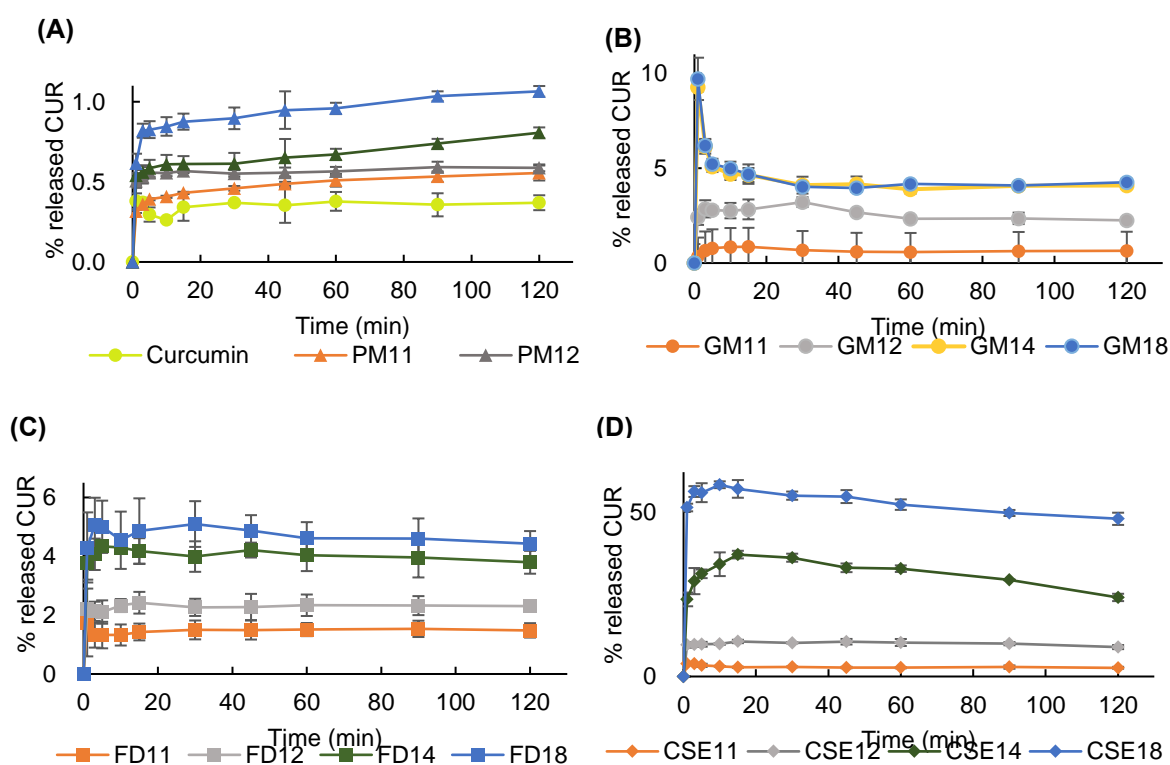
Figure 2.7. Dissolution behaviors of (A) curcumin (CUR), and physical mixtures (PMs) which showed higher dissolution rate in mixtures containing higher amount of hydroxypropyl-β-cyclodextrin; (B) ground mixtures (GMs) with the highest released CUR percentage of 9.71% for GM18 ; (C) freeze-drying mixtures (FDs) with the highest released CUR percentage of 5% for FD18; and (D) common solvent evaporation mixtures (CSEs) showing the superior dissolution rate of CUR compared to that of FDs and GMs with the same molar ratio and the greatest data 58.18% for CSE18 [63]

2.5.7. DE

The DEs of CUR crystals and SDs prepared using the grinding, FD, and CSE methods are displayed in Table 2.1. As the HPβCD molar was increased from 1 to 8 while

the CUR molar was kept constant at 1, the DE increased from 0.66 to 4.31% in GMs, from 1.48 to 4.69% in FDs, and from 2.82 to 52.21% in CSEs. The similarity in the dissolution profile of GM14 and GM18 was due to their DEs of 4.02 and 4.69, respectively. The CSE18 sample gave the best DE of 52.21%, 145-fold better than DE of CUR crystals (0.36%).

Because the CSE method was supposed to form ICs with the molar ratio of CUR:HPβCD = 1:2, the SD of CSE12 consisted of 1:2 ICs only. In other words, there was no CUR crystal, "empty" HPβCD, and 1:1 IC in the CSE12 whose DE was 10%. When the amount of HPβCD increased (in CSE14 and CSE18), the SD system was obtained and the DEs of CSE14 and CSE18 were 31.27 and 52.21%, respectively. This indicated that the dispersion of ICs in the matrix of HPβCD significantly increased the drug solubility compared to ICs.

2.6. Conclusion

The CSE method could realize a total formation of CUR-HPβCD SDs which consisted of 1:2 ICs and HPβCD "empty" and in which the 1:2 ICs were thoroughly dispersed in the matrix of HPβCD. When the molar ratio of drug: HPβCD was larger than 1:2, this proper CUR-HPβCD SD was obtained. The much greater than 1:2 of drug: HPβCD molar ratio, the more significantly increased the drug solubility compared to conventional 1:2 ICs.

Chapter 3. Preparation and characterization of solid dispersions composed of curcumin, hydroxypropyl cellulose and/or sodium dodecyl sulfate by grinding with vibrational ball milling [92]

3.1. Introduction

Hydroxypropyl cellulose (HPC) has been used in SD formation to improve drug solubility. Yamada et al. demonstrated that the co-ground mixtures (consisting of 3, 9-bis(N, N-dimethylcarbamoyloxy)-5H-benzofuro[3, 2-c]quinoline-6-one and HPC) increased the dissolution rate and maintained the high drug solubility by increasing particles surface area and forming amorphous state [93].

Sodium dodecyl sulfate (SDS) is an anionic surfactant widely used to improve drug wettability, solubility, and dissolution rate of poorly soluble APIs. Small amount of SDS resulted in a significant increase in the dissolution rate of fenofibrate samples obtained by salt assisted milling [94]. For prolonged contact with human skin, SDS concentrations should not excess 1% to avoid irritation [95].

For decades, to enhance CUR solubility, numerous methodologies forming CUR SDs with polymers have been accessed. Li et al. ameliorated CUR solubility by forming spray-dried SDs of CUR in cellulose derivative matrices [96]. Satomi et al. developed CUR SDs with HPC-SL and HPMC AS using wet milling and freeze-drying methods [97].

Among methods that formed SDs in previous chapter, vibrational ball milling was considered to develop ground and co-ground CUR because it is applicable not only in laboratory research but also in pilot and industrial scale studies [98]. This study focused on the effects of grinding time, role of HPC, and SDS in solubility enhancement of ground and co-ground CUR using vibrational ball milling.

Here, the amorphization was observed in molecularly pure drug, SDs that consist of

a drug and a polymer, and SDs that consist of a drug, a polymer, and a surfactant. The interactions between CUR-CUR and CUR-HPC after grinding were evaluated. The CUR formulations that significantly improved the drug dissolution rate were detected.

During the grinding process, various parameters can influence the efficiency of grinding, such as the frequency of the vibration, type of grinding jar (volume and material), type of media (quantity, material, and diameter), amount of powder filling, percentage of components, and grinding duration. Design of experiment (DoE) is an approach that can determine cause and effect relationships by introducing all possible inputs / factors acting on the process and all output(s) / response(s) based on the aims and statistical test performed. Then, the experimental resources are optimized while considering all the restrictions and limitations of the resources.

3.2. Materials

CUR was purchased from Tokyo Chemical Industry Co. Ltd (Tokyo, Japan). HPC-L (Mw 140,000 Da, viscosity 6.0-10.0 mPa.s at 20 °C/2% aq. solution) was purchased from Nippon Soda Co. Ltd (Tokyo, Japan). SDS (min 95.0%) was purchased from Wako Pure Chemical Industries Co. Ltd. (Osaka, Japan).

3.3. Preparation and characterization methods

3.3.1. Ground mixtures (GMs) preparation

The defined weight ratios of CUR, HPC and SDS were added to a 30-mL glass tube and mixed using a vortex mixer for 60 s to obtain the physical mixtures (PMs). A total of 300 mg of each PM was transferred to a 5-mL stainless steel jar that would fit the MM400 mixer mill (Retsch, Haan, Germany), and that contained a ball (stainless steel, Φ7 mm). The jar was immersed in liquid nitrogen for 5 min and then the material was

22

ground in the MM400 for 15 min at 30 Hz. The complete immersion for 5 min in liquid nitrogen and grinding process was repeated 1, 2, 3, and 4 times corresponding to 15, 30, 45, and 60 min of grinding time, respectively. Following this, the GMs were sieved through a 36-mesh sieve and stored in a desiccator until further evaluation.

3.3.2. Design of experiment (DoE)

For the DoE study, 6 levels of HPC (0, 10, 25, 50, 75, and 90%), 5 different grinding times (0, 15, 30, 45, and 60 min) and 2 levels of SDS (without-0 and with-1) were selected as inputs (Table 3.1). SDS amount was 1% of total amount of CUR and HPC. Design-Expert ® software version 11 and a full factorial design were utilized. These variables were set as categorical factors. The experimental design space consisted of 60 experiments. All the DoE runs were performed randomly, using similar process conditions. The output data was the dissolution efficiency (DE), with the goal being to achieve the highest DE.

Table 3.1. Samples of experiment based on factors and a response of DoE

Run	Factor 1 [7]HPC (%)	Factor 2 Grinding time (min)	Factor 3 Presence of [8]SDS	Response [9]DE (%)	Run	Factor 1 HPC (%)	Factor 2 Grinding time (min)	Factor 3 Presence of SDS	Response DE (%)
1	10	30	0	0.78	31	25	30	0	1.47
2	0	15	0	0.40	32	25	45	1	1.20
3	75	60	1	12.16	33	90	60	1	23.97
4	10	15	0	2.69	34	0	30	0	0.47
5	50	45	0	2.72	35	75	15	0	0.64

---

[7] HPC, Hydroxypropyl cellulose
[8] SDS, Sodium dodecyl sulfate
[9] DE, Dissolution efficiency

6	0	45	0	0.52	36	10	60	0	2.02
7	0	60	0	0.55	37	50	60	0	2.78
8	90	15	1	10.24	38	90	15	0	7.92
9	10	45	1	1.00	39	0	45	1	0.87
10	75	45	0	7.39	40	10	30	1	0.81
11	90	60	0	18.59	41	25	30	1	1.20
12	10	60	1	2.04	42	25	60	1	2.43
13	75	60	0	8.62	43	50	15	1	2.77
14	25	45	0	1.44	44	50	30	1	2.90
15	50	30	0	2.55	45	75	15	1	7.35
16	90	45	0	11.25	46	75	30	1	8.79
17	75	30	0	4.95	47	75	45	1	11.54
18	90	30	0	9.76	48	90	45	1	20.64
19	10	45	0	0.83	49	0	0	0	0.23
20	50	45	1	2.96	50	10	0	0	0.53
21	90	30	1	17.99	51	25	0	0	0.54
22	0	15	1	0.61	52	50	0	0	0.61
23	25	60	0	2.53	53	75	0	0	0.69
24	25	15	0	1.31	54	90	0	0	0.72
25	0	30	1	0.77	55	0	0	1	0.29
26	0	60	1	0.92	56	10	0	1	0.53
27	10	15	1	0.79	57	25	0	1	0.77
28	50	15	0	1.91	58	50	0	1	0.85
29	25	15	1	1.08	59	75	0	1	1.10
30	50	60	1	6.80	60	90	0	1	0.95

3.3.3. PXRD, FTIR, DSC, and dissolution test

The PXRD patterns, FTIR spectra, and DSC curves were recorded according to 2.4.4, 2.4.5, and 2.4.6 section, respectively.

The dissolution profiles of CUR in the GMs were evaluated as described in 2.4.7

section. Each sample was carried out in triplicate. The results were represented as mean $\pm$ std.

3.3.4. Fit factors

Moore and Flanner proposed procedures including different factor and similar factor to compare dissolution profiles in a pairwise fashion [99]. The difference factor (f_1) measures the percent error between two curves over all time points (Eq 2.1). The similarity factor (f_2) is a logarithmic transformation of the sum-squared error of differences between the test T_t and reference samples R_t over all time points (Eq 2.2).

$$f_1 = \frac{\sum_{t=1}^{n} |R_t - T_t|}{\sum_{t=1}^{n} R_t} \times 100 \qquad\qquad 3.1$$

$$f_2 = 50 \times \log \left[\frac{100}{\sqrt{\left(1 + \frac{1}{n} \sum (R_t - T_t)^2\right)}} \right] \qquad\qquad 3.2$$

where n: number of time points.

R_t: the mean dissolution value (%) for the reference product at time t.

T_t: the mean dissolution value (%) for the test product at the same time t.

The different factor f_1 is 0 when the test and reference profiles are identical and increase proportionally with the dissimilarity between two dissolution profiles. The similar factor f_2 fits the result between 0 and 100. It is 100 when the test and the reference profiles are identical and tends to 0 as the dissimilarity increases. In general, f_1 values lower than 15 (0-15) and f_2 values higher than 50 (50-100) show the similarity of the dissolution profiles [100].

In this study, to identify the formulations and conditions of the grinding method that can significantly enhance the kinetic solubility of drug, the f_1 and f_2 represented the dissimilarity of the dissolution profiles. In other words, f_1 value higher than 15 and f_2

values lower than 50 are noticed.

3.3.5. DE

DEs of 60 GMs were calculated as described in 2.4.8 section. The sample having the highest value of DE is the best formulation under the best conditions of grinding. The DEs were submitted in DoE as an output.

3.3.6. Stability

To evaluate stability, the 60-min GM containing 90% HPC and SDS was stored for 60 days at 40°C/ relative humidity (RH) 30% RH and 40°C/ RH 75%. The PXRD and dissolution profiles were examined at predetermined time intervals over this period (0, 7, 14, 30, and 60 days).

3.4. Results and discussion

3.4.1. PXRD

The PXRD patterns of 60 different ground mixtures (GMs) were examined. CUR crystals showed characteristic peaks at 2θ = 8.86, 12.28, 14.52, and 17.24° which represented their crystalline nature (data are not shown). PXRD pattern of HPC was observed as an amorphous form, whereas that of SDS showed a prominent peak at 6.8° (data are not shown).

The CUR characteristic peaks could be observed irrespective of the grinding time, but the peak intensity was decreased (Figure 3.1A). Colombo et al. [98] described that solid materials being processed in a mill received mechanical energy in pulse form. The transfer of mechanical energy through means of normal and shear stresses acting on solid material surfaces created growth of a strain field in the solid bulk. The strain field manifested atoms shift from equilibrium stable positions at lattice nodes or lattice collapse. Hence, the crystal transformation to amorphous phase could be explained and the

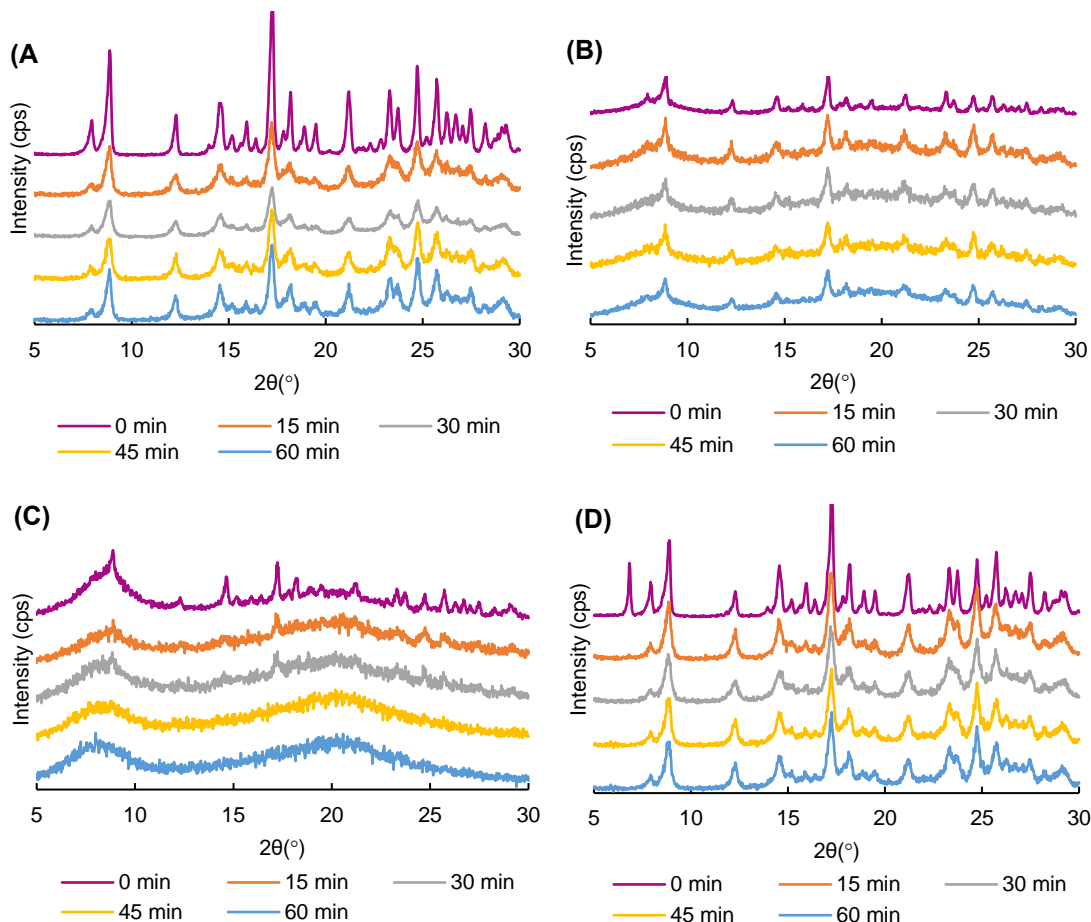reduction in the peak intensity was greater as the grinding time was prolonged.

Figure 3.1. X-ray patterns of (A) ground curcumin (CUR) crystals at various grinding time showing prominent peaks of CUR; (B) ground mixtures (GMs) containing CUR and 50% hydroxypropyl cellulose (HPC) showing decreases in the intensity of peaks as the grinding time increased; (C) GMs containing CUR and 75% HPC showing dramatical decreases in the intensity of peaks ; and (D) GMs containing CUR and sodium dodecyl sulfate (SDS) showing one prominent peak of SDS at 6.8º for physical mixture (0 min) but disappearance of the such peak for other GMs [92]

In binary ground mixtures (GMs) containing CUR and HPC (10, 25, and 50%), the characteristic peaks of CUR were visible but the reduction in the peak intensity clearly corresponded to the grinding time (Figure 3.1B). In GMs containing CUR and 75% HPC, some prominent peaks were observed at $2\theta =17.24$ and $24.76°$ for 15-min and 30-min GM. However, these peaks disappeared in the 45-min and 60-min GM (Figure 3.1C). In GMs containing CUR and 90% HPC, the characteristic peaks of CUR disappeared following

15 min of grinding (Figure S1F). Total transformation into amorphous nature of GMs showed that CUR was well dispersed within the matrix of HPC as the amount of HPC was triple that of CUR.

In ternary PMs (containing CUR, HPC, and SDS), regardless of the HPC amount, the prominent diffraction peak of SDS at 6.8° was observed (Figure 3.1D). However, this peak disappeared in all GMs (Figure S1 from D to L). Since the SDS amount in mixtures was very small, its dispersion was easily attained. In other words, the presence of SDS did not clearly influence the crystallinity of CUR in GMs. As a result, the crystallinity transformation behavior of ternary GMs was similar to that of binary GMs.

3.4.2. FTIR

The FTIR spectra of the 60 samples were examined. The prominent peaks observed in CUR were as follows [31]: (1) 3502 cm^{-1} for phenolic (-OH) vibrations; (2) 3017 cm^{-1} for aromatic C-H stretching vibrations; (3) 1626 cm^{-1} for conjugated alkene (C=C) stretching; (4) 1602 cm^{-1} for the stretching vibration of the benzene ring skeleton; (5) 1506 cm^{-1} for mixed (C=O) and (C=C) vibrations; 1274 cm^{-1} for methyl aryl ether (C-O) stretching vibrations (data are not shown).

In ground CUR crystals, there were increases in peaks intensity at 1507 cm^{-1} and 1275 cm^{-1} corresponding to carbonyl and ether group of CUR, respectively (Figure 3.2A). Also, peaks at 1274 cm^{-1} were shifted to 1276, 1280, 1281, and 1281 cm^{-1} corresponding to data of 15, 30, 45, and 60-min GMs, respectively. The increase in the intensity of peaks at 1507 cm^{-1} was due to the intra-molecule hydrogen bond of keto-enol forms (Figure 3.3). In addition, the shift of peaks at approximately 1274 cm^{-1} was due to the inter-molecule hydrogen bond of CUR and CUR (Figure 3.4a). However, it was impossible to observe the FTIR spectra of phenolic OH (at 3017 cm^{-1}) of CUR because they were over-imposed

by the broad peaks -OH group of HPC (at approximately 3200 – 3700 cm^{-1}).
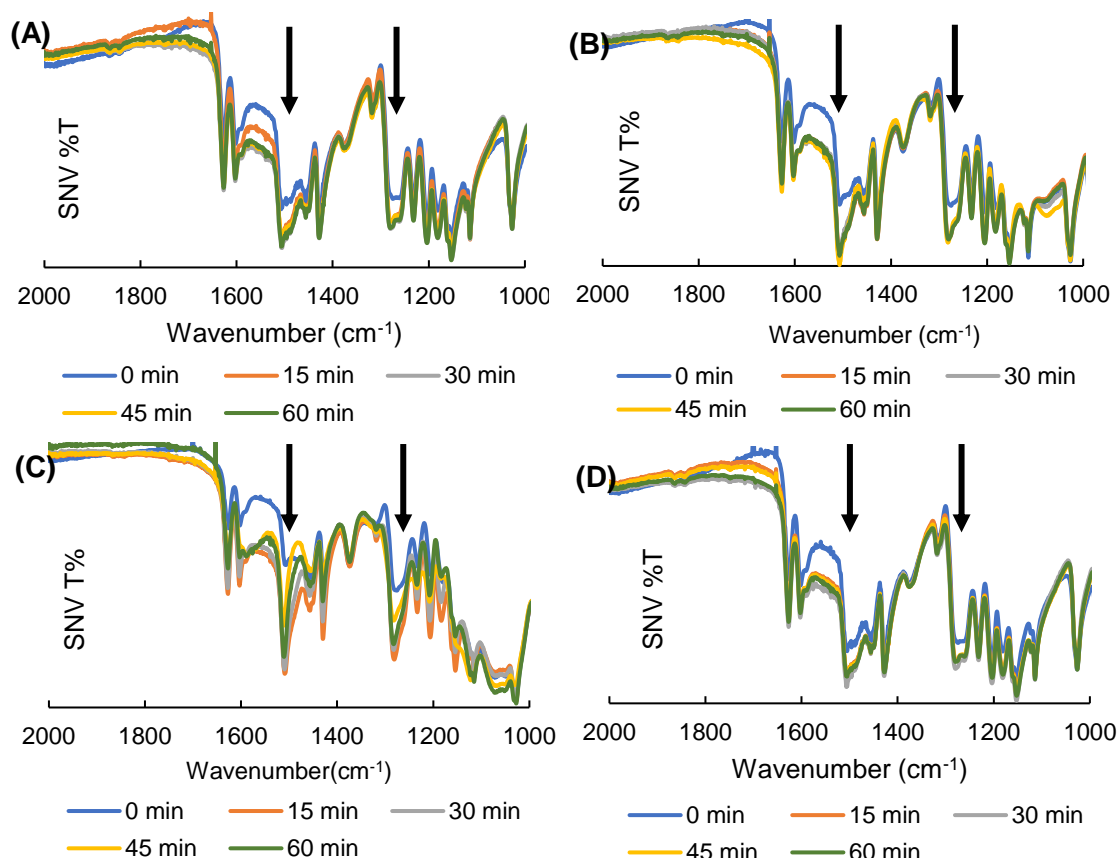
Figure 3.2. FTIR spectra of (A) ground curcumin (CUR) crystals in considering peaks at 1506 and 1275 cm^{-1} corresponding to carbonyl group (C=O) and benzyl methyl ether (OCH$_3$), respectively;; (B) ground mixtures (GMs) showing increases in the intensity of peaks at 1506 and 1275 cm^{-1} containing CUR and 50% HPC; (C) GMs containing CUR and 75% HPC showing appearance of new peaks at 1506 and 1275 cm^{-1} suggesting the formation of hydrogen bond between CUR and hydroxypropyl cellulose and (D) GMs containing CUR and sodium dodecyl sulfate [92]

Figure 3.3. Intra-molecule hydrogen bond of curcumin keto-enol form

As the amount of HPC in mixtures increased up to 50%, the variation of these peaks was also observed (Figure 3.2B). In addition to the CUR-CUR hydrogen bond, the hydrogen bonds between CUR-HPC were co-existed (Figure 3.4b).
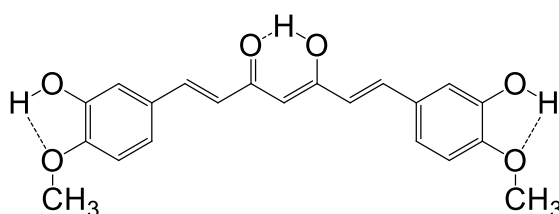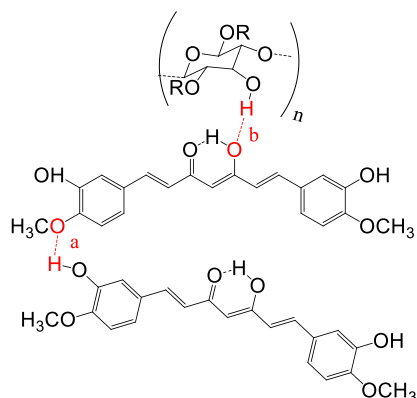

Figure 3.4. Estimated hydrogen bonds in ground mixtures between: (a) curcumin-curcumin; and (b) curcumin-hydroxypropyl cellulose

Particularly, in GMs containing over 75% HPC (Figure 3.2C), new peaks at 1507 cm^{-1} and 1275 cm^{-1} were observed and became more intensive when the grinding time increased. This suggests that the drug was thoroughly dispersed in the HPC and the only hydrogen bond between CUR and HPC was formed. In other words, the hydrogen bond between CUR and CUR did not exist. The SDS in both ternary PMs and GMs did not influence the FTIR spectra of these GMs (Figure 3.2D and Figure S2 from D to L) because of its small amount and being over-imposed by spectra of CUR and HPC.

3.4.3. DSC

DSC curve of CUR crystals shows one endothermic at 187 °C, due to the melting and that of HPC shows one endothermic peak at 206°C, due to its decomposition [101] (data are not shown). DSC thermograms of ground CUR crystals all showed melting peaks at approximately 190°C (Figure 3.5A). These peaks were stable regardless of the grinding time. However, exothermic peaks at approximately 80°C were observed. It indicated the recrystallization of CUR since the grinding method transformed CUR from crystalline to

amorphous phase [98]. In addition, the longer the grinding time, the higher the exothermic peaks were.

In GMs, DSC curves revealed both peaks of CUR and HPC, but they all were shifted to lower temperature because the mixtures of CUR and HPC are considered as impure material [91]. As the percentage of HPC in GMs increased, the melting peaks of CUR were broadened and more shifted to lower temperature (Figure 3.5B and Figure 3.5C). The recrystallization peaks could be observed in GMs containing up to 50% HPC.
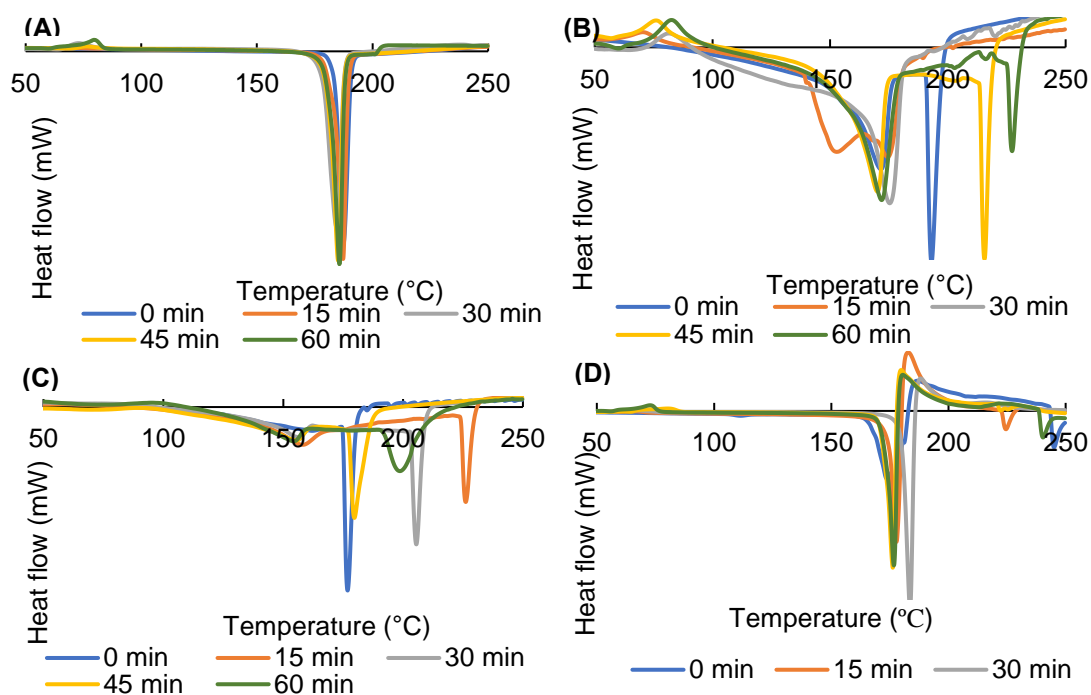
Figure 3.5. DSC curves of (A) ground curcumin (CUR) crystals showing endothermic peaks at approximately 190ºC corresponding to their melting temperature and exothermic peaks at approximately 80ºC corresponding to their recrystallization; (B) ground mixture (GMs) containing CUR and 50% hydroxypropyl cellulose (HPC) showing also the recrystallization phenomenon; (C) GMs containing CUR and 75% HPC showing the disappearance of CUR recrystallization; and (D) GMs containing CUR and sodium dodecyl sulfate (SDS) showing that the presence of SDS raised the right shoulders of CUR melting peaks and the recrystallization was visible [92]

In case of ternary GMs, the presence of SDS raised the right shoulders and un-stabilized the CUR melting peaks (Figure 3.5D). However, the recrystallization

phenomenon of ground CUR was similar to that of binary GMs. In other words, the CUR

crystallization was prevented as the HPC amount in GMs over 75%.

3.4.4. Dissolution study
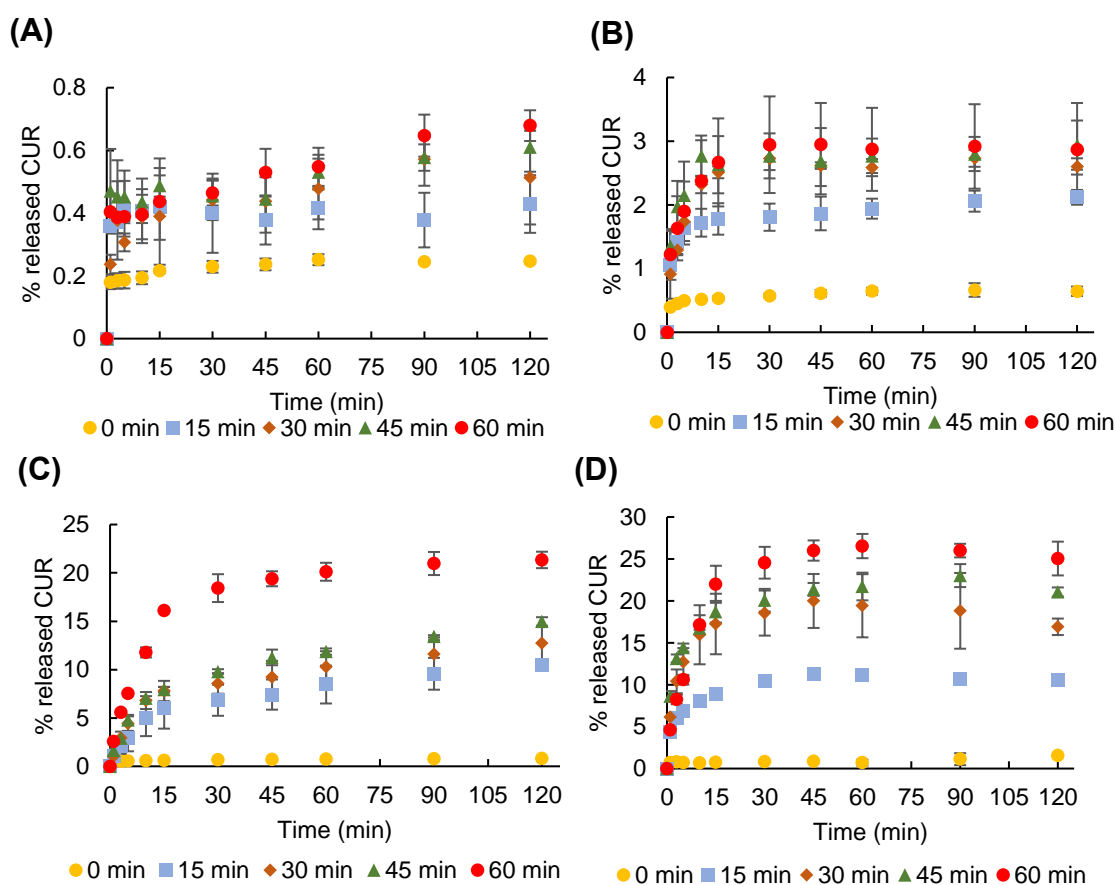
Figure 3.6. Dissolution profiles of (A) ground curcumin (CUR) crystals showing that the % released CUR positively increased to the grinding time; (B) ground mixtures (GMs) containing CUR and 50% hydroxypropyl cellulose (HPC); and (C) GMs containing CUR, 90% HPC, and (D) GMs containing CUR, 90% HPC, and sodium dodecyl sulfate. The presence of HPC and SDS significantly increased the released rate of CUR [92].

Dissolution profiles of ground CUR crystals are shown in Figure 3.6A. As grinding

time increased, the dissolution rate was enhanced, since CUR was partly transformed into

an amorphous phase whose solubility was higher than crystalline phase. Indeed, the

percentage of released CUR over 120 min was ameliorated from 0.25 (ground for 0 min)

to 0.68 (ground for 60 min).

Presence of HPC in PMs (0 min GMs) positively correlated with the dissolution rate of CUR (Figure 3.6B and C). Indeed, the released amounts of CUR over 120 min were 0.25, 0.55, 0.60, 0.64, 0.79, and 0.82% corresponding to 0, 10, 25, 50, 75, and 90% HPC, respectively. In addition, presence of SDS in ternary PMs could increase these numbers to 0.34, 0.65, 0.76, 0.95, 0.99, and 1.55%, correspondingly. The hydrophilicity of HPC and the surfactant characteristic of SDS can increase drug wettability and solubilization, thus, improve the CUR dissolution rate.

The dissolution rate of CUR in GMs increased as the amount of HPC increased and as the grinding time prolonged. Also, the presence of SDS in ternary GMs enhanced the CUR dissolution compared to corresponded binary GMs. The greatest dissolution rate of CUR was observed in the 120-min GMs containing 90% HPC and SDS: 25% (Figure 3.6D).

3.4.5. Fit factors

Fit factors are used to evaluate the significant differences in dissolution rate of CUR between formulations and their corresponding PM. The dissolution data of PMs were adopted as the reference during samples testing, which have the same amount of HPC and SDS. The difference factor (f_1) and similarity factor (f_2) values were calculated and are shown in Table 3.2. All samples had f_1 values > 15, indicating that ground samples and presence of SDS and / or HPC in samples led to a significant difference in CUR dissolution rate. In addition, an f_2 value of < 50 was observed in four GMs, namely, 60-min binary GM containing 90% HPC (40.6) as well as 30-min, 45-min, and 60-min ternary GMs containing 90% HPC (corresponding to 40.4, 37.5, and 34.9 respectively). There were significant differences the dissolution rate of these GMs. Therefore, the presence of SDS helped reduce the grinding time from 60 min to 30 min in order to develop a ground SDs

which significantly enhanced drug solubility.

Table 3.2. Fit factors of all samples with various percentage of HPC at various grinding time calculated from the dissolution data. The reference was CUR bulk and the dissimilarity in the dissolution rate of other samples with the reference was found when $f_1 > 15$ and $f_2 < 50$ [92]

Without [10]SDS												
Grinding time (min)	**[11]HPC 0%**		**HPC 10%**		**HPC 25%**		**HPC 50%**		**HPC 75%**		**HPC 90%**	
	f_1	f_2	f_1	f_2	f_1	f_2	f_1	f_2	f_1	f_2	f_1	f_2
15	54.8	99.6	48.4	99.1	70.8	93.7	77.2	88.5	81.7	82.3	91.9	59.8
30	56.6	99.5	58.3	98.2	66.0	92.3	82.0	83.3	90.3	68.2	93.5	54.9
45	63.5	99.2	59.8	97.8	72.9	92.6	84.0	81.3	93.1	59.9	94.3	51.8
60	63.2	99.2	81.6	87.7	84.8	82.2	83.7	81.5	93.8	57.0	96.6	**40.6**
With SDS												
Grinding time (min)	**HPC 0%**		**HPC 10%**		**HPC 25%**		**HPC 50%**		**HPC 75%**		**HPC 90%**	
	f_1	f_2	f_1	f_2	f_1	f_2	f_1	f_2	f_1	f_2	f_1	f_2
15	59.1	98.8	54.8	98.3	47.8	97.6	78.2	81.8	66.2	65.9	92.0	53.5
30	67.4	97.7	55.1	98.2	54.9	96.4	78.9	80.9	71.1	60.8	95.5	**40.4**
45	73.2	96.8	63.4	96.8	54.5	96.5	79.0	80.8	75.7	54.7	96.1	**37.5**
60	74.0	96.5	82.5	86.8	78.1	84.5	90.8	61.5	76.4	53.4	96.3	**34.9**

3.4.6. DE

DE (%) is a parameter reflected the area under the dissolution curve. The DEs of the 60 samples were calculated and are shown in Table 3.1; the values were in the ranged between 0.23 and 23.97; the smallest value corresponded to the DE of CUR crystals, and the highest value corresponded to the DE of 60-min GM containing 90% HPC and SDS. Hence, the DE value of later formulation increased 104-time as comparing to the DE of

---

[10] SDS, Sodium dodecyl sulfate
[11] HPC, Hydroxypropyl cellulose

CUR crystals.

In addition, because the DEs are comparative parameters to evaluate the differences among formulations, they were submitted into DoE as an output data whereas inputs were A-HPC (amount of HPC, %), B-grinding time (min), and C-presence of SDS. Following this, an analysis of variation was accessed to estimate the significance of DoE model.

3.4.7. DoE analysis

The half-normal plot of effects helps to observe what factor is significant. The vertical (y) axis displays the cumulative probability of getting a result and the horizontal (x) axis reveals the absolute value of effect [102]. In the half-normal plot (Figure 3.7), a model consisting of A-HPC, B-grinding time, and C-presence of SDS are shown as small squares on the right-hand side of the red line referring to their positive effects on the response. In addition, the distances from these three factors to the red line were in order of A-HPC, B-grinding time, and C-presence of SDS. This indicates that the influence of A-HPC on the DE was higher than that of B-grinding time and C-presence of SDS.

Figure 3.7. Half normal plot showing the positive effects of hydroxypropyl cellulose (A-HPC), B-grinding time, and C-presence of sodium dodecyl sulfate (SDS) factors on the response (dissolution efficiency). The distance from the factors to the red line showed the degree of their influence on the response [92]

35

The half-normal plot of effects helps to observe what factor is significant. The vertical (y) axis displays the cumulative probability of getting a result and the horizontal (x) axis reveals the absolute value of effect [102]. In the half-normal plot (Figure 3.7), a model consisting of A-HPC, B-grinding time, and C-presence of SDS are shown as small squares on the right-hand side of the red line referring to their positive effects on the response. In addition, the distances from these three factors to the red line were in order of A-HPC, B-grinding time, and C-presence of SDS. This indicates that the influence of A-HPC on the DE was higher than that of B-grinding time and C-presence of SDS.
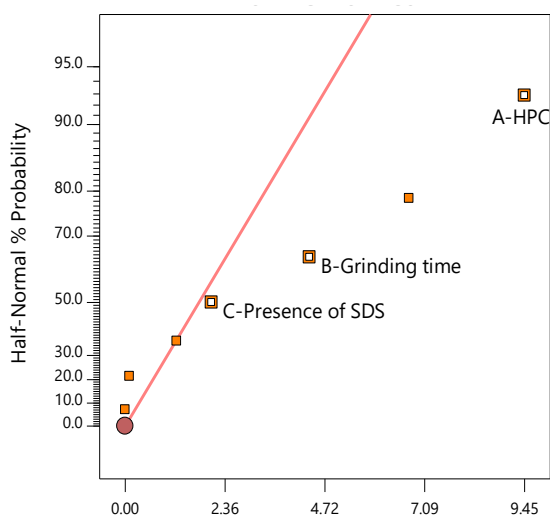
A model F-value of 13.77 implies model significance; there was only a 0.01% chance that such an F-value could occur due to noise (Table 3.3). Because p-values > 0.05 indicate that model terms are significant, A-HPC, B-grinding time, and C-presence of SDS were significant model terms whose p-values were <0.0001, 0.0002, and 0.0465, respectively. In other words, A-HPC, B-grinding time, and C-presence of SDS factors significantly influenced on the DE. The smaller p-value is the greater influence of factor on DE is. This fact illustrated the mentioned analysis observed from the half-normal plot.

Table 3.3. Result of '**analysis of variation**'

Source	Sum of Squares	[12]df	Mean Square	F-value	p-value	
Model	1314.82	10	131.48	13.77	< 0.0001	significant
A-[13]HPC	1008.40	5	201.68	21.12	< 0.0001	
B-Grinding time	266.59	4	66.65	6.98	0.0002	
C-Presence of [14]SDS	39.84	1	39.84	4.17	0.0465	

The interactions of the three factors are shown in Figure 3.8. Samples grounded for longer time expressed higher DE while samples containing larger amount of HPC showed

---

[12] df, degree of freedom
[13] HPC, Hydroxypropyl cellulose
[14] SDS, Sodium dodecyl sulfate

better DE. Moreover, the presence of SDS in GMs significantly increased DE compared to GMs in the absence of SDS (p-value < 0.05).
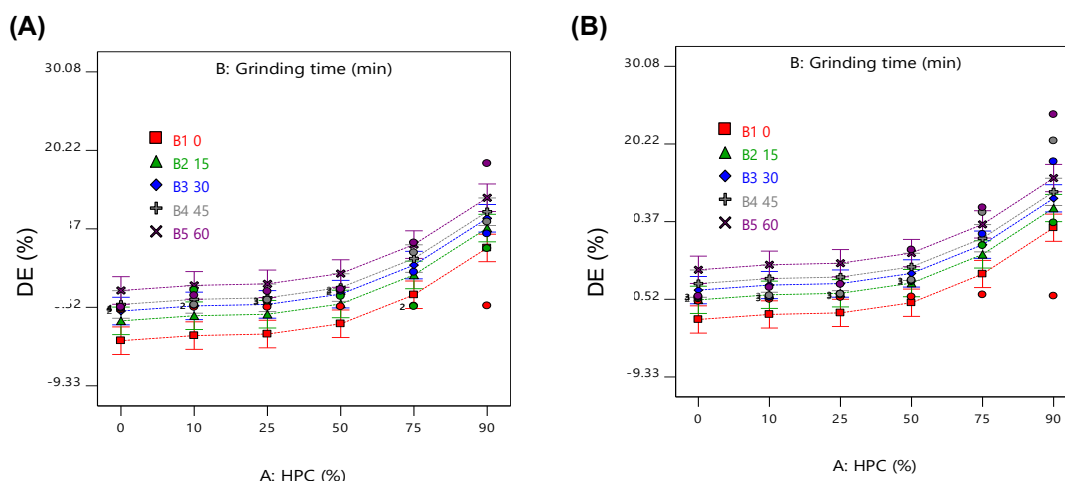

Figure 3.8. Interactions among factors of: (A) Ground mixtures (GMs) without sodium dodecyl sulfate (SDS), and (B) GMs with SDS. There were stronger interactions in GMs containing SDS compared to GMs without SDS.

B1 0, 0-min grinding; B2 15, 15-min grinding; B3 30, 30-min grinding; B4 45, 45-min grinding; and B5 60, 60-min grinding

3.4.8. Stability

To explore the effect of the storage time and HPC under high temperature and low/high humidity condition on 60-min GMs containing 90% HPC and SDS, the PXRD patterns and dissolution profiles over 7, 14, 30, and 60 days at 40°C/ 30% RH and 40°C/ 75% RH were recorded as in Figure 3.9. The halo patterns of samples were stable up to 30 days in both two stored conditions (Figure 3.9A). However, CUR characteristic peaks appeared in samples after 60 days of storing. HPC may have protected the drug from crystallization for up to 30 days in the stored conditions.

After 7 days of storing, the dissolution rate of CUR was decreased (Figure 3.9B). In the condition of RH 30%, the CUR was continuously released over the initial period ranging from 0 to 15 min and gradually decreased over the remaining time (from 30 to

120 min). However, samples stored in RH 75% released the drug very slowly during the 0-15 min initial time followed by a gradual increase. Since the HPC can easily absorb water from the atmosphere, the samples become lumpy and slowly decomposed.

After 14 days of storing, the dissolution rate of CUR in RH 30% was higher than that in RH 75%. During the initial 15 min, CUR was gradually released, then decreased over the remaining time (from 30 to 120 min). The samples stored at RH 75% released CUR continuously over 120 min.

However, after 30 days of storing, the samples in RH 30% progressively released CUR over 15 min, fluctuated during the period of 15 and 60 min, and then decreased over the remaining time. Whereas the samples in RH 75% released drug continuously over 60 min then decreased over the remaining time. In addition, after 60 days of storing, the samples in both RH 30% and RH 75% released CUR gradually over 120 min. Nevertheless, the sample dissolution rate in RH 75% was lower than that in RH 30%.

Obviously, the moisture in the stored environment had prominent effects on CUR crystallinity and dissolution rate and the temperature at 40°C accelerated the storage process. The presence of HPC in samples absorbed such water and protected the drug from the influence of moisture and heat. It was suggested that the sample should be stored at room temperature (25°C) and RH under 30% to assure the drug stability over 30 days.

Concerning restraints of this study, we used the DoE as a statistical equipment in analyzing data and did not confer to its capacity of design experiments. Indeed, the accessed full factorial design of DoE required 60 runs of experiment. Instead, a fractional factorial design should be used, and the number of samples could be reduced to at least twice the number of runs. This could reduce resources, but error effects and a power loss due to the reduction in runs are inevitable consequences [102].
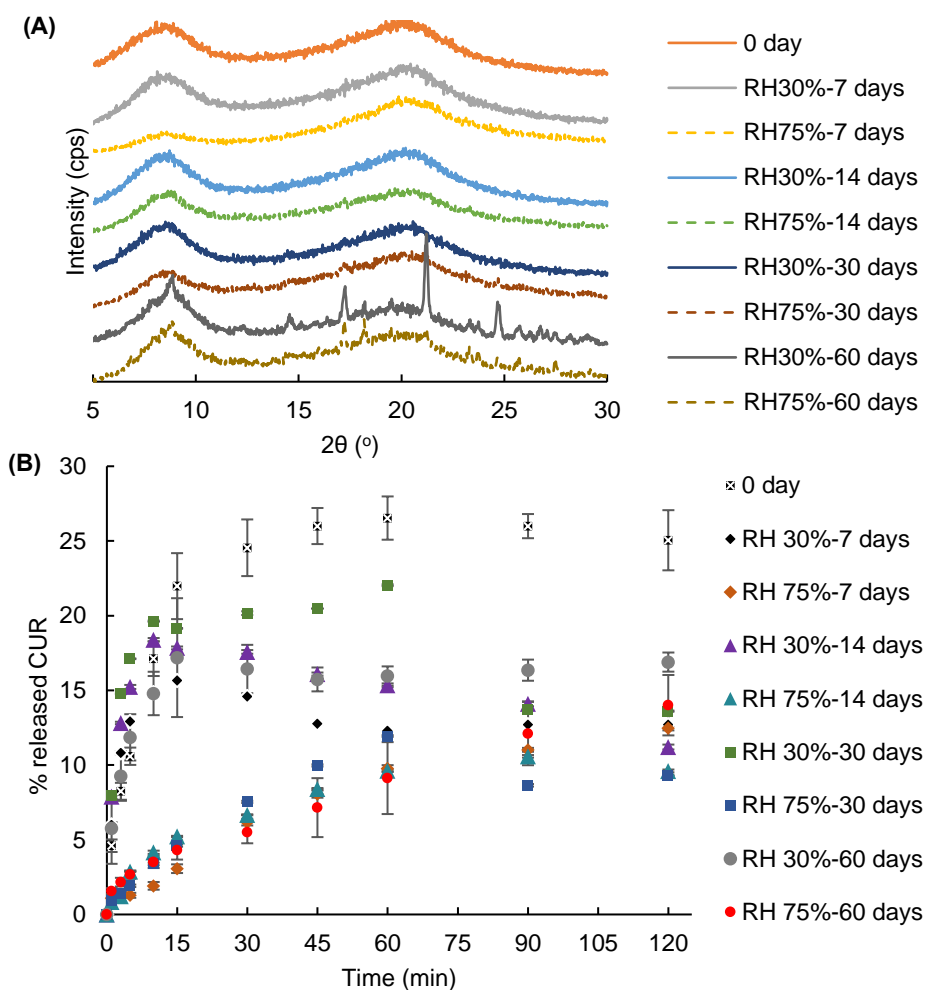
Figure 3.9. Stability results of 60-min ground mixtures containing 90% hydroxypropyl cellulose (HPC) and sodium dodecyl sulfate (SDS) after 0, 7, 14, 30, and 60-day storage at 40°C/ 30% RH and 40°C/ 75% RH, showing (A) X-ray patterns, and (B) dissolution profiles

3.5. Conclusion

In this study, amorphization of CUR and CUR SDs consisting of CUR, HPC and / or SDS were developed by the vibrational ball milling. The resulting ground samples were characterized using PXRD, FTIR, DSC, and a dissolution test. The 60-min GM containing 90% HPC significantly increased the CUR solubility. Presence of SDS in GMs containing 90% HPC reduced grinding time from 60 min to 30 min in forming a ground SD which significantly increased the drug dissolution rate. This amorphous state was stable for 30 days when stored at 40°C/ RH 75%.

Supplementary Materials

Figure S1. PXRD patterns of (A) ground curcumin (CUR) crystals; (B) ground mixtures (GMs) containing CUR and 10% hydroxypropyl cellulose (HPC); (C) GMs containing CUR and 25% HPC, and SDS; (D) GMs containing CUR and 50% HPC; (E) GMs containing CUR and 75% HPC; (F) GMs containing CUR and 90% HPC; (G) GMs containing CUR and sodium dodecyl sulfate (SDS), (H) GMs containing CUR, 10% HPC, and SDS; (I) GMs containing CUR, 25% HPC, and SDS; (J) GMs containing CUR, 50% HPC, and SDS; (K) GMs containing CUR, 75% HPC, and SDs; (L) GMs containing CUR, 90% HPC, and SDS

Figure S2. FTIR spectra of (A) ground curcumin (CUR) crystals; (B) ground mixtures (GMs) containing CUR and 10% hydroxypropyl cellulose (HPC); (C) GMs containing CUR and 25% HPC, and SDS; (D) GMs containing CUR and 50% HPC; (E) GMs containing CUR and 75% HPC; (F) GMs containing CUR and 90% HPC; (G) GMs containing CUR and sodium dodecyl sulfate (SDS), (H) GMs containing CUR, 10% HPC, and SDS; (I) GMs containing CUR, 25% HPC, and SDS; (J) GMs containing CUR, 50% HPC, and SDS; (K) GMs containing CUR, 75% HPC, and SDs; (L) GMs containing CUR, 90% HPC, and SDS

Figure S3. DSC curves of (A) ground curcumin (CUR) crystals; (B) ground mixtures (GMs) containing CUR and 10% hydroxypropyl cellulose (HPC); (C) GMs containing CUR and 25% HPC, and SDS; (D) GMs containing CUR and 50% HPC; (E) GMs containing CUR and 75% HPC; (F) GMs containing CUR and 90% HPC; (G) GMs containing CUR and sodium dodecyl sulfate (SDS), (H) GMs containing CUR, 10% HPC, and SDS; (I) GMs containing CUR, 25% HPC, and SDS; (J) GMs containing CUR, 50% HPC, and SDS; (K) GMs containing CUR, 75% HPC, and SDs; (L) GMs containing CUR,

90% HPC, and SDS

Figure S4. Dissolution profiles of (A) ground curcumin (CUR) crystals; (B) ground mixtures (GMs) containing CUR and 10% hydroxypropyl cellulose (HPC); (C) GMs containing CUR and 25% HPC, and SDS; (D) GMs containing CUR and 50% HPC; (E) GMs containing CUR and 75% HPC; (F) GMs containing CUR and 90% HPC; (G) GMs containing CUR and sodium dodecyl sulfate (SDS), (H) GMs containing CUR, 10% HPC, and SDS; (I) GMs containing CUR, 25% HPC, and SDS; (J) GMs containing CUR, 50% HPC, and SDS; (K) GMs containing CUR, 75% HPC, and SDs; (L) GMs containing CUR, 90% HPC, and SDS
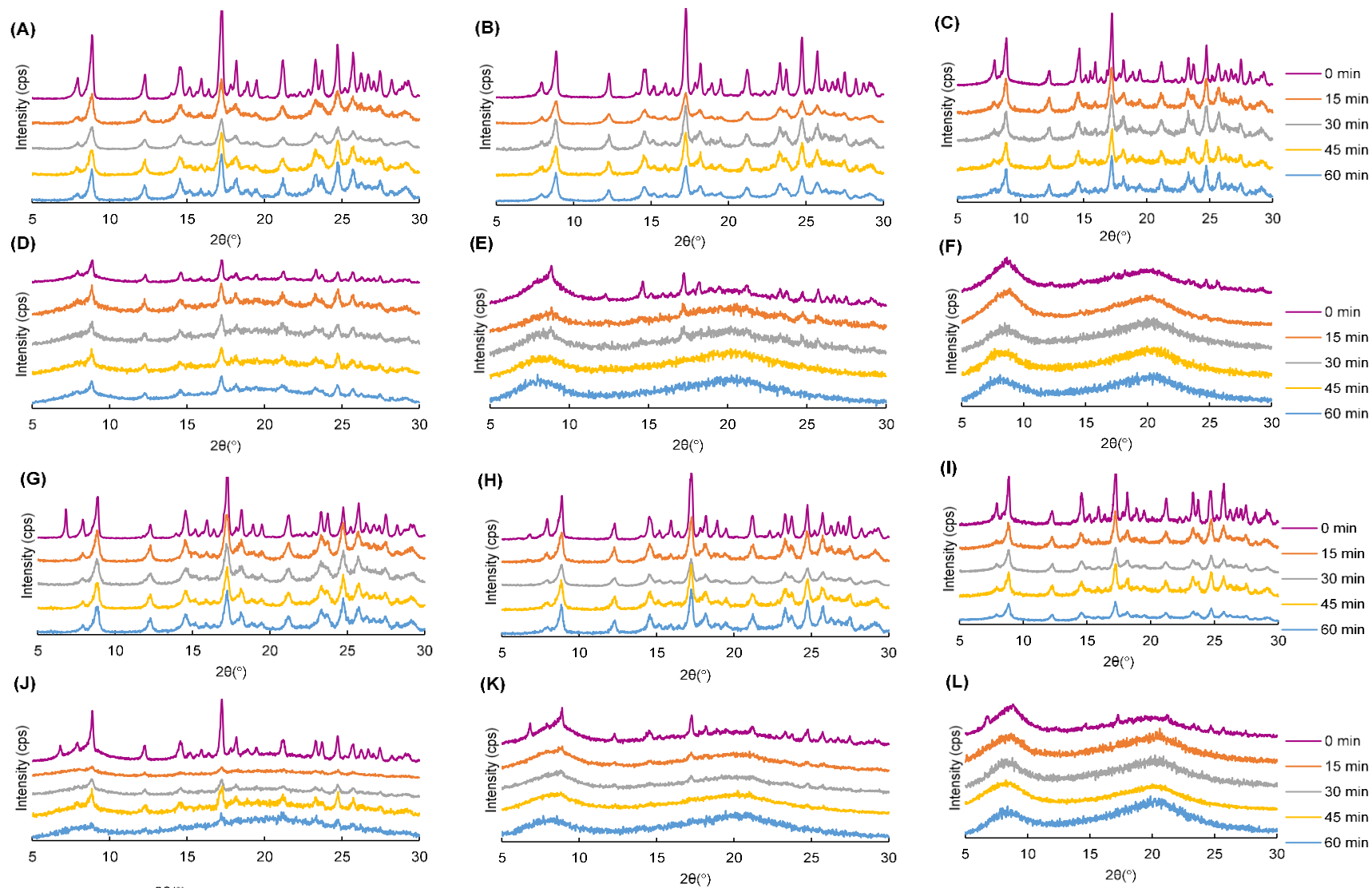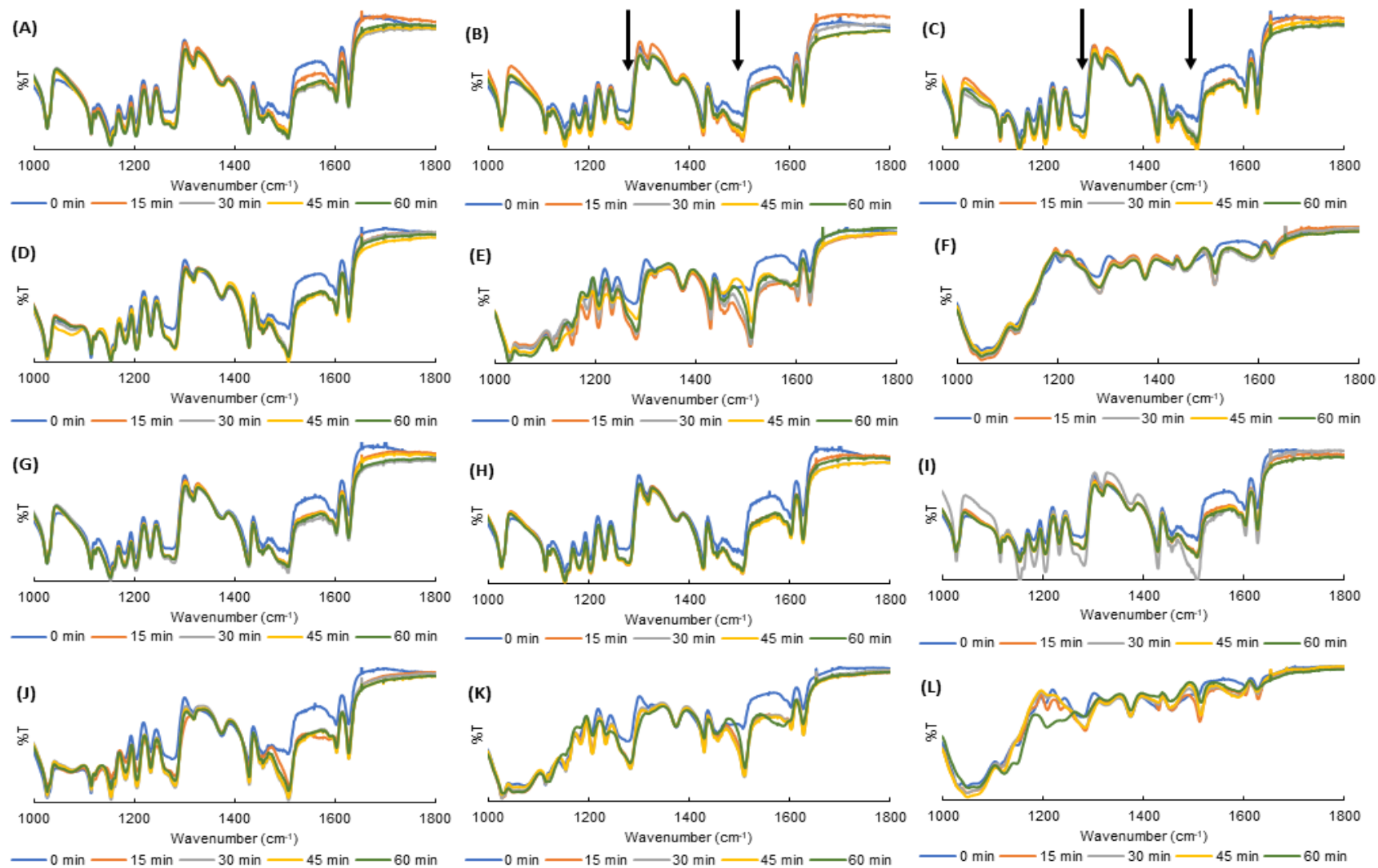
Figure S1. PXRD patterns of various samples

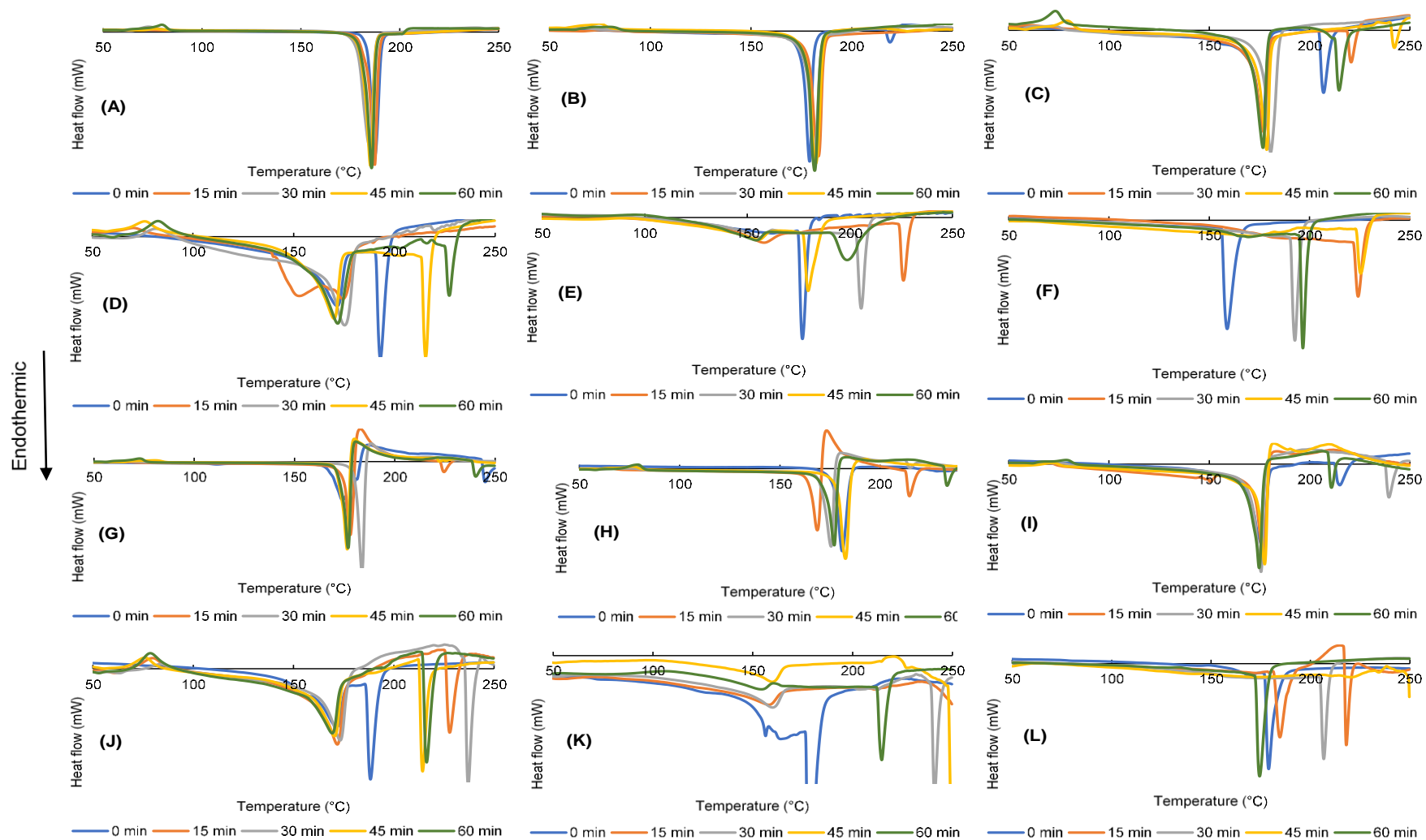**Figure S2. FTIR spectra of various samples**

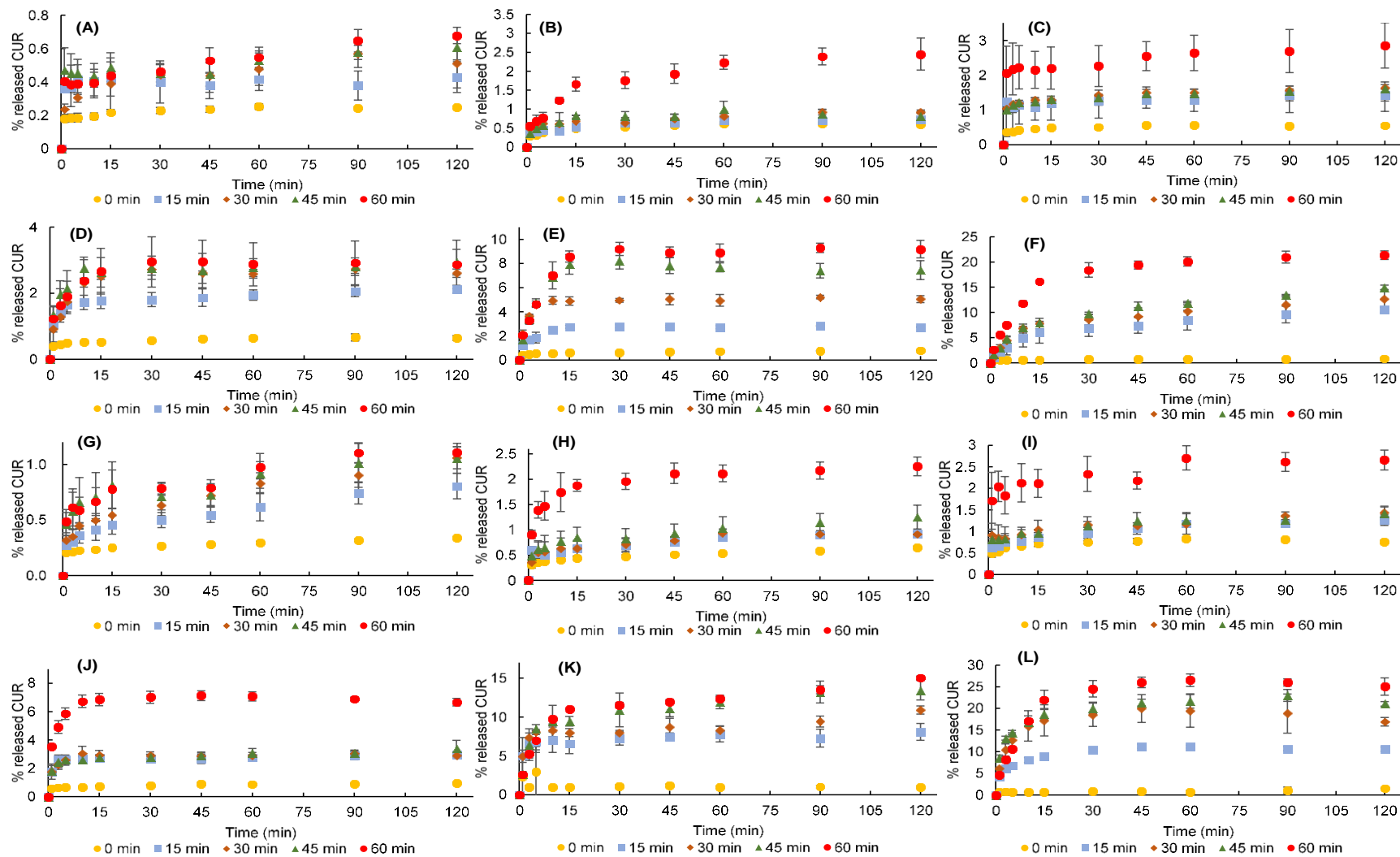**Figure S3. DSC curves of various samples**

Figure S4. Dissolution profiles of CUR from various samples

Chapter 4. Effects of polymer molecular weight on curcumin amorphous solid dispersion: at-line monitoring system based on attenuated total reflectance mid-infrared and near-infrared spectroscopy [103]

4.1. Introduction

Many strategies were demonstrated to form a CUR ASD system with hydrophilic polymers such as cellulose derivatives [104,105], polyvinylpyrrolidone [106], Soluplus® [107], and Eudragit® [108]. Moreover, addition of a surfactant in a polymer-drug SD facilitated fast dissolution of poorly water-soluble drugs and prevention of drug precipitation [109]. Qi et al. suggested that the ASD consisting of a nonionic polymer and an anionic surfactant significantly contributed to the solubilization and stabilization of supersaturated solution of poorly water-soluble drug via the adsorption of surfactant clusters on the polymer chain [109].

Hydroxypropyl cellulose (HPC) is a nonionic water-soluble cellulose ether and plays important roles in ASD such as attaining and maintaining supersaturation, preventing API from crystallization, and controlling the hygroscopicity of the amorphous API [110]. Sodium dodecyl sulfate (SDS) is an anionic surfactant widely used to improve drug wettability, solubility and dissolution rate, due to prevent a hydrophobic barrier forming on contact with water or agglomeration of recrystallized drug particles after dispersion [111]. Many studies investigated the combination of HPC and SDS in drug SD formation [112-115].

An at-line process analytical technology helps in understanding and monitoring a preparation process. Dagge et al. defined it as a method characterized by manual sampling

followed by discontinuous sample preparation, measurement, and evaluation [116]. Analytical instruments (e.g. near-infrared, mid-infrared, and ultra-violet spectroscopy) and chemometric techniques (e.g. principal components analysis-PCA, partial least-squares-PLS, and hierarchical cluster analysis-HCA) are applied in pharmaceutical science for at-line monitoring process [117-119]. Chemometrics is an approach that uses mathematical, statistical methods to design procedures and experiments, and to provide maximum relevant chemical information by analyzing chemical datasets [120].

Particularly, PCA is a dimensionality-reduction approach that simplifies the complexity in high-dimensional datasets [121] by transforming a large set of variables into a smaller one [122] while minimizing information loss [123]. PCA can be obtained from the singular value decomposition (SVD) of the data matrix. Principal components (PCs) are vectors but they are not chosen at random. The first PC (PC1) accounts for the greatest amount of variance in the dataset. The second component (PC2) which is orthogonal to the first accounts for the greatest amount of variance left after the PC1, and so on. As considering the significance of PCs, some components are kept while others are discarded. As the result, the data matrix is simplified (i.e., 100-dimensional dataset can be reduced up to 2-dimensional one).

Zidan et al. monitored tacrolimus crystallization behavior in SDs with HPMC using Fourier transformation-Raman and NIR datasets using PCA approach [124]. Otsuka et al. investigated effect of (polyvinyl pyrrolidone and SDS) and relative humidity on ASD rebamipide based PCA of powder X-ray patterns and NIR spectra [113]. Leimann et at. developed an SD system consisting of CUR, polymers and Tween 80, evaluated particles and color stability after heating using PCA technique [125].

Additionally, PCA can also be performed via singular value decomposition (SVD) of

the data matrix A. SVD is the factorization of A into three matrices $A = U\Sigma V^T$ where U and V are orthogonal and Σ is square diagonal. The matrix U is called the scores matrix, the matrix V is called the loadings matrix, and Σ is called singular values [126]. Overfitting is modeling error that occurs when a function is too closely fit to a limited set of data points. Model validation is a most frequently preventative measure against overfitting [127].

Here, an ASD system consisting of CUR, HPC, and SDS was developed using vibration ball milling. The aim of this study was to investigate the effects of the molecular weight (Mw) of HPC and grinding time on SD formation and the accompanying physicochemical characteristics of SDs. To the best of our knowledge, based on the obtained datasets of mid-infrared and near-infrared spectra, chemometrics analysis was performed to at-line monitor the formation process of these ternary ASDs.

4.2. Materials

CUR was purchased from Tokyo Chemical Industry Co. Ltd (Tokyo, Japan). HPC-SSL (Mw 40,000 Da, viscosity 2.0-2.9 mPa.s at 20 °C/2% aq. solution), HPC-L (Mw 140,000 Da, viscosity 6.0-10.0 mPa.s at 20 °C/2% aq. solution), and HPC-M (Mw 700,000 Da, viscosity 150-400 mPa.s at 20 °C/2% aq. solution) were purchased from Nippon Soda Co. Ltd (Tokyo, Japan). SDS (min 95.0%) was purchased from Wako Pure Chemical Industries Co. Ltd. (Osaka, Japan).

4.3. Preparation and characterization methods

4.3.1. Preparation method

The defined weight ratios of CUR, HPC, and SDS at 30%, 69%, and 1%, respectively, were gently mixed using a glass mortar and pestle for 60 s to obtain PMs.

This weight ratio was the result of previous experiment in chapter 3 [92] where the ground CUR, binary SDs and ternary SDs were evaluated. This chapter demonstrated that the HPC concentration was at about 70% and presence of SDS could increase the solubility and dissolution rate of CUR. The used amount of SDS (1%) assured not to create irritation in case of long usage.

Then, 700 mg of each PM was transferred to a 10-mL stainless steel jar of appropriate size for the MM400 mixer mill (Retsch, Haan, Germany) containing a ball (stainless steel, Φ12 mm). The jar was immersed in liquid nitrogen for 5 min, and then the material was ground in the MM400 mixer mill for 15 min at 30 Hz. The complete immersion for 5 min in liquid nitrogen and grinding process was repeated 1, 2, 3, 4, 6, and 8 times, corresponding to 15, 30, 45, 60, 90, and 120 min of grinding time, respectively. Following grinding, the GMs were sieved through a mesh 36 sieve, stored in a desiccator, and protected from light exposure until further evaluation. All samples were nominated as in Table 4.1.

Table 4.1. Samples used in the experiment [103]

	Grinding time (min)	**Ingredients**
[15]**PM1**	0	[16]CUR, [17]HPC-SSL, [18]SDS
[19]**GM1-15**	15	CUR, HPC-SSL, SDS
GM1-30	30	CUR, HPC-SSL, SDS
GM1-45	45	CUR, HPC-SSL, SDS
GM1-60	60	CUR, HPC-SSL, SDS
GM1-90	90	CUR, HPC-SSL, SDS

[15] PM, Physical mixture
[16] CUR, Curcumin
[17] HPC, Hydroxy propyl cellulose
[18] SDS, Sodium dodecyl sulfate
[19] GM, Ground mixture

GM1-120	120	CUR, HPC-SSL, SDS
PM2	0	CUR, HPC-L, SDS
GM2-15	15	CUR, HPC-L, SDS
GM2-30	30	CUR, HPC-L, SDS
GM2-45	45	CUR, HPC-L, SDS
GM2-60	60	CUR, HPC-L, SDS
GM2-90	90	CUR, HPC-L, SDS
GM2-120	120	CUR, HPC-L, SDS
PM3	0	CUR, HPC-M, SDS
GM3-15	15	CUR, HPC-M, SDS
GM3-30	30	CUR, HPC-M, SDS
GM3-45	45	CUR, HPC-M, SDS
GM3-60	60	CUR, HPC-M, SDS
GM3-90	90	CUR, HPC-M, SDS
GM3-120	120	CUR, HPC-M, SDS

4.3.2. Scanning electron microscopy (SEM)

Samples were attached on a brass specimen club using double-side adhesive tape and made electrically conductive by coating in a vacuum (6 Pa) with platinum (6 nm/min) using an auto-fine coater JFC-1600 (Jeol Ltd., Tokyo, Japan) for 300s at 20 mA. The microscopic features were observed using an analytical SEM (JSM-6060 LA; Jeol Ltd., Tokyo, Japan) at 7 kV, connected to a low-temperature CoolAce circulator EYELA CA-1112 (EYELA Ltd., Tokyo, Japan) at 22°C.

4.3.3. Particle size measurement

Five mg of samples were dispersed in 10 mL ultrapure water, then sonicated for 1 min using an Ultrasonic Homogenizer (Microtec Co. Ltd., Chiba, Japan). The particle size was evaluated using a Zeta potential and particle size analyzer (ELSZ-2000, Otsuka Electronics Co. Ltd., Osaka, Japan) at 25°C. The results are presented as the mean ± std

of three measurements.

4.3.4. PXRD, DSC, MIR, dissolution test

The PXRD patterns, MIR spectra, and DSC curves were recorded according to 2.4.4, 2.4.5, and 2.4.6 section, respectively. The obtained MIR and DSC spectra were normalized by the standard normal variate (SNV) method.

The dissolution profiles of CUR in the GMs were evaluated as described in 2.4.7 section. The results were represented as mean ± std of six measurements.

4.3.5. Near-infrared (NIR)

NIR spectra of samples were obtained in the range of 900-1700 nm using an NIR spectrometer NIR-S-G1 (InnoSpectra Co., Hsinchu, Taiwan). The measurements were performed using the reflectance mode in a glass bottle at 25°C. Wavelength resolution was 4 nm. The obtained spectra were normalized by the SNV method.

4.3.6. Chemometric techniques

Unscrambler X (ver. 10.5.1) software was used to access SNV, PCA, and SVD techniques.

4.4. Results and discussion

Not all samples were physicochemically characterized. The procedure of characterization was summarized in Table 4.2.

Table 4.2. Procedure of physicochemical characterization**.** Not all samples were characterized [103]

Grinding time (min)	0	15	30	45	60	90	120
[20]SEM	O						O
Particle size	O						O

---

[20] SEM, Scanning electron microscopy

[21]PXRD	O					O	O
[22]DSC	O					O	O
Dissolution	O						O
[23]MIR	O	O	O	O	O	O	O
[24]NIR	O	O	O	O	O	O	O

4.4.1. SEM

SEM images of raw materials, PMs, and 120-min GMs are shown in Figure 4.1. CUR particles (Figure 4.1A) exhibited rectangular and parallelepiped morphologies in three-dimensional view: 45-75 µm, 15-20 µm, and 4-5 µm in height. SDS particles (Figure 4.1B) had a multilayer, oval-like shape, with a maximum length of approximate 175 µm and a maximum width of approximate 90 µm. The particles of HPC-SSL (Figure 4.1C) were multilayered, whereas those of HPC-L and HPC-M were round angled and stone-like (Figure 4.1D and Figure 4.1E, respectively). The dimensions of PMs involving CUR particles and the three types of HPC (SSL, L, and M) are shown in Figure 4.1F, Figure 4.1G, and Figure 4.1H, respectively. CUR particles were slightly larger than HPC-SSL particles ((Figure 4.1F) but were smaller than HPC-L and HPC-M particles.

At a magnification of 1000×, Figure 4.1I, Figure 4.1J, and Figure 4.1K show the particles after grinding for 120 min. However, it was impossible to differentiate between CUR and HPC particles. All particles were much smaller (<10 µm) than before they were ground. Dry milling can significantly reduce the particle size of ingredients; thus, API solubility can be remarkably increased by increasing the surface area and improving wettability.

---

[21] PXRD, Powder X-ray diffraction
[22] DSC, Differential scanning calorimetry
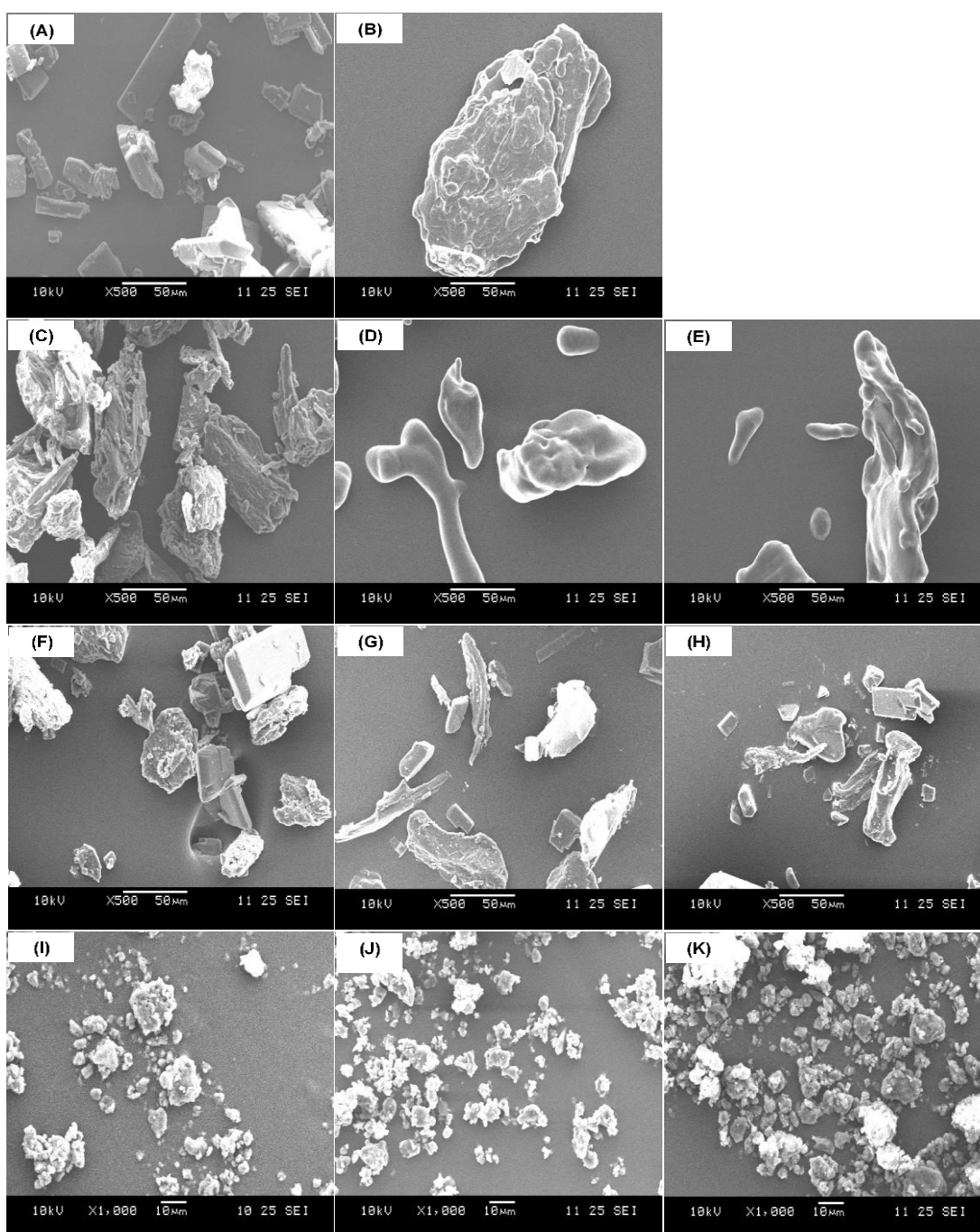[23] MIR, Mid-infrared
[24] NIR, Near-infrared

Figure 4.1. Scanning electron microscopy images of (A) curcumin (CUR); (B) sodium dodecyl sulfate (SDS); (C) hydroxy propyl cellulose (HPC)-SSL; (D) HPC-L, (E) HPC-M, and (F) physical mixture (PM) of CUR, HPC-SSL, and SDS; (G) PM of CUR, HPC-L, and SDS; (H) PM of CUR, HPC-M, and SDS; (I) 120-min ground mixture (GM) of CUR, HPC-SSL, and SDS; (J) 120-min GM of CUR, HPC-L, and SDS; and (K) 120-min GM of CUR, HPC-M, and SDS. The size of particles was minimized up to 10 μm after 120-min grinding [103]

4.4.2. Particle size

Median particle size and particle size distribution for PMs and 120-min GMs were shown in Table 4.3 and Figure 4.2, respectively. When dispersed in water, the HPC and SDS in mixtures were soluble. Thus, the particle size of CUR reflected that of mixtures. The particle size was greatly reduced after 120 min of grinding. Indeed, as compared to its corresponding PM, the particle size of GM1-120, GM2-120, and GM3-120 decreased 139-, 118-, and 139-fold, respectively.

Table 4.3. Particle size and polydispersity index of samples (n = 3) [103]

Sample	Particle size (nm)	Polydispersity index
[25]PM1	30546 ± 5573	1.978 ± 0.822
PM2	41447 ±3857	2.039 ± 0.882
PM3	69948 ± 7013	1.683 ± 0.581
[26]GM1-120	266.2 ± 33	0.215 ± 0.031
GM2-120	350.2 ± 60	0.23 ± 0.029
GM3-120	502.5 ± 16	0.204 ± 0.032

Interestingly, the particle size was greater when the viscosity of HPC was higher. Because CUR is poorly aqueous soluble, the PMs or GMs are dispersed in water as a suspension. In this case, the CUR is rapidly precipitated, and only the floating particles of CUR were screened. The higher viscosity of the liquid is, the larger size of floating particles is. Hence, the particle size of mixtures containing HPC-M was larger than that of HPC-L, and HPC-SSL, respectively (viscosity of HPC: -M > -L > -SSL)

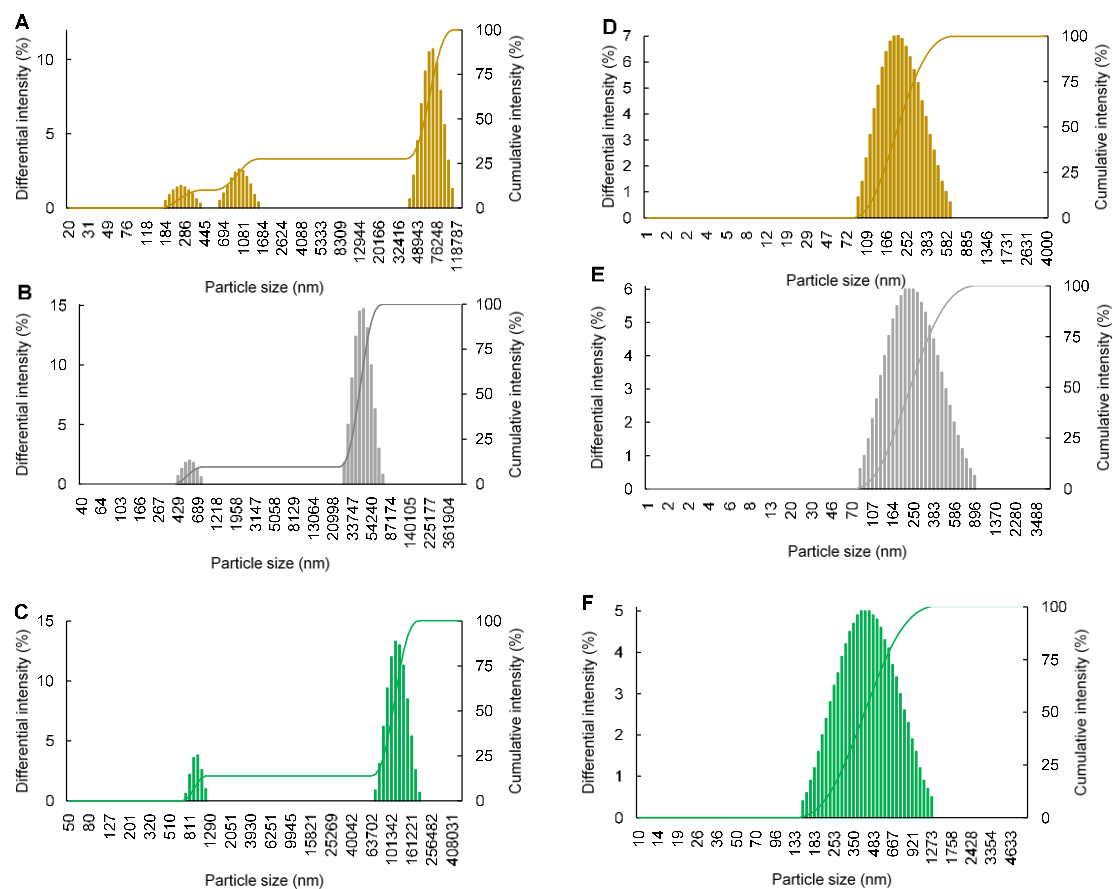[25] PM, Physical mixture
[26] GM, Ground mixture

Figure 4.2. Particle size distribution of (A) physical mixture (PM) containing curcumin (CUR), hydroxypropyl cellulose (HPC)-SSL, and sodium dodecyl sulfate (SDS); (B) PM containing CUR, HPC-L, and SDS; (C) PM containing CUR, HPC-M, and SDS; (D) 120-min ground mixture (GM) of CUR, HPC-SSL, and SDS; (E) 120-min GM of CUR, HPC-L, and SDS; and (F) 120-min GM of CUR, HPC-M, and SDS [103]

4.4.3. PXRD

PXRD patterns of the raw materials are presented in Figure 4.3A. CUR crystals displayed prominent peaks at 2θ = 8.86, 12.28, 14.54, 17.24, 18.18°, 21.2, 23.32, 24.72, and 25.74°, which represent their crystalline nature. The pattern of SDS also indicated a crystalline form, with some prominent peaks at 2θ = 6.82, 9.00, 11.52, 13.78, and 18.42°. The spectra of HPC revealed amorphous features, which were characterized by two halos centered at approximately 2θ = 9 and 21°. Figure 4.3B showed the PXRD profiles of PMs

which reflected one prominent peak of SDS at 6.8° and characteristic peaks of CUR.

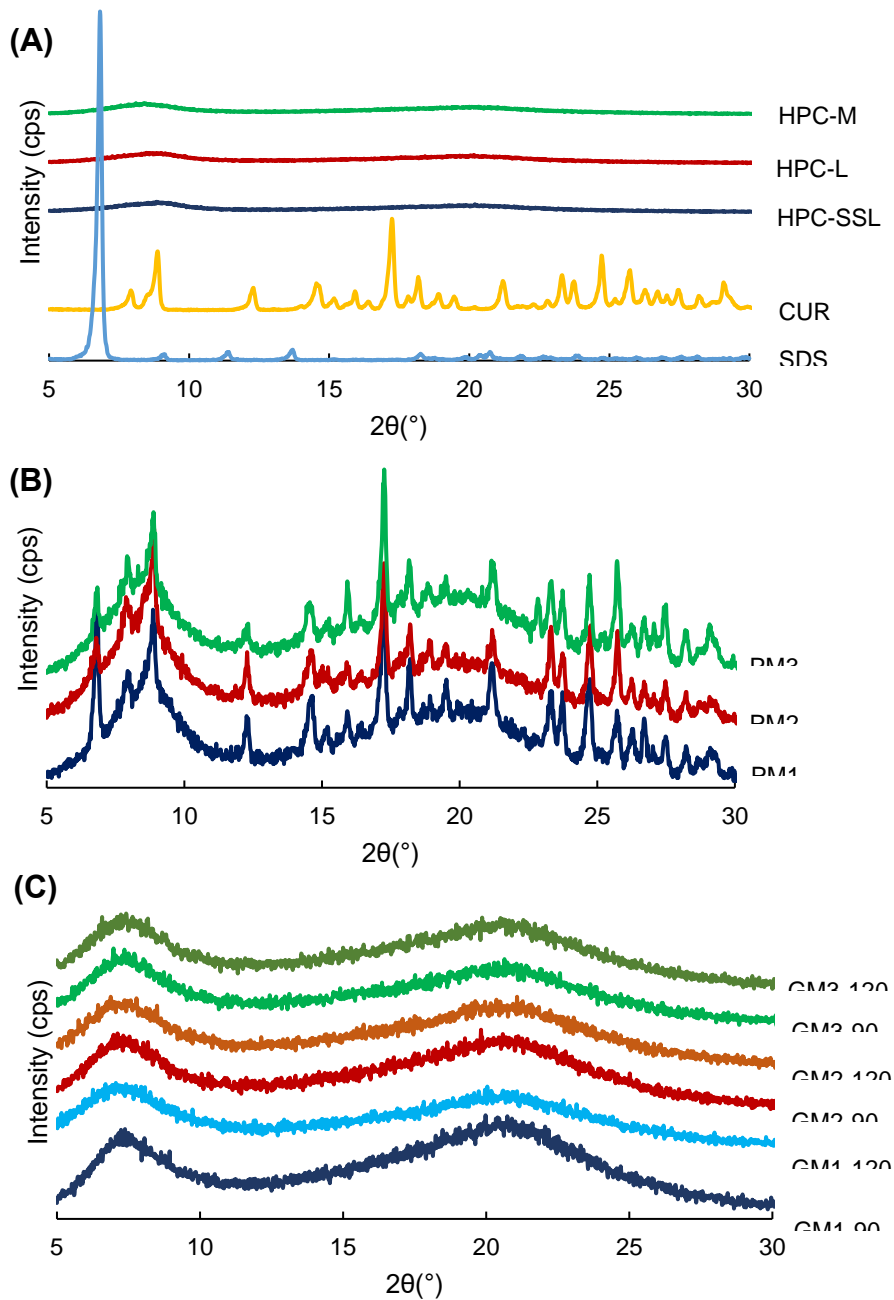

Figure 4.3. X-ray diffraction patterns of (A) raw materials, (B) physical mixtures, and (C) 90- and 120-min ground mixtures showing the transformation from crystalline forms to amorphous forms of curcumin after being ground

After grinding for 120 min, the prominent peaks of CUR in the GMs were hardly visible (Figure 4.3C). Colombo et al.[98] described that solid materials being processed

in a mill received mechanical energy, which manifested atoms shift from equilibrium stable positions at lattice nodes or lattice collapse. Hence, the crystal transformation to amorphous phase could be explained. There was a formation of ASD after 120 min of grinding.

4.4.4. DSC

The DSC thermograms of raw materials, PMs, 90-min GMs, and 120-min GMs are shown in Figure 4.4. In the thermogram of CUR crystals, an endothermic peak attributed to melting was observed at 191°C. The DSC curve of HPC-SSL had a broad endothermic peak at 110 - 170 °C, an exothermic peak at 170 – 210°C, and an endothermic peak at 202 °C; whereas that of HPC-L had a broad endothermic peak at 120 – 170°C, an exothermic peak at 170 – 205°C, and a visible endothermic peak at 221 °C. Moreover, the curve of HPC-M showed a broad exothermic peak at 170 – 185°C, an exothermic peak at 189 °C, and an endothermic peak at 209 °C. In this study, although the cause of these thermal behaviors could not be fully clarified, in general, the amorphous region of HPCs (observed from PXRD patterns) shows the glass transition temperature [128]. Hence, it is supposed that the broad exothermic peaks were the glass transition, following the crystallization (corresponding to exothermic peaks) and melting temperature.

In PMs (Figure 4.4B, Figure 4.4C, and Figure 4.4D; the green lines), the glass transition temperatures (the red circle) were observed at 75, 76, and 81 °C corresponding to mixtures containing HPC-SSL, HPC-L, and HPC-M, respectively. Because these mixtures are considered to impure materials [91], the observed peaks will shift to lower temperatures. Moreover, the melting peaks of CUR also shifted to 161, 156, and 168°C; whilst the decomposition peaks of HPC shifted to 189, 197, and 198°C corresponding to PM1, PM2, and PM3, respectively.

As shown in Figure 4.4B, Figure 4.4C, and Figure 4.4D, the crystallization temperatures (the blue circles) were 119-130°C for 90-min GMs and 112-140°C for 120-min GMs. We supposed these temperatures corresponding to CUR because the grinding process will transform the crystalline to amorphous form of drug [98] and they differed from that of HPCs.
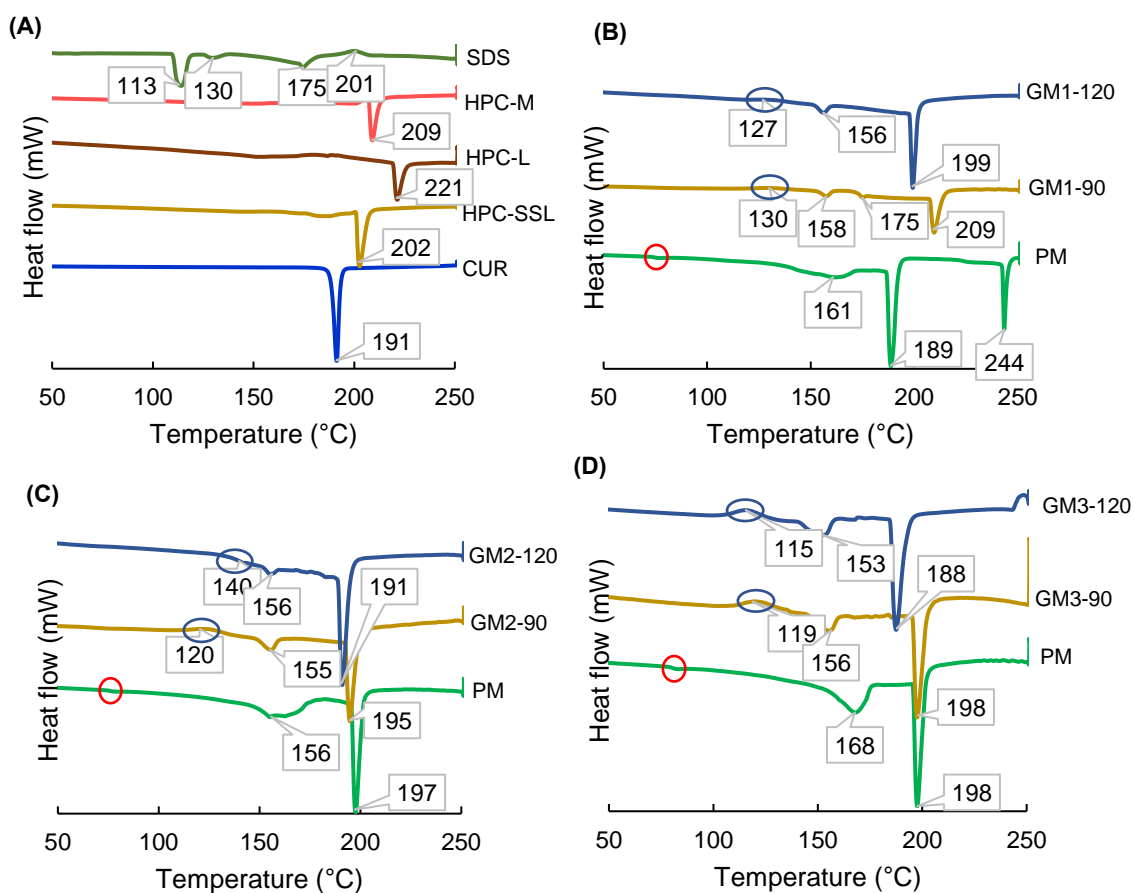

Figure 4.4. DSC curves of (A) raw materials; (B) physical mixture (PM), 90-min ground mixture (GM), and 120-min GM of curcumin (CUR), hydroxypropyl cellulose (HPC)-SSL, and sodium dodecyl sulfated (SDS); (C) PM, 90-min GM, and 120-min GM of CUR, HPC-L, and SDS; and (D) PM, 90-min GM, and 120-min GM of CUR, HPC-M, and SDS [103]

4.4.5. Dissolution study

The dissolution profiles of CUR crystals, PMs, and 120-min GMs were obtained for a period of 120 min (Figure 4.5). The rate of CUR release from PMs was always greater

than that from CUR crystals (Figure 4.5A). PM1 showed a gradual increase in drug concentration, whereas PM2 and PM3 showed fluctuations over the measurement period (120 min).

The 120-min GM had a superior dissolution rate of CUR than the PMs over the measurement period (120 min). An explanation for this is that after 120 min of grinding, the particle size of the components was reduced, leading to a large increase in the surface area of the particles, which enhanced the wettability and solubility of the drug. In addition, API particles were well dispersed in the HPC matrix; thus, the hydrophilic nature of HPC possibly increased the dissolution rate of the drug.
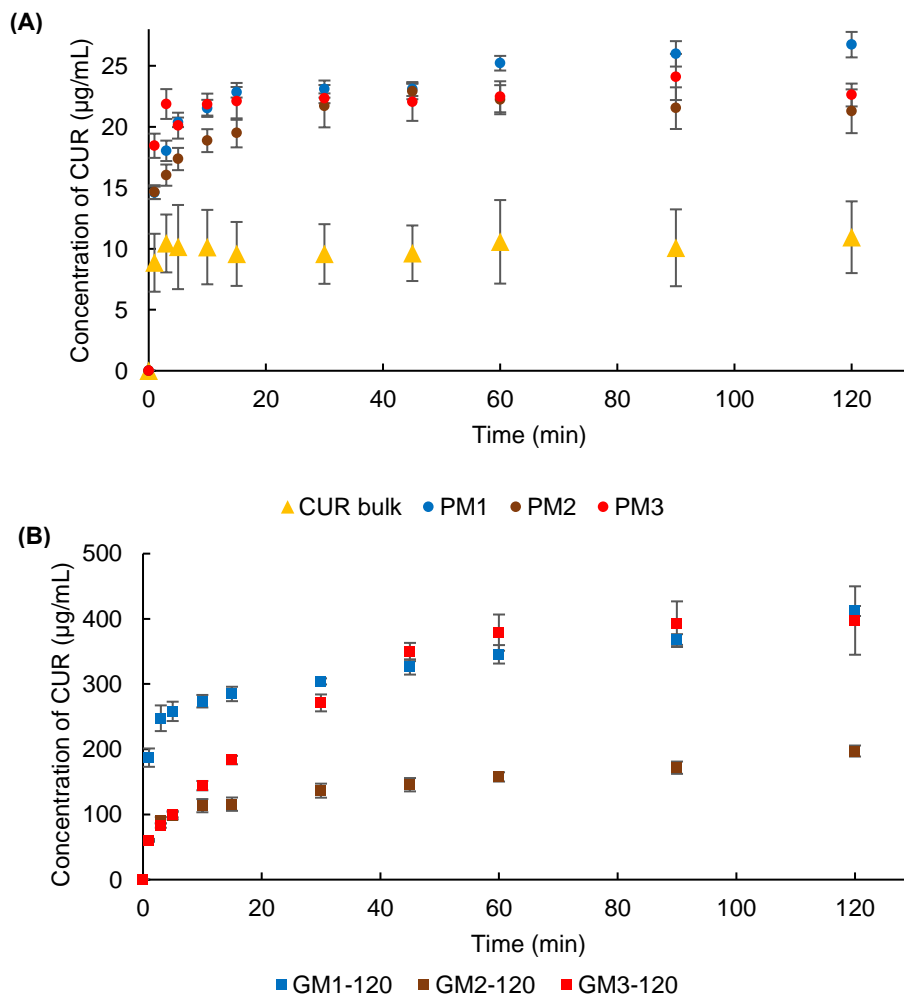

Figure 4.5. Dissolution profiles of (A) curcumin, physical mixtures, and (B) 120-min ground mixtures (mean ± standard deviation, n = 6) [103]

Over the first minute of the study, the amount of CUR released from GM1-120 (187.13 µg/mL) was 3.1-fold greater than that released from GM2-120 (59.22 µg/mL) and GM3-120 (60.72 µg/mL) (Figure 4.5B), and this continuously increased over a period of 120 min from 247.53 µg/mL to 412.01 µg/mL. A similar drug-release profile was noted from GM2-120 and GM3-120 over a period of 1-5 min, corresponding to 59.22-98.86 µg/mL and 60.72-99.53 µg/mL, respectively. However, over the period of 10-120 min, CUR release from GM2-120 increased slowly from 113.45 µg/mL to 197.23 µg/mL, whereas that from GM3-120 increased rapidly from 144.15 µg/mL to 391.82 µg/mL.

4.4.6. MIR spectroscopy

The MIR spectra of CUR, HPCs, and SDS were shown in Figure 4.6A at wavelength 2000 to 1000 cm^{-1}. The prominent peaks observed in CUR spectra (yellow line) were as follows: (1) 1602 cm^{-1} corresponding to the stretching vibration of the benzene ring skeleton; (2) 1506 cm^{-1} corresponding to the mixed (C=O) and (C=C) vibrations; and (3) 1275 cm^{-1} corresponding to the methyl aryl ether (O-CH$_3$) stretching vibrations [31]. The spectra of HPCs displays a prominent peak at 1042 cm^{-1} and a small peak at 1375 cm^{-1} corresponding to C-O stretching and O-H bending [129]. Additionally, the spectra of SDS (blue line) exhibits a prominent peak at 1215 cm^{-1} corresponding to S=O stretching of sulfonate.

The MIR spectra of GM1, GM2, and GM3 with their corresponding PMs were scored in Figure 4.6B, Figure 4.6C, and Figure 4.6D respectively. In general, after grinding, some characteristic peaks of CUR were covered by that of HPCs, resulting in the disappearance of peaks at 1507-1137 cm^{-1}. However, the peaks at around 1280 cm^{-1} increased their intensity. Interestingly, a new broad peak at 1606-1534 cm^{-1} and a new sharp peak at 1512 cm^{-1} were observed. The reason for the increase in the intensity and the appearance of two

new peaks were supposed to be the formation of hydrogen bonds (see also 3.4.2).

Because the percentage of SDS in the system was very low (1%), it was totally dispersed within the matrix of HPC and its interaction with CUR and HPC could not clearly observed.
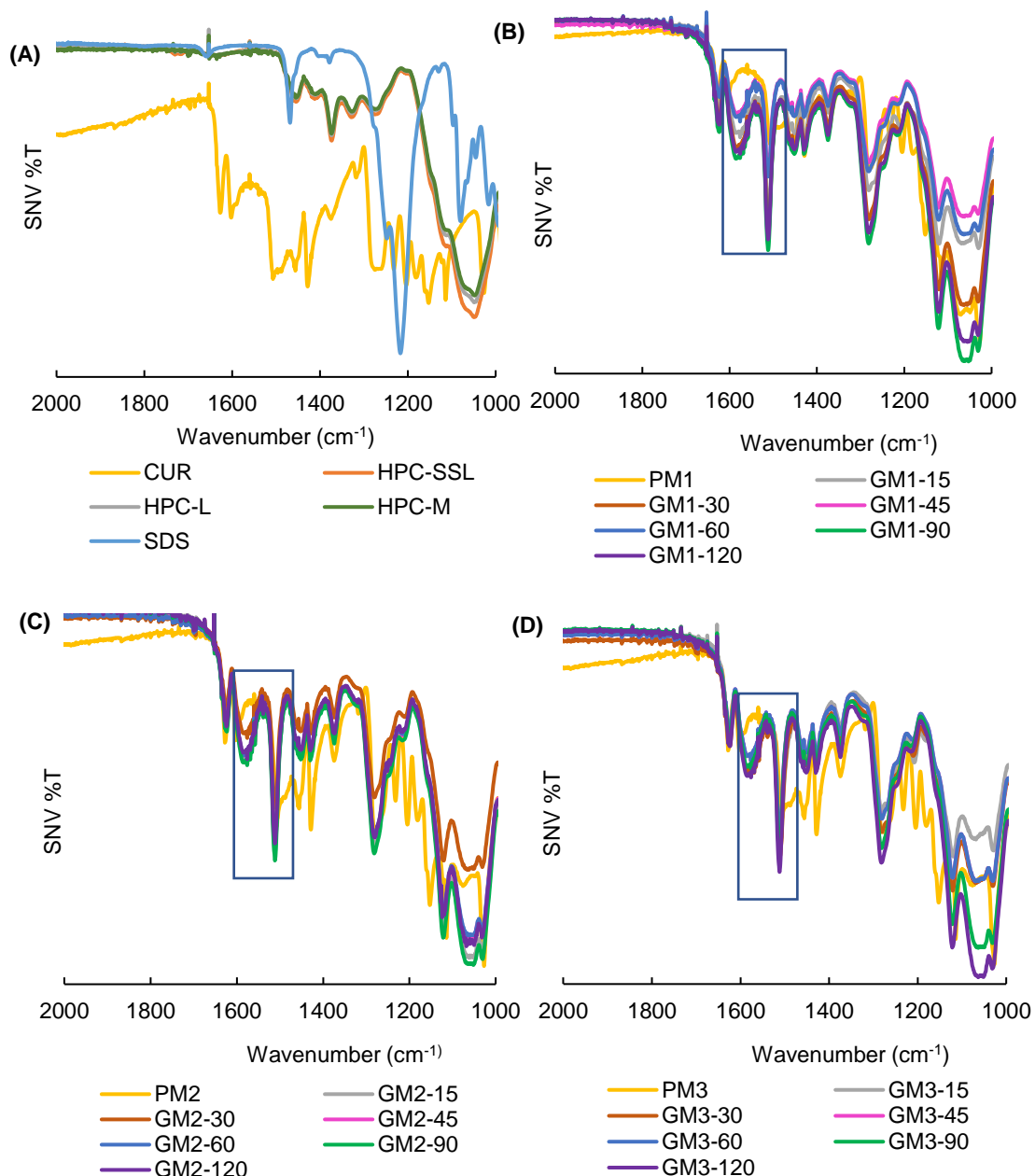

Figure 4.6. Mid-infrared spectra of (A) raw materials, (B) mixtures of curcumin (CUR), hydroxy propyl cellulose (HPC)-SSL, and sodium dodecyl sulfate (SDS); (C) mixtures of CUR, HPC-L, and SDS; and (D) mixtures of CUR, HPC-M, and SDS [103]

4.4.7. Analysis of MIR spectra

The SVD results of MIR spectra in the range from 2000 to 1000 cm^{-1} are shown in Table 4.4. We assumed that the value was sufficient to explain the variance in the MIR spectra. To prevent overfitting [127], the PC number was estimated for two. The validation values for PC1 and PC2 were 63.81% and 92.15%, respectively. In general, the PC1 shows bulk CUR spectra and implies a simple dispersion with grinding time under 30 min, while the PC2 shows CUR molecules randomly dispersed into HPC. To address this, Figure 4.7 was observed and analyzed.

Table 4.4. Cumulative explanatory variance based on mid-infrared spectra dataset [103]

	[27]PC1	PC2	PC3	PC4	PC5	PC6	PC7
Singular value	20.78	6.50	0.93	0.35	0.08	0.03	0.02
Calibration	72.33	94.96	98.20	99.42	99.69	99.80	99.85
Validation	63.81	92.15	96.08	98.16	98.69	98.87	98.88

Figure 4.7 displays loadings and scores of PC1 and PC2 obtained from the MIR spectra in the range from 2000 to 1000 cm^{-1}. The loading of PC1 (blue line) in Figure 4.7A revealed the characteristic peaks of CUR at 1627, 1604, 1484, 1428, 1231, 1202, 1182, 1153, 1114, and 1027 cm^{-1}, as shown in the bulk CUR spectra (Figure 4.7A). Interestingly, a peak of loading at 1534 cm^{-1} was not correlated with any peak of CUR, SDS, or HPC MIR spectra (data not shown). It was considered to be a new peak associated with the formation of SDs.

Moreover, the loading of PC2 (orange line) in Figure 4.7A reveals some characteristic peaks at 1628, 1507, and 1261 cm^{-1} corresponding to the peak shift, mixed vibrations of (C=O) and (C=C) of CUR, and new peak, respectively. This loading suggested a change

---

[27] PC-Principle component

in the second step of SD formation; thus, the microcrystals of CUR were randomly solid-dispersed in HPC to promote amorphization.
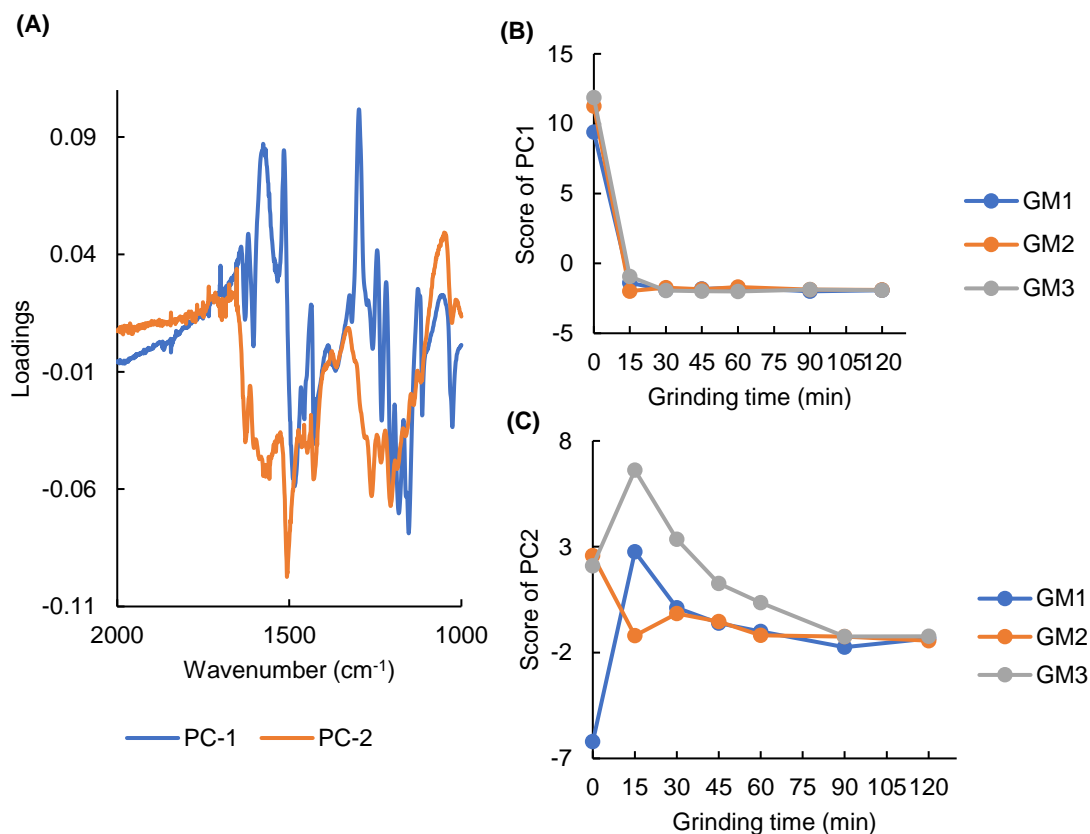

Figure 4.7. (A) Loadings, (B) score of principle component (PC)1, and (C) score of PC2 based on the mid-infrared spectra dataset [103]

The time-course profiles of the score for PC1 are shown in Figure 4.7B. Data at 0 min corresponded to the PMs which were used for reference. The score values of PC1 decreased for all samples at the initial period of mechanochemical synthesis from 0-30 min. This indicated that there was a dramatical reduction in the crystallinity of CUR after 30 min of grinding. We supposed that there were two steps in the SDs formation process: before and after 30 min of grinding, which corresponded to simple and randomized dispersion, respectively.

As shown in Figure 4.7C, the score of PC2 at 0 min was random. Over the 30-min grinding time, the PC2 score of GMs gradually decreased as the grinding time increased.

In addition, the PC2 score of GM3 was higher than that of GM2 and GM1 and there was a similarity in the PC2 values of GM2 and GM1. We assumed that the M_w of HPC influences the formation of SDs in GMs. Indeed, for the high-M_w HPC-M (700,000 Da) (in GM3), a superior dispersion formation was obtained while the M_w of HPC-SSL (40,000) and HPC-L (140,000 Da) (in GM1 and GM2, respectively), the degree of dispersion formation was similar.

4.4.8. NIR spectroscopy

The SNV-transformed NIR spectra of bulk materials and GMs are shown in Figure 4.8. The prominent peaks observed for CUR (yellow line in Fig. 8A) are as follows: 1005

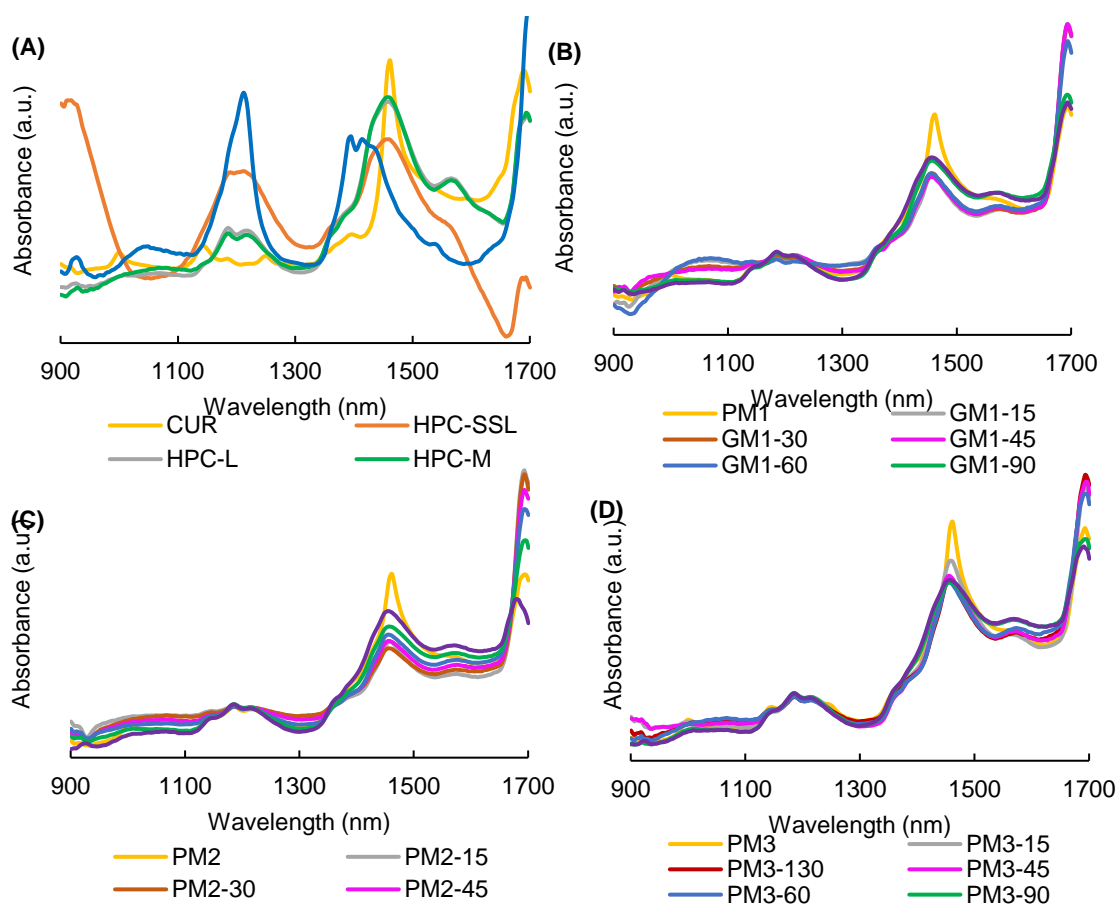
Figure 4.8. Near-infrared spectra of (A) raw materials; (B) ground mixtures (GMs) of curcumin (CUR), hydroxypropyl cellulose (HPC)-SSL, and sodium dodecyl sulfate (SDS); (C) GMs of CUR, HPC-L, and SDS; and (D) GMs of CUR, HPC-M, and SDS [103]

nm for the ROH third overtone, 1136 nm for the CH_3 second overtone, 1461 nm for the ROH second overtone, and 1686 nm for the CH_3 overtone. In the spectra of HPC-L, HPC-M, and HPC-SSL (orange, gray, and green line in Figure 4.8A, respectively), there were pronounced peaks at 1100-1300 nm owing to presence of CH, CH_2, and CH_3 second overtones; at 1398-1536 nm owing to the CH, CH_2, CH_3, and ROH second overtones; and at 1658-1700 nm owing to CH, CH_2, and CH_3 third overtones. SDS spectra (blue line in Figure 4.8A) displays pronounced peaks at 1217, 1398, and 1700 nm, which were attributed to the carbonyl chain second, second, and third overtones, respectively.

The time-course NIR spectra of GMs are shown in Figure 4.8B, Figure 4.8C, and Figure 4.8D. The pronounced peaks at 1464 nm, which indicate the ROH second overtones of CUR, are broadened as the grinding time increased. The peak of CUR at 1686 nm, corresponding to the CH_3 overtone, showed a red shift in mixtures with HPC and SDS, regardless of the grinding time.

4.4.9. Analysis of NIR spectra

The SVD results of NIR spectra for GMs are presented in Table 4.5. We assumed that the value was sufficient to explain the variance in the NIR spectra. To prevent overfitting [127], the PC number was estimated for two. The validation values for PC1 and PC2 were 83.42% and 91.66%, respectively.

Table 4.5. Cumulative explanatory variance based on near-infrared spectra dataset [103]

	[28]PC-1	PC-2	PC-3	PC-4	PC-5	PC-6	PC-7
Singular value	7.08	0.69	0.44	0.11	0.05	0.03	0.01
Calibration	84.09	92.25	97.49	98.77	99.31	99.71	99.80
Validation	83.42	91.66	97.30	98.67	99.19	99.68	99.76

---

[28] PC-Principle component

Figure 4.9 exhibits the loadings and scores of PC1 and PC2 based on NIR spectra of GMs. The loading of PC1 (blue line in Figure 4.9A) shows a remarkable peak at 1697 nm owing to the carbon chain third overtone of HPC, whereas the loading of PC2 (red line in Figure 4.9A) exhibits a noticeable peak at 1461 nm owing to the ROH second overtones of CUR. We supposed that PC1 and PC2 showed respectively randomized dispersion of HPC and CUR.
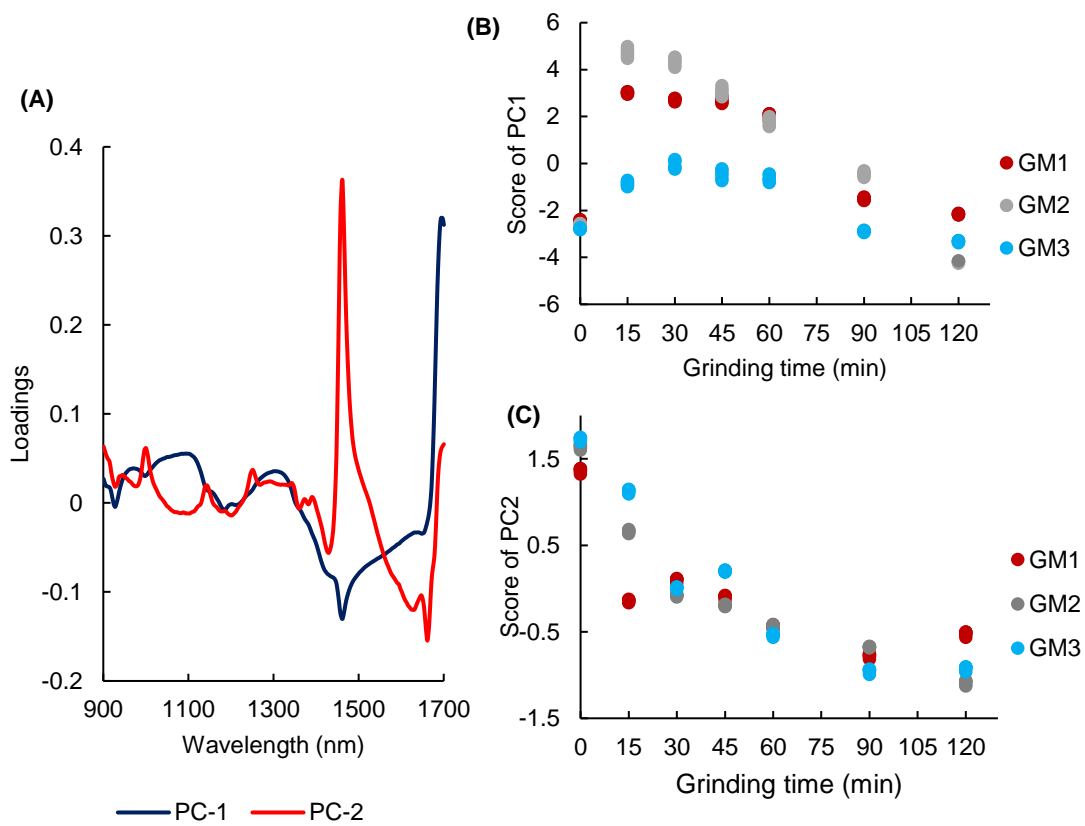
Figure 4.9. (A) Loadings, (B) score of principal component (PC)1, and (C) score of PC2 based on the near-infrared spectra dataset [103]

The time-course profiles of scores for PC1 and PC2 are shown in Figure 4.9B and Figure 4.9C, respectively. The PC1 score values for GM1 and GM2 increased at initial period of grinding time from 0-15 min, then gradually decreased during 15-120 min. Differently, the PC1 score value for GM3 increased for grinding times of 0-30 min and then decreased during 30-120 min. These variances suggested that two steps were

involved in SD formation: before and after 15 min for GM1 and GM2 and before and after 30 min for GM3. The score of PC2 (Figure 4.9C) decreased in GMs for grinding times between 0 and 120 min. Because the loading of PC2 resembles the spectrum of CUR, the reduction in score of PC2 was considered to indicate the decrease in the crystallinity of CUR. In other words, the CUR was amorphized and the degree of amorphization was increased as the grinding time prolonged.

The NIR spectroscopy is a non-destructive approach and demands a relatively inexpensive hand-held piece of equipment. The NIR spectra can be easily manipulated and scored. Associated with MIR spectroscopy, using chemometrics, IR spectra help at-line monitor mechanochemical transformation of samples during SD formation which obtained by grinding.

4.5. Conclusion

In this study, ternary ASD systems containing CUR, HPC, and SDS were developed using the milling method and characterized their physicochemical and mechanochemical properties. After 120-min grinding, the particle size reduced to under 1 μm and the GMs totally transformed into amorphous phase. The release behavior of CUR depended on the grade of HPCs due to their Mw and corresponding viscosity. During the SD formation process, the grinding time and Mw of HPC could be monitored by analyzing data obtained from MIR and NIR spectra based on chemometrics. There were two steps in SD formation: (1) simple dispersion with grinding time under 30 min and (2) random dispersion of mixtures with grinding time from 30 to 120 min. The HPC-M (700,000 Da) resulted in more effectively forming SD systems.

Chapter 5.   Conclusion

CUR SDs were developed with HPβCD, HPCs of various grades, and SDS using freeze-drying, solvent evaporation as well as grinding methods. The obtained SDs were physicochemically characterized using PXRD, FTIR, DSC, dissolution study as well as SEM, particle size measurement, NIR. The carrier(s) where the drug was dispersed could influence the SD forming process due to its (their) chemical structure(s), molecular weight, proportion, and interactions with other components.

The DoE approach gave a global vision of SD formation due to its ability to determine relationship among factors, or to reveal optimize conditions of formulation preparation. It is promising to be a useful tool for researchers to apply in laboratory as well as in pilot and industrial scale.

The SD formation process could be at-line monitored by analyzing MIR and NIR associated with chemometrics. As a results, the effects of SD components and process factors could be evaluated. This monitoring is simple, fast, cheap, and convenient for researchers to apply in pharmaceutical formulation.

Once CUR solubility is increased using SDs, they are loaded onto some formulations which are used as a dermal delivery system for accelerating wound healing process. There have been experiments of loading CUR SDs on non-woven textiles (PET textiles), which are then evaluated *in vitro* and *in vivo* abilities of curing some skin diseases. By the way, the enhancement in the permeability of CUR SDs is evaluated as references when comparing to CUR SDs loaded on the textiles.

References

[1] Rams-Baron, M.; Jachowicz, R.; Boldyreva, E.; Zhou, D.; Jamroz, W.; Paluch, M. Amorphous drug solubility and absorption enhancement. In: Amorphous drugs, Cham: Springer International Publishing Co. 2018, 41–68.

[2] Ngono, F.; Willart, J.F.; Cuello, G.J.; Jimenez-Ruiz, M.; Yelles, C.H.; Affouard, F. Impact of amorphization methods on the physico-chemical properties of amorphous lactulose. Mol. Pharm. 2020, 17, 1–9.

[3] Zeng, Y.; Alzate-Vargas, L.; Li, C.; Graves, R.; Brum, J.; Strachan, A.; Koslowski, M. Mechanically induced amorphization of small molecule organic crystals. Modelling Simul. Mater Sci. Eng. 2019, 27, 1–19.

[4] Shen, W.; Wang, X.; Jia, F.; Tong, Z.; Sun, H.; Wang, X.; Song, F.; Ai, Z.; Zhang, L.; Chai, B. Amorphization enables highly efficient anaerobic thiamphenicol reduction by zero-valent iron. In Appl. Catal. B. 2020, 264, 118550.

[5] Nuno, F.C.; João, F.P.; Ana, I.F. Co-amorphization of olanzapine for solubility enhancement. Ann. Med. 2019, 51, 87.

[6] Zhang, W.; Zhao, Y.; Xu, L.; Song, X.; Yuan, X.; Sun, J.; Zhang, J. Superfine grinding induced amorphization and increased solubility of α-chitin. Carbohydr. Polym. 2020, 237, 116145.

[7] Brough, C.; Williams, R.O. 3rd. Amorphous solid dispersions and nano-crystal technologies for poorly water-soluble drug delivery. Int. J. Pharm. 2013, 453, 157–166.

[8] DiNunzio, J.C.; Miller, D.A.; Yang, W.; McGinity, J.W.; Williams, R.O. 3rd. Amorphous compositions using concentration enhancing polymers for improved bioavailability of itraconazole. Mol. Pharm. 2008, 5, 968–980.

[9]   Hancock, B.C.; Parks, M. What is the true solubility advantage for amorphous pharmaceuticals? Pharm. Res. 2000, 17, 397–404.

[10] Vo, C.L.N.; Park, C.; Lee, B.J. Current Trends and future perspectives of solid dispersions containing poorly water-soluble drugs. Eur. J. Pharm. Biopharm. 2013, 85, 799–813.

[11] Shaikh, A.; Bhide, P.; Nachinolkar, R. Solubility enhancement of celecoxib by solid dispersion technique and incorporation into topical gel. Asian J. Pharm. Clin. Res. 2019, 12, 294–300.

[12] Palanisamy, V.; Sanphui, P.; Prakash, M.; Chernyshev, V. Multicomponent solid forms of the uric acid reabsorption inhibitor lesinurad and cocrystal polymorphs with urea: DFT simulation and solubility study. Acta Crystallogr. Sect. C 2019, 75, 1102–1117.

[13] Das, S.; Mandal, P. Design, formulation, and evaluation of solid dispersion tablets of poorly water-soluble antidiabetic drug using natural polymer. Asian J. Pharm. Clin. Res. 2019, 12, 195–207.

[14] Kapourani, A.; Vardaka, E.; Katopodis, K.; Kachrimanis, K.; Barmpalexis, P. Crystallization tendency of APIs possessing different thermal and glass related properties in amorphous solid dispersions. Int. J. Pharm. 2020, 579, 119149.

[15] Thais, F.R.A.; Cecília, T.B.; Denicezar, B.; Venâncio, A.A.; Mirella, S.; Carolina, S.; Patrícia, S.; Marco, V.C. Preparation, characterization and ex vivo intestinal permeability studies of ibuprofen solid dispersion. J. Disper. Sci. Technol. 2019, 40, 546–554.

[16] Uchiyama, H.; Wada, Y.; Hatanaka, Y.; Hirata, Y.; Taniguchi, M.; Kadota, K.; Tozuka, Y. Solubility and permeability improvement of quercetin by an interaction

between α-glucosyl stevia nano-aggregates and hydrophilic polymer. J. Pharm. Sci. 2019, 108, 2033–2040.

[17] Trapani, A.; Catalano, A.; Carocci, A.; Carrieri, A.; Mercurio, A.; Rosato, A.; Mandracchia, D.; Tripodo, G.; Schiavone, B.I.P.; Franchini, C.; et al. Effect of methyl-β-cyclodextrin on the antimicrobial activity of a new series of poorly water-soluble benzothiazoles. Carbohydr. Polym. 2019, 207, 720–728.

[18] Curcuma longa in India Materia. In: Nadkarni KM. Indian materia medica, Mumbai: Popular Prakashan Co. 1976, 414–418.

[19] Narayanacharyulu, R.; Krishna, S.C.; Mudit, D. Design and development of sustained release tablets using solid dispersion of beclomethasone dipropionate. Res. Rev. J. Drug Formulation Dev. Prod. 2015, 2, 30–41.

[20] Niederau, C.; Göpfert, E. The effect of chelidonium- and turmeric root extract on upper abdominal pain due to functional disorders of the biliary system. Results from a placebo-controlled double-blind study. Med. Klin. (Munich) 1999, 94, 425–430.

[21] Abouhussein, D.M.N.; El Nabarawi, M.A.E.; Shalaby, S.H.; El-Bary, A.A. Sertraline-cyclodextrin complex orodispersible sublingual tablet: optimization, stability, and pharmacokinetics. J. Pharm. Innov. 2019, 1–14.

[22] Vasconcelos, T.; Sarmento, B.; Costa, P. Solid dispersions as strategy to improve oral bioavailability of poor water-soluble drugs. Drug Discov. Today 2007, 12, 1068–1075.

[23] Abd El-Bary, A.; Kamal, I.H.; Haza'a, B.S.; Al Sharabi, I. Formulation of sustained release bioadhesive minitablets containing solid dispersion of levofloxacin for once daily ocular use. Pharm. Dev. Technol. 2019, 24, 824–838.

[24] Modi, A.; Tayade, P. Enhancement of dissolution profile by solid dispersion

(kneading) technique. AAPS PharmSciTech 2006, 7, E87.

[25] Paradkar, A.; Ambike, A.A.; Jadhav, B.K.; Mahadik, K. R. Characterization of curcumin–PVP solid dispersion obtained by spray drying. Int. J. Pharm. 2004 271(1-2), 281–286.

[26] Liu, X.; Lu, M.; Guo, Z.; Huang, L.; Feng, X.; Wu, C. Improving the chemical Stability of amorphous solid dispersion with cocrystal technique by hot melt extrusion. Pharm. Res. 2012, 29, 806–817.

[27] Wu, J.X.; Yang, M.; Berg, F.van den, Pajander, J.; Rades, T.; Rantanen, J. Influence of solvent evaporation rate and formulation factors on solid dispersion physical stability. Eur. J. Pharm. Sci. 2011, 44(5), 610–620.

[28] Sethia, S.; Squillante, E. Physicochemical Characterization of Solid Dispersions of Carbamazepine Formulated by Supercritical Carbon Dioxide and Conventional Solvent Evaporation Method. J. Pharm. Sci. 2002, 91(9), 1948–1957.

[29] Betageri, G.V.; Makarla K.R. Enhancement of dissolution of glyburide by solid dispersion and lyophilization techniques. Int. J. Pharm. 1995, 126(1-2), 155–160.

[30] Łyszczarz, E.; Hofmanová, J.; Szafraniec-Szczęsny, J.; Jachowicz, R. Orodispersible films containing ball milled aripiprazole-poloxamer®407 solid dispersions. Int. J. Pharm. 2020, 575, 118955.

[31] Tønnesen, H. H.; Karlsen, J.; Mostad, A. Structural studies of curcuminoids. I. The crystal structure of curcumin. Acta Chem. Scand. Ser. B 1982, 36, 475–479.

[32] Mague, J.T.; Alworth, W.T.; Payton, F.L. Curcumin and derivatives. Acta Cryst. 2004, C60, 608–610.

[33] Benassi, R.; Ferrari, E.; Lazzari, S.; Spagnolo, F.; Saladini, M. Theoretical study on curcumin: A comparison of calculated spectroscopic properties with NMR, UV-vis

and IR experimental data. J. Mol. Struct. 2008, 892, 168–176.

[34] Duke, J.A.; Bogenschutz-Godwin, M.J.; duCellier, J.; Duke, P.K. CRC Handbook of Medicinal Spices, 1st ed.; CRC Press LLC: Florida, USA, 2002; pp. 137–144.

[35] Niederau, C.; Gopfert, E. The effect of chelidonium- and turmeric root extract on upper abdominal pain due to functional disorders of the biliary system. Results from a placebo-controlled double-blind study. Med. Klin. (Munich) 1999, 94, 425–430.

[36] Li, C.; Li, L.; Luo, J.; Huang, N. Effect of turmeric volatile oil on the respiratory tract. Zhongguo Zhong Yao Za Zhi 1998, 23, 624–625.

[37] Curcuma longa (turmeric). Monograph. Altern. Med. Rev. 2001, 6, S62–66.

[38] Shoba, G.; Joy, D.; Joseph, T.; Majeed, M.; Rajendran, R.; Srinivas, P.S. Influence of piperine on the pharmacokinetics of curcumin in animals and human volunteers. Planta Med. 1998, 64, 353–356.

[39] Bouvier, G.; Hergenhahn, M.; Polack, A.; Bornkamm, G.W.; Bartsch, H. Validation of two test systems for detecting tumor promoters and EBV inducers: comparative responses of several agents in DR-CAT Raji cells and in human granulocytes. Carcinogenesis 1993, 14, 1573–1578.

[40] Saikia, A.P.; Ryakala, V.K.; Sharma, P.; Goswami, P.; Bora, U. Ethnobotany of medicinal plants used by Assamese people for various skin ailments and cosmetics. J Ethnopharmacol 2006, 106, 149–157.

[41] Sharma, R.A.; Steward, W.P.; Gescher, A.J. Pharmacokinetics and pharmacodynamics of curcumin. Adv. Exp. Med. Biol. 2007, 595, 453–470.

[42] Kulac, M.; Aktas, C.; Tulubas, F.; Uygur, R.; Kanter, M.; Erboga, M.; Ozen, O. A. The effects of topical treatment with curcumin on burn wound healing in rats. J. Mol. Histol. 2012, 44, 83–90.

[43] Cianfruglia, L.; Minnelli, C.; Laudadio, E.; Scirè, A.; Armeni, T. Side effects of curcumin: epigenetic and antiproliferative implications for normal dermal fibroblast and breast cancer cells. Antioxidants 2019, 8, 382.

[44] Liu, X.; Zhang, R.; Shi, H.; Li, X.; Li, Y.; Taha, A.; Xu, C. Protective effect of curcumin against ultraviolet A irradiation-induced photoaging in human dermal fibroblasts. Mol. Med. Rep. 2018, 17, 7227–7237.

[45] Mohanty, C.; Sahoo, S.K. Curcumin and its topical formulations for wound healing applications. Drug Discov. Today 2017, 22(10), 1582–1592.

[46] Gopinath, D.; Ahmed, M.R.; Gomathi, K; Chitra, K.; Sehgal, P.K.; Jayakumar, R. Dermal wound healing processes with curcumin incorporated collagen films. Biomaterials, 2004, 25(10), 1911-1917.

[47] Li, X.; Nan, K.; Li, L.; Zhang, Z.; Chen, H. In vivo evaluation of curcumin nanoformulation loaded methoxy poly(ethylene glycol)-graft-chitosan composite film for wound healing application. Carbohydr. Polym. 2012, 88, 84–90.

[48] Merrell, J.G.; McLaughlin, S.W.; Tie, L.; Laurencin, C.T.; Chen, A.F.; Nair, L.S. Curcumin-loaded poly(epsilon-caprolactone) nanofibres: diabetic wound dressing with anti-oxidant and anti-inflammatory properties. Clin. Exp. Pharmacol. Physiol. 2009, 36(12), 1149-1156.

[49] El-Refaie, W.M.; Elnaggar, Y.S.; El-Massik, M.A.; Abdallah, O.Y. Novel curcumin-loaded gel-core hyalurosomes with promising burn-wound healing potential: Development, in-vitro appraisal and in-vivo studies. Int. J. Pharm. 2015, 486(1-2), 88-98.

[50] Thomas, L.; Zakir, F.; Mirza, M.A.; Anwer, M.K.; Ahmad, F.J.; Iqbal, Z. Development of Curcumin loaded chitosan polymer based nanoemulsion gel: In

vitro, ex vivo evaluation and in vivo wound healing studies. Int. J. Biol. Macromol. 2017, 101, 569-579.

[51] Li, X.; Chen, S.; Zhang, B.; Li, M.; Diao, K.; Zhang, Z.; Li, J.; Xu, Y.; Wang, X.; Chen, H. In situ injectable nano-composite hydrogel composed of curcumin, N,O-carboxymethyl chitosan and oxidized alginate for wound healing application. Int. J. Pharm. 2012, 437(1-2), 110-119.

[52] Gong, C.; Wu, Q.; Wang, Y.; Zhang, D.; Luo, F.; Zhao, X.; Wei, Y.; Qian, Z. A biodegradable hydrogel system containing curcumin encapsulated in micelles for cutaneous wound healing. Biomaterials 2013, 34, 6377–6387.

[53] Manca, M.L.; Castangia, I.; Zaru, M.; Nácher, A.; Valenti, D.; Fernàndez-Busquets, X.; Fadda, A.M.; Manconi, M. Development of curcumin loaded sodium hyaluronate immobilized vesicles (hyalurosomes) and their potential on skin inflammation and wound restoring. Biomaterials 2015, 71, 100-109.

[54] Chereddy, K.K.; Coco, R.; Memvanga, P.B.; Ucakar, B.; des Rieux, A.; Vandermeulen, G.; Préat, V. Combined effect of PLGA and curcumin on wound healing activity. J. Control. Release 2013, 171, 208–215.

[55] Seo, S.-W.; Han, H.-K.; Chun, M.-K.; Choi, H.-K. Preparation and pharmacokinetic evaluation of curcumin solid dispersion using Solutol® HS15 as a carrier. Int. J. Pharm. 2012, 424(1-2), 18–25.

[56] Li, J.; Lee, I.W.; Shin, G.H.; Chen, X.; Park, H.J. Curcumin-Eudragit® E PO solid dispersion: A simple and potent method to solve the problems of curcumin. Eur. J. Pharm. Biopharm. 2015, 94, 322–332.

[57] Hu, L.; Shi, Y.; Li, J.H; Gao, N.; Wang, S. Enhancement of oral bioavailability of curcumin by a novel solid dispersion system. AAPS Pharm. Sci. Tech 2015, 16,

1327–1334.

[58] Zhang, Q.; Suntsova, L.; Chistyachenko, Y.S.; Evseenko, V.; Khvostov, M.V.; Polyakov, N.E.; Dushkin, A.V.; Su, W. Preparation, physicochemical and pharmacological study of curcumin solid dispersion with an arabinogalactan complexation agent. Int. J. Biol. Macro. 2019, 128, 158–166.

[59] Dharmalingam, K.; Anandalakshmi R.; Shashank Shekhar. Microwave-induced diffusion method for solid dispersion of curcumin in HPMC matrix using water as hydration carrier, J. Dispers. Sci. Technol. 2020,

[60] Zhang, M.; Zhuang, B.; Du, G.; Han, G.; Jin, Y. Curcumin solid dispersion-loaded in situ hydrogels for local treatment of injured vaginal bacterial infection and improvement of vaginal wound healing. J. Pharm. Pharmacol. 2019, 71(7), 1044-1054.

[61] Du, L.; Feng, X.; Xiang, X.; Jin, Y. Wound healing effect of an in situ forming hydrogel loading curcumin-phospholipid complex. Curr Drug Deliv. 2016, 13(1), 76-82.

[62] Zhang, W.; Cui, T.; Liu, L.; Wu, Q.; Sun, L.; Li, L.; Wang, N.; Gong, C. Improving anti-tumor activity of curcumin by polymeric micelles in thermosensitive hydrogel system in colorectal peritoneal carcinomatosis model. J. Biomed. Nanotechnol. 2015, 11(7), 1173–1182.

[63] Mai, N.N.S.; Nakai, R.; Kawano, Y.; Hanawa, T. Enhancing the solubility of curcumin using a solid dispersion system with hydroxypropyl-β-cyclodextrin prepared by grinding, freeze-drying, and common solvent evaporation methods. Pharmacy 2020, 8, 203.

[64] Rachmawati, H.; Edityaningrum, C.A.; Mauludin, R. Molecular inclusion Complex

of curcumin–β-cyclodextrin nanoparticle to enhance curcumin Skin permeability from hydrophilic matrix gel. AAPS Pharm. Sci. Tech. 2013, 14, 1303–1312.

[65] Maurice, R.E.; Maria, L.A.; Katarina, B.; Howard, D.P.; David, S.K. Cyclodextrin inclusion complexes: Studies of the variation in the size of alicyclic guests. J. Am. Chem. Soc. 1989, 111, 6765–6772.

[66] Swati, R.; Sanjay, K. Solubility enhancement of celecoxib using b-cyclodextrin inclusion complexes, Eur. J. Pharm. Biopharm. 2004, 57, 263-267.

[67] Liu, L.; Zhu, S. Preparation and characterization of inclusion complexes of prazosin hydrochloride with β-cyclodextrin and hydroxypropyl-β-cyclodextrin. J. Pharm. Biomed. Anal. 2006, 40, 122–127.

[68] Wen, X.; Tan, F.; Jing, Z.; Liu, Z. Preparation and study the 1:2 inclusion complex of carvedilol with β-cyclodextrin. J. Pharm. Biomed. Anal. 2004, 34, 517–523.

[69] Karathanos, V.T.; Mourtzinos, I.; Yannakopoulou, K.; Andrikopoulos, N.K. Study of the solubility, antioxidant activity and structure of inclusion complex of vanillin with β-cyclodextrin. Food Chem. 2007, 101, 652–658.

[70] Sambasevam, K.P.; Mohamad, S.; Sarih, N.M.; Ismail, N.A. Synthesis and characterization of the inclusion complex of β-cyclodextrin and azomethine. Int. J. Mo. Sci. 2013, 14, 3671–3682.

[71] Menezes, P.P.; Serafini, M.R.; Quintans-Júnior, L.J.; Silva, G.F.; Olivera, J.F.; Carvalho, F.M.S.; Souza, J.C.C.; Matos, J.R.; Alves, P.B.; Matos, I.L.; et al. Inclusion complex of (−)-linalool and β-cyclodextrin. J. Therm. Anal. Calorim. 2014, 115, 2429–2437.

[72] Wen, P.; Zhu, D.H.; Feng, K.; Liu, F.J.; Lou, W.Y.; Li, N.; Zong, M.H.; Wu, H. Fabrication of electrospun polylactic acid nanofilm incorporating cinnamon

essential oil/β-cyclodextrin inclusion complex for antimicrobial packaging, Food Chem. 2015, 196, 996–1004.

[73] Li, N.; Wang, N.; Wu, T.; Qiu, C.; Wang, X.; Jiang, S.; Zhang, Z.; Liu, T.; Wei, C.; Wang, T. Preparation of curcumin-hydroxypropyl-β-cyclodextrin inclusion complex by cosolvency-lyophilization procedure to enhance oral bioavailability of the drug. Drug Dev. Ind. Pharm. 2018, 44(12), 1966–1974.

[74] Jantarat, C.; Sirathanarun, P.; Ratanapongsai, S.; Watcharakan, P.; Sunyapong, S.; Wadu, A. Curcumin-hydroxypropyl-β-cyclodextrin inclusion complex preparation methods: effect of common solvent evaporation, freeze drying, and ph shift on solubility and stability of curcumin. Trop. J. Pharm. Res. 2014, 13(8), 1215.

[75] Jun, S. W.; Kim, M.S.; Kim, J.S.; Park, H. J.; Lee, S.; Woo, J.S.; Hwang, S.J. Preparation and characterization of simvastatin/hydroxypropyl-β-cyclodextrin inclusion complex using supercritical antisolvent (SAS) process. Eur. J. Pharm. Biopharm. 2007, 66(3), 413–421.

[76] Loftsson, T.; Másson, M.; Brewster, M.E. Self-association of cyclodextrins and cyclodextrin complexes. J. Pharm. Sci. 2004, 93, 1091–1099.

[77] Loftsson, T.; Magnúsdóttir, A.; Másson, M.; Sigurjónsdóttir, J.F. Self-association and cyclodextrin solubilization of drugs. J. Pharm. Sci. 2002, 91, 2307–2316.

[78] Syed, H.K; Peh, K.K. Comparative curcumin solubility enhancement study of β-cyclodextrin and its derivative hydroxypropyl-β-cyclodextrin. Lat. Am. J. Pharm. 2013, 32, 52–59.

[79] Martín, L.; León, A.; Olives, A.I.; Castillo, B.; Martín, M.A. Spectrofluorimetric determination of stoichiometry and association constants of the complexes of harmane and harmine with β-cyclodextrin and chemically modified β-cyclodextrins.

Talanta 2020, 60, 493–503.

[80] Akbik, D.; Ghadiri, M.; Chrzanowski, W.; Rohadizadeh, R. Curcumin as a wound healing agent. Life Sci. 2014, 116, 1–7.

[81] 2-Hydroxypropyl-β-cyclodextrin. Available online: https://www.applichem.com/en/shop/product-detail/as/2-hydroxypropyl-beta-cyclodextrin/(accessed on 4 June 2020).

[82] Zhang, Q.; Ren, W.; Dushkin, A.V.; Su, W. Preparation, characterization, in vitro and in vivo studies of olmesartan medoxomil in a ternary solid dispersion with N-methyl-D-glucamine and hydroxypropyl-β-cyclodextrin. J. Drug Deliv. Sci. Technol. 2020, 56, 101546.

[83] Center for drug evaluation and research. Q2 (R1) Validation of analytical procedures: Text and methodology; FDA Beltsville, MD, USA, 1995.

[84] Higuchi T, Connors KA. Phase solubility techniques. Adv. Anal. Chem. Instrum 1965, 4, 117–212.

[85] Dhanoa, M.S.; Lister, S.J; Sanderson, R.; Barnes, R.J. The link between multiplicative scatter correction (MSC) and standard normal variate (SNV) transformations of NIR spectra. J. Near Infrared Spec, 1994, 2, 43–47.

[86] Dissolution test, in: *The Pharmacopeia of Japan.* 17th ed, Eng ver., Yakuji Nippo Ltd, Japan, 2016, pp. 157–161.

[87] Khan, K.A.; Rhodes, C.T. Effect of compaction pressure on the dissolution efficiency of some direct compression systems. Pharm. Acta Helv. 1972, 47, 594–700.

[88] Jahed, V.; Zarrabi, A.; Bordbar, A.; Hafezi, M.S. NMR (1H, ROESY) spectroscopic and molecular modelling investigations of supramolecular complex of β-

cyclodextrin and curcumin. Food Chem, 2014, 165, 241–246.

[89] Li, N.; Wang, N.; Wu, T.; Qiu, C.; Wang, X.; Jiang, S.; Zhang, Z. Liu, T.; Wei, C.; Wang, T. Preparation of curcumin-hydroxypropyl-β-cyclodextrin inclusion complex by cosolvency-lyophilization procedure to enhance oral bioavailability of the drug, Drug Dev. Ind. Pharm. 2018, 44, 1966-1974.

[90] Kolev, T.M.; Velcheva, E.A.; Stamboliyska, B.A.; Spiteller, M. DFT and experimental studies of the structure and vibrational spectra of curcumin. Int. J. Quantum Chem. 2005, 102, 1069–1079.

[91] Allen, E. The melting point of impure organic compounds. J. Chem. Educ. 1942, 19, 278.

[92] Mai, N.N.S.; Otsuka, Y.; Kawano, Y.; Hanawa, T. Preparation and characterization of solid dispersions composed of curcumin, hydroxypropyl cellulose and/or sodium dodecyl sulfate by grinding with vibrational ball milling. Pharmaceuticals (Basel). 2020, 13(11), 383.

[93] Yamada, T.; Saito, N.; Imai, T.; Otagiri, M. Effect of Grinding with Hydroxypropyl Cellulose on the Dissolution and Particle Size of a Poorly Water-Soluble Drug. Chem. Pharm. Bull. 1999, 47, 1311–1313.

[94] Mochalin, V. N.; Sagar, A.; Gour, S.; Gogotsi, Y. Manufacturing nanosized fenofibrate by salt assisted milling. Pharm. Res. 2009, 26, 1365–1370.

[95] Final report on the safety assessment of sodium lauryl sulfate and ammonium lauryl sulfate. J. Am. Coll. Toxicol. 1983, 2, 127-181.

[96] Li, B., Konecke, S.; Wegiel, L. A.; Taylor, L. S.; Edgar, K. J. Both solubility and chemical stability of curcumin are enhanced by solid dispersion in cellulose derivative matrices. Carbohyd. Polym. 2013, 98, 1108–1116.

[97] Satomi, O.; Takahashi, H.; Kawabata, Y.; Seto, Y.; Hatanaka, J.; Timmermann, B.; Yamada, S. Formulation design and photochemical studies on nanocrystal solid dispersion of curcumin with improved oral bioavailability. J. Pharm. Sci. 2010, 99, 1871–1881.

[98] Colombo, I.; Grassi, G.; Grassi, M. Drug mechanochemical activation. J. Pharm. Sci. 2009, 98, 3961–3986.

[99] Moore, W.; Flanner, H.H. Mathematical comparison of curves with an emphasis on in vitro dissolution profiles. Pharm. Technol. 1996, 20, 64–74.

[100] Polli, J.E.; Rekhi, G.S.; Augsburger, L.L.; Shah, V.P. Methods to compare dissolution profiles and a rationale for wide dissolution specifications for metoprolol tartarate tablets. J. Pharm. Sci. 1997, 86, 690–700.

[101] Kararli, T.T.; Hurlbut, J.B.; Needham, T.E. Glass–rubber transitions of cellulosic polymers by dynamic mechanical analysis. J. Pharm. Sci. 1990, 79, 845–848.

[102] Mark, J.A.; Patrick, J.W. DoE simplified. CRC Press, 3rd ed. 2015, 106.

[103] Mai, N.N.S; Otsuka, Y.; Goto, S.; Kawano, Y.; Hanawa, T. Effects of polymer molecular weight on curcumin amorphous solid dispersion; at-line monitoring system based on attenuated total reflectance mid-infrared and near-infrared spectroscopy. J. Drug Deliv. Sci. Technol. 2021, 61, 102278,

[104] Wan, S.; Sun, Y.; Qi, X.; Tan, F. Improved bioavailability of poorly water-soluble drug curcumin in cellulose acetate solid dispersion. AAPS Pharm. Sci. Tech. 2011, 13(1), 159–166.

[105] Li, B.; Konecke, S.; Wegiel, L.A.; Taylor, L.S.; Edgar, K.J. Both solubility and chemical stability of curcumin are enhanced by solid dispersion in cellulose derivative matrices. Carbohyd. Polym. 2013, 98(1), 1108–1116.

[106] Paradkar, A.; Ambike, A.A.; Jadhav, B.K.; Mahadik, K.R. Characterization of curcumin–PVP solid dispersion obtained by spray drying. Int. J. Pharm. 2004, 271(1-2), 281–286.

[107] Al-Akayleh, F.; Al-Naji, I.; Adwan, S.; Al-Remawi, M.; Shubair, M. Enhancement of curcumin solubility using a novel solubilizing polymer Soluplus®. J. Pharm. Inno. 2020, 271.

[108] Fan, W., Zhu, W.; Zhang, X.; Di, L. The preparation of curcumin sustained-release solid dispersion by hot melt extrusion. I. Optimization of the formulation. J. Pharm. Sci. 2020, 109(3), 1242–1252.

[109] Qi, S.; Roser, S.; Edler, K.J.; Pigliacelli, C.; Rogerson, M.; Weuts, I.; Frederic, V.D.; Stokbroekx, S. Insights into the role of polymer-surfactant complexes in drug solubilization/stabilization during drug release from solid dispersions. Pharm. Res. 2020, 30(1), 290–302.

[110] Vaka, S.R.K.; Bommana, M.M.; Desai, D.; Djordjevic, J.; Phuapradit, W.; Shah. N. Excipients for amorphous solid dispersion, in: Shah, N.; Sandhu, H.; Choi, D.S.; Chokshi, H. Malick, A.W. (Eds.), Amorphous solid dispersion, Springer-Verlag New York Inc., New York, 2014, pp. 123–164.

[111] Pouton. C.W. Formulation of poorly water-soluble drugs for oral administration: Physicochemical and physiological issues and the lipid formulation classification system. Eur. J. Pharm. Sci. 2006, 29, 278–287.

[112] Tascón-Otero, E.; Torre-Iglesias, P.; García-Rodríguez, J.J.; Peña, M.A.; Álvarez-Álvarez, C. Enhancement ò the dissolution rate of indomethacin by solid dispersions in low-substituted hydroxypropyl cellulose. Indian J. Pharm. Sci. 2019, 81(5), 824–833.

[113] Otsuka, Y.; Utsunomiya, Y.; Umeda, D.; Yonemochi, E.; Kawano, Y.; Hanawa, T. Effect of polymers and storage relative humidity on amorphous rebamipide and its solid dispersion transformation: multiple spectra chemometrics of powder x-ray diffraction and near-infrared spectroscopy. Pharmaceuticals 2020, 13(7), 147.

[114] Kawano, Y.; Ishii, N.; Shimizu; Y.; Hanawa, T. Development and characterization of suspension containing nanoparticulated rebamipide for a mouth wash for stomatitis. J. Pharm. Sci. Technol., Jpn. 2017, 77(2), 104–115.

[115] Rahman, M.; Ahmad, S.; Tarabokija, J.; Parker, N.; Bilgili, E. Spray-dried amorphous solid dispersions of griseofulvin in HPC/Soluplus/SDS: Elucidating the multifaceted impact of SDS as a minor component. Pharmaceutics 2020, 12(3), 197.

[116] Dagge, L.; Harr, K.; Schnedl, G. Classification of process analysis: offline, atline, online, inline. Cem. Int. 2009, 72–81.

[117] Behbahani, P.; Qomi, M.; Ghasemi, N.; Tahvildari, K. Ephedrine analysis in real urine sample via solvent bar microextraction technique coupled with HPLC-UV and chemometrics. Curr. Pharm. Anal. 2019, 15(1), 24–31.

[118] Rodionova, O.Y.; Titova, A.V.; Demkin, N.A.; Balyklova, K.S.; Pomerantsev, A.L. Qualitative and quantitative analysis of counterfeit fluconazole capsules: A non-invasive approach using NIR spectroscopy and chemometrics. Talanta 2019, 195, 662–667.

[119] Soliman, S.S.; Elghobashy, M.R.; Abdalla, O.M. ATR-FTIR coupled with Chemometrics for quantification of vildagliptin and metformin in pharmaceutical combinations having diverged concentration ranges. Vib. Spectrosc. 2020, 116, 102995.

[120] Héberger. K. Chemoinformatics—multivariate mathematical–statistical methods

for data evaluation, in: Vékey, K.; Telekes, A.; Vertes A. (Eds.), Medical Applications of Mass Spectrometry, Elservier Science Publisher B.V., Netherlands, 2008, pp. 141–169.

[121] Lever, J.; Krzywinski, M.; Altman, N. Points of Significance: Principal component analysis. Nat. Methods 2017, 14(7), 641–642.

[122] Zakaria, J. https://builtin.com/data-science/step-step-explanation-principal-component-analysis, 2020 (accessed 12 November 2020).

[123] Jolliffe, I.T.; Cadima, J. Principal component analysis: a review and recent developments. Philos. T. R. Soc. A. 2016, 374, 20150202.

[124] Zidan, A.S.; Rahman, Z.; Sayeed, V.; Raw, A.; Yu, L.; Khan, M.A. Crystallinity evaluation of tacrolimus solid dispersions by chemometric analysis. Int. J. Pharm. 2012, 423(2) 341–350.

[125] Leimann, V.F.; Gonçalves, O.H.; Sorita, G.D.; Rezende, S.; Bona, E.; Fernandes I.P.M.; Ferreira, I.C.F.R.; Barreiro, M.F. Heat and pH stable curcumin-based hydrophilic colorants obtained by the solid dispersion technology assisted by spray-drying. Chem. Eng. Sci. 2019, 205, 248–258.

[126] Klema, V.; Laub, A. The singular value decomposition: Its computation and some applications. IEEE Trans. Automat. Contr. 1980, 25(2), 164-176.

[127] Faber, N.M.; Rajkó R. How to avoid over-fitting in multivariate calibration – The conventional validation approach and an alternative. Analytica Chimica Acta 2007, 595, 98–106.

[128] Trivedi, M.K.; Nayak, G.; Patil, S.; Tallapragada, R.M.; Mishra, R. Influence of biofield treatment on physicochemical properties of hydroxyethyl cellulose and hydroxypropyl cellulose. J. Mol. Pharm. Org. Process Res. 2015, 3, 126.

[129] Sigma-Aldrich Co. LLC, USA https://www.sigmaaldrich.com/technical-documents/articles/biology/ir-spectrum-table.html/, 2020 (accessed 10 November 2020).